THE EVALUATION, DEVELOPMENT, AND APPLICATION OF THE CORRELATION CONSISTENT BASIS SETS

Scott Yockel, B.S.

Dissertation Prepared for the Degree of

DOCTOR OF PHILOSOPHY

UNIVERSITY OF NORTH TEXAS

December 2006

APPROVED:

Angela K. Wilson, Major Professor
Martin Schwartz, Committee Member
Mohammad A. Omary, Committee Member
Ralph A. Wheeler, Committee Member
Thomas R. Cundari, Committee Member and Departmental Coordinator of Graduate Studies
Ruthanne Thomas, Chair of the Department of Chemistry
Sandra L. Terrell, Dean of the Robert B. Toulouse School of Graduate Studies

Yockel, Scott, The evaluation, development, and application of the correlation consistent basis sets. Doctor of Philosophy (Physical Chemistry), December 2006, 189 pp., 30 tables, 11 illustrations, references, 241 titles.

Employing correlation consistent basis sets coupled with electronic structure methods has enabled accurate predictions of chemical properties for second- and third-row main group and transition metal molecular species. For third-row (Ga-Kr) molecules, the performance of the correlation consistent basis sets (cc-pV*n*Z, *n*=D, T, Q, 5) for computing energetic (*e.g.*, atomization energies, ionization energies, electron and proton affinities) and structural properties using the *ab initio* coupled cluster method including single, double, and quasiperturbative triple excitations [CCSD(T)] and the B3LYP density functional method was examined. The impact of relativistic corrections on these molecular properties was determined utilizing the Douglas-Kroll (cc-pV*n*Z-DK) and pseudopotential (cc-pV*n*Z-PP) forms of the correlation consistent basis sets. This work was extended to the characterization of molecular properties of novel chemically bonded krypton species, including HKrCl, $FKrCF_3$, $FKrSiF_3$, $FKrGeF_3$, FKrCCF, and FKrCCKrF, and provided the first evidence of krypton bonding to germanium and the first di-krypton system. For second-row (Al-Ar) species, the construction of the core-valence correlation consistent basis sets, cc-pCV*n*Z was reexamined, and a revised series, cc-pCV(*n*+*d*)Z, was developed as a complement to the augmented tight-*d* valence series, cc-pV(*n*+*d*)Z. Benchmark calculations were performed to show the utility of these new sets for second-row species. Finally, the correlation consistent basis sets were used to study the structural and spectroscopic properties of Au(CO)Cl, providing conclusive evidence that luminescence in the solid-state can be attributed to oligomeric species rather than to the monomer.

ACKNOWLEDGEMENTS

Within this section I wish to acknowledge the many people that have been instrumental throughout the process of earning this doctoral degree at the University of North Texas (UNT). Foremost, I extend my greatest gratitude to my Ph.D. advisor Professor Angela K. Wilson, whom I have the utmost respect and admiration. Her passion for theoretical chemistry influenced me as an undergraduate and continues to inspire me even today. Furthermore, she is a kind, compassionate advisor who will always be a friend and colleague. I would like to thank Dr. Wilson for her editorial corrections and scientific comments on all my publications. Also, I must thank my committee for their time and comments on this dissertation. Thank you to the Wilson Group graduate students and postdoctoral fellows N. DeYonker and G. R. Shelton for proofreading this dissertation. I wish to also thank D. Gustavus, D. Fuller, and D. Hrovat who have worked diligently to provide great computational resources at UNT. Thank you to D. Gustavus for all the knowledge in system administration that he has taught me. Support for the following work has been provided by the National Science Foundation, U.S. Dept. of Education, National Center for Supercomputing Applications, and UNT's Faculty Research Grant, Academic Computing Services, and Center for Scientific Computing and Modeling. Thank you to the collaborators who contributed to a small portion of the computational work in this dissertation: B. Mintz (Ch. 3), A. Garg (Ch. 7) and E. Gawlik (Ch. 8). Experimental work in Chapter 9 was provided by O. Elbjeirami and Professor Mohammad A. Omary. Finally I would like to thank my family and friends for their consistent support through encouraging words, prayer, and love, especially my parents David and Nancy Yockel and my wife Lauren Yockel.

TABLE OF CONTENTS

LIST OF TABLES

LIST OF ILLUSTRATIONS

CHAPTER 1

INTRODUCTION

Solving the fundamental equation of quantum mechanics, the Schrödinger equation, enables the prediction of many chemical properties such as geometric structures, vibrational frequencies, electronic energy levels, ionization potentials, electron affinities, potential energy surfaces, and enthalpies. However, solutions to the Schrödinger equation are complex, and cannot be solved exactly, with the exception of one-electron systems. This is due largely to the significant computing resources (disk space, memory, and time) required. Therefore, a computational "method" must be chosen, which refers to the level of sophistication at which the Schrödinger equation will be addressed. Additionally a "basis set" must be chosen, which is a predefined set of basis functions (*s,p,d,f,* …) that is used by the method for the description of atomic orbitals.

The use of approximate methods and incomplete basis sets to solve the Schrödinger equation introduces error into the prediction of chemical properties. To understand the error, the interplay between methods and basis sets must be gauged. The reliability of a method and basis set combination in the prediction of chemical properties helps to establish the historical performance of a given computational approach. When established experimental data are not available or experimental data have large uncertainties, it is the historical performance that allows computational chemists to gauge the reliability of the predicted chemical properties. Additionally, when large discrepancies or uncertainties in experimental values are encountered,

accurate computational chemistry calculations can help decipher which experimental values should be accepted.

The ability to predict chemical properties with "chemical accuracy" is crucial to the understanding of many chemical phenomena. Predicting accurate chemical properties can lead to the confirmation of experimental findings, provide supporting evidence to better explain experimental observations, or provide valuable guidance to experimentalists for future research. A major advantage of computational approaches is their use for studying systems, such as reaction intermediates, short-lived transient species, or excited state complexes, which often are either difficult, if not impossible, to study directly in the laboratory, or are too cost prohibitive to study.

The focus of the present work is based on the evaluation, development, and application of the correlation consistent basis sets, a special family of basis sets that were originally developed by T. H. Dunning, Jr. in 1989 for the atoms B-Ne (first-row) and hydrogen.[1] (A more in-depth discussion on the composition of the correlation consistent sets is detailed in Chapter 2.) Further development of the standard correlation consistent basis sets included extensions to second-row atoms (Al-Ar)[2] and to third-row atoms (Ga-Kr).[3] The basis sets for first- and second-row atoms have been used in numerous studies and their reliability and accuracy have been demonstrated in a number of benchmark studies,[1,2,4-25] which provide accurate descriptions of molecular properties. These previous studies provide a precedent for the accuracy that should be achievable for future calculations on first- and second-row molecules using the correlation consistent basis sets and electron correlation methods. Even though the third-row sets have been used many times in the literature, no comprehensive study on a large test suite of molecules had been performed. Thus, the work in Chapter 3 provides a benchmark for the third-row sets. More

recent developments in the correlation consistent basis sets have encompassed relativistic effects. The effect relativity has on the structural and electronic properties of molecules containing third-row atoms is the focus of Chapter 4.[26-28]

The correlation consistent basis set family also includes sets where both core- and valence-electron interactions are considered. The core-valence correlation consistent basis sets (cc-pCV*n*Z) augment the standard valence sets (cc-pV*n*Z) with a set of high-exponent basis functions to describe the core region of a molecule.[9,16] Recently a deficiency was noted in the original formulation of the valence basis sets for second-row atoms,[29-32] which is discussed in more detail in Chapter 5 (see Sec 5.1). This deficiency has been remedied, resulting in a new basis set formulation, cc-pV(*n*+*d*)Z.[15] However a deficiency still exists for the core-valence basis sets for second-row atoms. Chapter 5 examines this problem and introduces a new core-valence basis set series, cc-pCV(*n*+*d*)Z.

The correlation consistent basis sets have also been used to study krypton-bonded compounds. Historically, krypton was thought to be inert and non-reactive, however, experimental and theoretical efforts have shown that krypton is capable of forming real chemical bonds.[33,34] While these studies have provided insight about krypton-bonded species, there is still much to be learned. Chapter 6 focuses on the characterization of the compound HKrCl, which has been synthesized experimentally,[33,35] while the aim of Chapters 7 and 8 is to predict and characterize new noble gas-bonded systems. This can be done with certainty because of the results of the benchmarking studies and Chapter 6.

Recently, the development of the correlation consistent basis sets has expanded beyond main group chemistry into transition metal chemistry.[36,37] These new series of basis sets have enabled a more balanced description of transition metal atoms as compared to main group atoms,

which allows for a more accurate evaluation of transition metal chemistry. Chapter 9 is a study which utilizes these new basis sets to gain further understanding about the structure-luminescence relationship in Au(CO)Cl. The work in Chapter 9 has been done in collaboration with the M. A. Omary group at the University of North Texas, Department of Chemistry.[38]

CHAPTER 2

GENERAL COMPUTATIONAL CHEMISTRY METHODOLOGY

The Schrödinger equation[39-42] (Eqn. 2.1) is central to quantum mechanics, and in its simplest form is comprised of a Hamiltonian operator ($\hat{H}$) that operates on a wavefunction (Ψ).

$$\hat{H}\Psi = E\Psi \tag{2.1}$$

In molecular quantum chemistry, the wavefunction is described by the basis set – a set of mathematical functions (or basis functions) that represent the atomic orbitals. Solving Eqn 2.1 yields the total energy eigenvalue (E) and eigenvector wavefunction (Ψ). The Hamiltonian,

$$\hat{H} = -\sum_{i}^{N}\frac{1}{2}\nabla_i^2 - \sum_{A}^{M}\sum_{i}^{N}\frac{Z_A}{r_{iA}} + \sum_{i>j}^{N}\frac{1}{r_{ij}} - \sum_{A}^{M}\frac{1}{2M_A}\nabla_A^2 + \sum_{A>B}^{M}\frac{Z_A Z_B}{r_{AB}} \tag{2.2}$$

is the total energy operator for a system with electrons (i,j) and nuclei (A,B) and is comprised of five terms: (1) electronic kinetic energy, (2) potential energy of electron attraction to the nuclei, (3) potential of the Columbic electron-electron repulsion, (4) nuclear kinetic energy, (5) potential energy of the nuclear-nuclear repulsion.

The complexity of the Schrödinger equation makes it feasible to solve exactly for one-electron species. In order to study chemical systems, solving the Schrödinger equation, therefore requires an approximate treatment of the theoretical method within a finite one-electron particle basis. In general, there are three major factor which must be considered: the level of accuracy desired for the property of interest, the computational cost of the method employed, and the size of the molecular system. The accuracy at which properties can be computed relies heavily upon the method chosen to solve the Schrödinger equation. The method employed and the size of the

molecular system studied are limited by the amount of computational resources available (*i.e.* time, memory, disk space …). In fact, the computational resources needed, or the "cost" of a calculation, is dramatically increased by both the size of the system and the sophistication of the method used to solve the Schrödinger equation.

Computations utilizing *ab initio* methods entail solving the Schrödinger equation directly from theoretical principles and do not include parameters based on experimental data. However, there are some basic assumptions that are generally made in typical *ab initio* calculations. As noted in Eqn. 2.2, the coordinates of both nuclei and electrons are present, thus the nuclear and electronic motions are coupled when solving the Schrödinger equation. However, the electronic and nuclear motions can be separated because the speed of the nuclei is minuscule in comparison to the speed of the electrons. Decoupling the electronic and nuclear motions is referred to as the Born-Oppenheimer approximation.[43] Thus, for electronic calculations the nuclei are kept fixed and the electron Hamiltonian ($\hat{H}_{elec}$) is used, which only solves the first three parts of Eqn. 2.2. This approximation usually has very little effect on the electronic structure or the prediction of chemical properties. For example, in an elaborate study by Rusic *et al.*, which revisits the gas-phase bond dissociation energy of water, they predict that the non-Born-Oppenheimer effects contribute only 0.10 kcal/mol to the computed atomization energy of water.[23]

The non-relativistic Schrödinger equation, as shown in Eqn. 2.1, assumes that the speed of the electrons is insignificant relative to the speed of light, which is considered infinite. Thus, in Eqn. 2.1 the effects due to relativity are excluded, which is generally acceptable for molecules composed of the lighter elements. This assumption breaks down as the velocity of the electrons in the 1*s* orbital increase and approach significant fractions of the finite speed of light. This

becomes more prevalent as the effective nuclear charge increases. A more in-depth discussion on the impact that relativity has on chemical properties is presented in Chapter 4.

Another approximation that is central to much of *ab initio* quantum chemistry is the Hartree-Fock (HF) approximation.[44-48] In the HF method, the direct Coulombic electron-electron repulsion is not specifically considered and instead, only the net effect of each electron interaction with the average electronic potential is considered. This generally recovers ~99% of the total electronic energy. The computational cost of a typical HF calculation scales as N^4, where N is the number of basis functions. The lowering in energy due to the individual electron-electron interactions is referred to as electron correlation,

$$E_{\text{corr}} = \mathcal{E}_0 - E_0 \tag{2.3}$$

which is defined as the difference in the exact ground state energy ($\mathcal{E}_0$) and the ground state HF energy (E_0).[49] Even though the electron correlation generally accounts for ~1% of the total electronic energy, a good description of electron correlation is generally necessary for the accurate prediction of chemical properties. Electron correlation methods have schemes that account for (or correlate) specific electron-electron interactions, causing a dramatic increase in the computational cost due to the number of direct electron-electron interactions that must be considered. Most of these approaches are much more "expensive" as compared to HF and scale as $\geq N^5$. The primary correlated method used throughout this study is the coupled cluster method (CCSD(T)), which incorporates the correlation of electrons in a cluster operator (Eqn. 2.4) that includes all single and double excitations along with quasiperturbative triple excitations from the ground state wavefunction.[50-52]

$$e^{\hat{T}} = 1 + T_1 + \left(T_2 + \frac{1}{2}T_1^2\right) + \left(T_3 + T_2T_1 + \frac{1}{6}T_1^3\right) + \ldots \tag{2.4}$$

As shown in Eqn. 2.4, e^T is a general cluster operator that includes all excitations of a given reference wavefunction grouped together by the type of excitation. The first term (1) comes from the zeroth order wavefunction, the second term (T_1) includes all single excitations, the third term ($T_2 + \frac{1}{2}T_1^2$) includes both the product of two single excitations ($\frac{1}{2}T_1^2$) and a double excitation (T_2), and so on. A full discussion of this methodology is beyond the scope of this dissertation and can be found in Ref. 50-54 Figure 2.1 provides a diagram of the occupied and virtual orbitals of a given system and illustrates the concept of single (S), double (D), and triple (T) excitations. The iterative CCSD steps of the CCSD(T) method scale as N^6 while the single perturbation (T) part scales as N^7, providing in one of the more efficient ways to include electron correlation due to the triple's contribution. When using expensive correlated methods, it is usually not feasible to correlate all of the electrons in the system. Normally, the correlation of the core electrons is not included in electron correlated methods. This approach is known as the frozen-core approximation because only valence electrons are included in the correlation space – the orbital space that is included in the electron correlation calculation. Since the majority of chemical bonding involves only the valence electrons, this approximation generally has only a small effect on the energetics. For example, in a benchmark study on first-row diatomics by Peterson *et al.,* correlating the 1*s* core electrons only increased the dissociation energy (D_e) of O_2 by 0.22 kcal/mol and shortened the bond distance by 0.0019 Å.[10]

An alternative to solving Schrödinger wavefunction based equations to solve for the total energy in a given system is to use density functional theory (DFT). The central premise to DFT is that the ground state energy of a system can be expressed as a "function" of the electron density (ρ). Kohn and Sham (KS) were the first to introduce the use of orbitals (namely the KS orbitals) to DFT, which allow for a more realistic description of molecules.[55] As shown in Eqn.

2.5, using DFT to solve for the ground state energy of a system includes terms which describe the various interactions in the molecule, which are analogous to the terms in the Hamiltonian (Eqn. 2.2).

$$E = E^{T}(\rho) + E^{V}(\rho) + E^{J}(\rho) + E^{XC}(\rho) \qquad (2.5)$$

In Eqn. 2.4, the ground state energy is the sum of the kinetic energy (E^{T}), potential energy of the nuclear-electronic attraction (E^{v}), Columbic electron-electron repulsion (E^{J}), and the electronic exchange and correlation energy (E^{XC}). The last term, E^{XC}, can be separated into two different parts, the exchange (E^{X}) and the correlation (E^{C}). There are many different means for constructing these two components, and these various means define the type of "functional", or method, that is used. Difficulties arise in providing the exact formalism (*i.e.* a functional) which correctly links the electronic density to the kinetic, potential, exchange (energy that arises from the correlation electrons of like spins), and correlation (energy that emerges from the interaction electrons of opposite spins) energies. Over the past years, a multitude of different functionals have been developed to address this problem. These functionals have seen widespread utilization for the study of molecular properties, largely due to the means to account for electron correlation at a low computational cost (formally N^4, but in practical use scales as N^3).

While there is an extensive number of functionals available, including newer "generations" of functionals, the discussion here will be limited to B3LYP, as it continues to be the most widely used functional, as well as the best established functional in terms of overall reliability in the prediction of energetics such as dissociation energies. which includes Becke's three parameter (B3)[56] exchange term and Lee, Yang, and Parr's (LYP)[57] correlation term. This functional is considered a "hybrid" density functional because it mixes in a portion of the exchange energy from HF and is parameterized to best reproduce a given test suite of molecular

energies. In general, B3LYP is not known to be as reliable as an *ab initio* method such as CCSD(T), as the typical error in energetics for B3LYP is ~2-3 kcal/mol from reliable experiment.[56] However, the much smaller computational cost of B3LYP and other DFT methods makes these methods a highly desirable computational approach.

Beyond the approximations common in most electronic structure calculations, the main sources of error in calculated properties arise from the use of an incomplete (or finite) basis set and the choice of electron correlation method. The error arising from the use of an incomplete basis can be eliminated when a set of basis functions completely spans the molecular orbital space so that additional basis functions no longer affect the electronic energy; this is known as the complete basis set (CBS) limit. Similarly, when all possible electron-electron interactions have been accounted for, as in the full configuration interaction (Full CI) method,[58,59] the electron correlation limit has been reached. With the performance of today's computers, it is possible to study the electronic structure of extremely small systems at or very near the complete basis set (CBS) and electron correlation limits (Full CI). The solution to the Schrödinger equation at these limits approaches the "exact" solution. For energy calculations, such as atomization energy, ionization energy, and electron affinity, the normal target accuracy is within 1.0 kcal/mol and bond lengths within 0.01 Å of high quality experimental results for typical chemically bonded main-group molecules. However, this level of accuracy may not be attainable when using some of the standard approximations such as the Born-Oppenheimer, frozen-core, and non-relativistic approximations.

Series of basis sets which allow energetic and structural properties to be extrapolated to the CBS limit are advantageous because they enable the decoupling of the error in the approximate method and incomplete basis. The correlation consistent basis sets have been used

throughout the remaining chapters because the systematic nature of these sets provides a means to extrapolate computed energies and other properties to the CBS limit.[19] The uniqueness of this family of basis sets stems from their construction – basis functions that contribute similar amounts of correlation energy are grouped together, and these groups of functions are added to the basis set to form successively larger sets as shown in Fig. 2.1. This approach allows for systematically constructed basis sets rather than a somewhat arbitrary addition of basis functions. Therefore, beyond the minimal HF set of functions (*s*, *p*), additional *s* and *p* functions are added together with higher angular momentum functions, also known as polarization functions (*d, f, g, h*) to form the cc-pV*n*Z series of basis sets (where *n*=D(2), T(3), Q(4), 5), namely, the correlation consistent polarized valence *n*-ζ ("zeta") sets. These sets were designed for calculations which include only valence electrons in the correlation space. Throughout the present work, the cc-pV*n*Z correlation consistent series of basis sets will be referred to as the "standard sets". Augmenting the standard sets with a set of low-exponent diffuse functions led to the aug-cc-pV*n*Z sets,[4] which have been proven useful in the study of anionic species and van der Waals-type complexes – species where accounting for or describing more diffuse electron-electron interactions is critical.[13,14,60]

The CBS limit enables the direct comparison of the performance of methodologies, as the error arising from the use of an incomplete basis set has been eliminated at this limit. Furthermore, at the CBS limit the errors intrinsic to the method can be realized by comparison with well-established, reliable experimental data. When the types of errors associated with the approximate methods are fully understood, then the development of more efficient and accurate methods can be accomplished.

Figure 2.1. Pictorial representation of the single (S) double (D) and triple (T) excitations that are included in methods like CCSD(T).

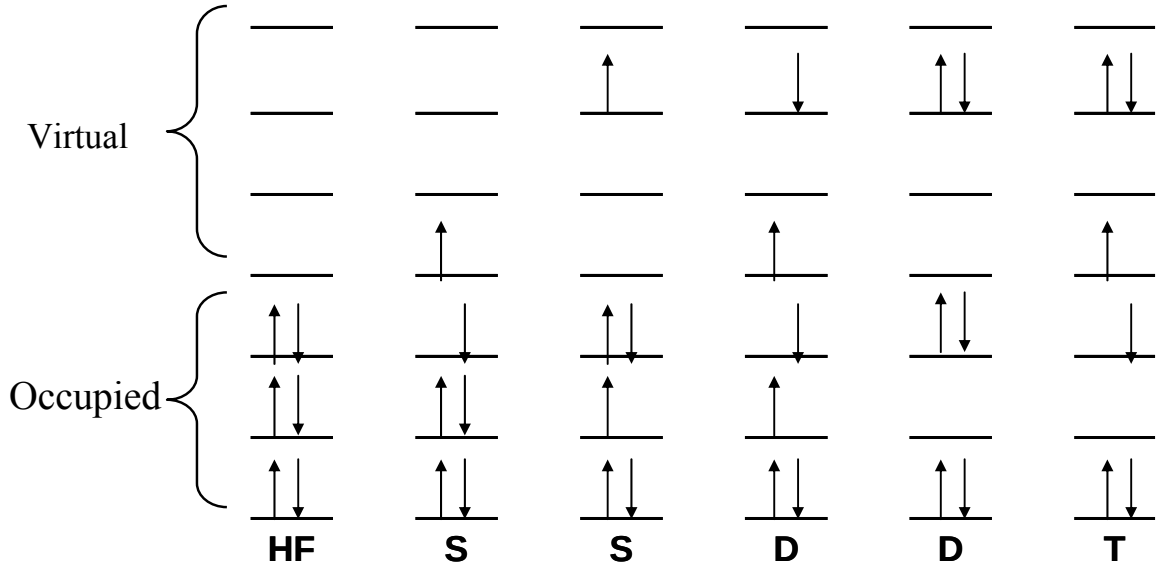

Figure 2.2. Pictorial diagram showing the groups of functions that are added to the HF orbitals to make successively larger cc-pV*n*Z basis sets.

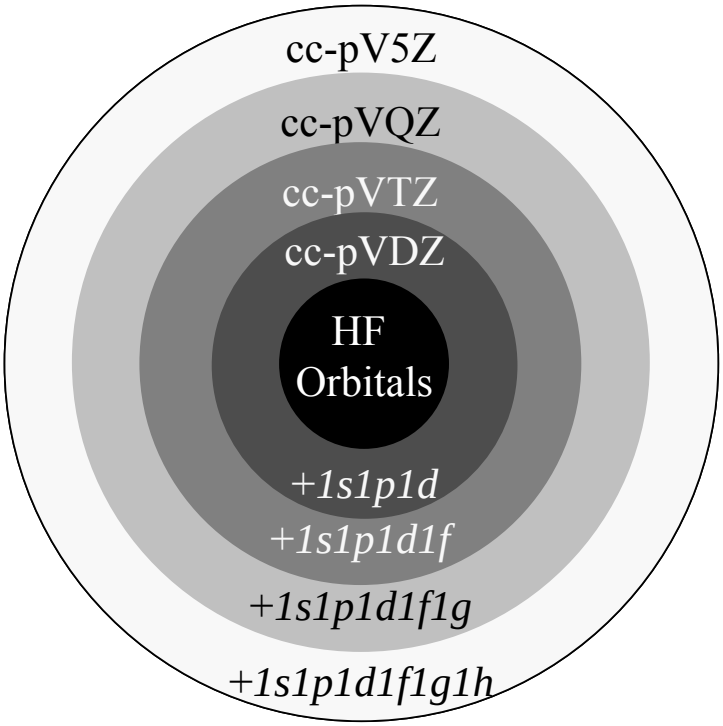

CHAPTER 3

PERFORMANCE OF THE CORRELATION CONSISTENT BASIS SETS FOR THIRD-ROW ATOMS Ga-Kr: A COMPARISON OF ADVANCED *AB INITIO* AND DENSITY FUNCTIONAL THEORY[§]

3.1. Introduction

Over the last few decades, there has been growing interest in the thermochemical and energetic properties of third-row (Ga-Kr) molecules. This is due to their importance in areas such as semiconductor, organometallic, and atmospheric chemistry. To illustrate, AsH_3 is important in the fabrication of GaAs, which is used in the semiconductor industry; HOBr is believed to have a role in ozone depletion; and germanium species are important in chemical vapor deposition mechanisms leading to the formation of films for new ceramic materials.

The increased interest in molecules containing third-row atoms has resulted in a need for reliable structural and energetic properties for these systems. One way to predict these properties is through the use of quantum chemical electronic structure methods, which have the ability to compute chemical and structural properties that rival the accuracy of the best laboratory experiments. Reliance upon computational methods can only be established after sufficient benchmark calculations are performed on a wide test suite of molecules for which well-established experimental data are available. Benchmarking of methods is critical, particularly

[§] This chapter has been adapted from the publication of *J. Chem. Phys.*, Vol. 121, Scott Yockel, B. Mintz and Angela K. Wilson, "Accurate energetics of small molecules containing third-row atoms Ga—Kr: A comparison of advanced *ab initio* and density functional theory", Pages 60-77, Copyright (2004), with permission from American Institute of Physics.

when studying molecular properties of species for which little or no experimental data are available, as only the historical performance of the method can be used to validate new findings. Further, because there are a large number of computational chemistry approaches available, understanding the typical accuracy and limitations of these methods is crucial.

For first- and second-row atoms, there have been a large number of benchmark studies demonstrating the effectiveness of specific theoretical treatments in the description of electronic structure. Examples include the correlation consistent benchmark series by Dunning, *et al.*;[5-7,10,14] the G1, G2, and G3 studies by Pople, *et al.*;[61-63] the CBS-*n* work by Petersson, *et al.*;[64,65] and the ccCA method of Wilson *et al.*[66,67] Other than employing the Gaussian-*n* and CBS-*n* methods, there have been very few other extended studies that compute the chemical properties of molecules containing third-row atoms, especially studies which use the correlation consistent basis sets.[68-73]

The correlation consistent basis sets of Dunning and co-workers[1,2,4] are unique among basis sets, as discussed in Chapter 2, in that their systematic construction has provided the means to decouple errors arising from basis set and method. Thus, determining the *inherent accuracy* of correlated electronic structure methods can be studied at the complete basis set (CBS) limit, where basis saturation has been reached. The systematic convergence behavior of energetics and other properties resulting from the use of a series of sets enables determination of the CBS limit, or Kohn-Sham (KS) limit as in the case of density functional theory. While at the CBS limit, understanding of the true performance of electron correlation methods can be ascertained in the calculation of molecular properties and energetics without relying upon embedded empirical parameters to achieve accuracy (as is the case in composite approaches such as G2 and G3).

In this chapter, the performance of the correlation consistent basis sets[3] has been investigated for third-row atoms with the *ab initio* method, CCSD(T). Additionally benchmark calculations have been done in collaboration with undergraduate Benjamin Mintz, using B3LYP, a density functional method. The CCSD(T) method was selected due to its well-established reliability in accurate molecular property prediction, (*e.g.* ± 1.0 kcal/mol for energies and ± 0.01 Å for bond lengths from firmly-established experimental values). On the other hand, B3LYP was chosen due to its success in structural prediction, and usefulness in thousands of studies, in part, due to its low computational cost in comparison to CCSD(T). Chemical and structural properties were computed for a set of third-row molecules from the Gaussian-2 (G2) extended test set. This G2 test set represents a collection of accurate experimental data including nineteen atomization energies, fifteen ionization potentials, four electron affinities, and two proton affinities. For these third-row systems, the optimized structures, atomization energies, ionization energies, electron affinities, and proton affinities were determined for each method and level of basis set. Additionally, several schemes were utilized to extrapolate the computed energies and bond lengths to the CBS and KS limits,. These schemes were compared to each other and contrasted to the energies obtained from the composite G2 and G3 methods.

Thousands of studies have been done using the family of correlation consistent basis sets for first row (B-Ne) and second row (Al-Ar) atoms, resulting in some of the most accurate theoretical predictions to date for a wide range of molecules and their molecular properties and energetics. There have been several recent studies such as those by Peterson, *et al.*,[74-77] and Schaefer, *et al.*[78-81] that have used the correlation consistent basis sets to investigate novel third-row compounds. It is anticipated that the third-row basis sets will see similar usefulness as the first and second row basis set families have already, once the reliability of the sets has been

further established through extended studies such as in this chapter, and the standard diatomic benchmarks of Wilson and Dunning.[82]

3.2. Methodology

In this study, the *ab initio* coupled cluster method, CCSD(T), [50-52] was used. This method includes single, double, and quasiperturbative excitations to the reference HF wavefunction and scales as N^7. (As discussed in Chapter 2, N= number of basis functions.) Additionally, B3LYP density functional method was chosen for comparison, due in part to its wide spread use and success in the prediction of chemical properties of many first- and second-row atoms.[83,84] This method is comprised of Becke's three-parameter hybrid exchange functional (B3)[56] coupled with Lee, Yang, and Parr's (LYP)[57] correlation functional, and scales as N^3. In both cases, the basis sets employed were the standard and augmented correlation consistent basis sets. All CCSD(T) calculations have been performed with the MOLPRO[85] chemistry software package, and all B3LYP calculations were done with GAUSSIAN98[86] software package. The default numerical grid (75, 302) in GAUSSIAN98 was used to evaluate the density functional theory integrals. This grid includes 75 radial shells and 302 angular points per shell, resulting in approximately 7000 quadrature points per atom. In general, this grid is known to provide energies accurate to five places past the decimal.

Optimized structures and frequencies were obtained for both CCSD(T) and B3LYP with each basis set. Zero point energy (ZPE) corrections were applied to the total energy for each molecule, since the total energies are measured at the bottom of the potential well, and experimental values are measured at the first vibrational levels. Additionally, spin-orbit corrections were made to the total energy of the atoms and molecules in this test suite. Spin-

orbit correction are needed because the spin (S) and angular momentum (L) quantum numbers couple and cause the degenerate orbitals to split, which causes a lowering in the total energy. Spin-orbit corrections were not computed in this study for third-row systems, and instead was taken from previous studies so that direct comparisons in computational methods could be made.[87,88] For third-row atoms and molecules, spin orbit corrections have been obtained from Blaudeau and Curtiss configuration interaction calculations,[88] just as in G2 and G3 theory for third-row systems, which have only a 0.10 millihartree mean absolute deviation from experiment. For systems containing second row atoms, the corrections were determined using the Moore Tables.[87] As the magnitude of the spin orbit effect on first row atoms is below one millihartree, it was not included.[87] It must be noted that in G2 and G3 theory, the 3*d* orbitals were included in the valence space during the frozen-core computations. However, in this study frozen-core calculations were done without inclusion of the *3d* orbitals in the valence space, since the basis functions in the cc-pV*n*Z sets were optimized with only the 4*s* and 4*p* in the valence space.

Several approaches have been used to establish complete basis set (CBS) and Kohn-Sham (KS) limits. The first approach, which is quite simple to implement, requires values from only two basis set levels (ζ-levels) such as cc-pVDZ and cc-pVTZ and was developed by Halkier *et al.*[89]

$$E_{\infty} = \frac{E_X X^3 - E_Y Y^3}{X^3 - Y^3} \qquad (3.1)$$

In Eqn. 3.1, E_X and E_Y represent the molecular property at two ζ-levels, "X" and "Y", while the X and Y are the cardinal number for the ζ-level. Within the context of this work, the notation of the two-point extrapolation will be $CBS_{X\text{-}Y}$ representing the two ζ-levels involved in the extrapolation. The second approach used is the Feller exponential extrapolation,[19]

$$D_e(n) = D_e(\infty) + Ae^{-Bn} \quad (3.2)$$

where *A* and *B* are parameters determined in a nonlinear fit. This exponential extrapolation was implemented in two ways. In the first implementation, a given property was extrapolated as in Eqn. 3.2 – denoted as the "CBS_{prop}" exponential extrapolation. In the second formulation of the Feller scheme, extrapolations were done using the total energies for both the atoms and the molecule, rather than directly using the dissociation energies.

$$E(n) = E(\infty) + Ae^{-Bn} \quad (3.3)$$

Once the CBS, or KS limits were determined for the total energies of the atoms and molecules, the dissociation energy was then obtained from this data - denoted as the "CBS_{total}" exponential extrapolation. In total, five different CBS limit extrapolations were performed.

3.3. Results and Discussion

3.3.1. Equilibrium Geometries

Optimized bond lengths and bond angles are reported in Table 3.1 for B3LYP and CCSD(T) for each level of basis set. Overall, the bond lengths and angles are in good agreement with experiment, with most calculated bond lengths within 0.01 Å, and most calculated bond angles within 1° of experiment at the quintuple-ζ basis set level. There are several notable exceptions such as GeH_4, where CCSD(T)/aug-cc-pVQZ predicts a Ge–H bond length of 1.541 Å, and the experiment observe a bond length of 1.514 Å. Other theoretical prediction are in agreement with the Ge–H bond lengths predicted in this study, and for example the G2 computed bond length of GeH_4 was 1.543 Å.[69] Both B3LYP and CCSD(T) methods provide similar geometries in most cases. There are a few exceptions where predicted bond lengths are nearer to

experiment with CCSD(T) than with B3LYP at the quintuple-ζ basis set level, including BrF (0.01 Å), BrCl (0.02 Å), and Br_2 (0.03 Å). In general, both B3LYP and CCSD(T) produce bond lengths that slightly overestimate those from experiment.

The CCSD(T) calculated bond lengths for GaCl and NaBr have the largest disagreement (~0.05 Å) with experiment. As illustrated by Hofmann *et al.*[90] and Petrie,[91] the inclusion of the inner valence 2*s* and 2*p* orbitals for Na in the correlation space for coupled cluster calculations is important when Na is bonded to a highly electronegative species such as F. Similarly, Radom and Duke[71] have included 3*d* orbitals in their correlation space for third-row electropositive elements which are bonded to electronegative atoms. For example, in their investigation of GaO they noted significant orbital mixing between the oxygen 2*s* and gallium 3*d* orbitals. For such compounds, neglect of this orbital mixing as in the standard frozen-core approximation, leads to an appreciable amount of error and is thought to be the reason for the larger differences in bond length between theory and experiment for GaCl.

The bond angles obtained from CCSD(T) are slightly closer to experiment than those obtained from B3LYP. The maximum deviation in angle from experiment for CCSD(T) occurs for HOBr which deviates by 1.0°. For B3LYP, the largest differences observed are for HOBr (1.6°) and CH_3Br (1.2°).

As shown in Table 3.2, the mean absolute deviation in the bond length from experiment is very similar for B3LYP (0.012 Å for both cc-pV5Z and aug-cc-pV5Z) and for CCSD(T) (0.014 Å for cc-pV5Z and 0.011 Å for aug-cc-pV5Z). These deviations are reduced slightly (~0.001 Å) by using a two-point extrapolation scheme based upon geometries obtained at the quadruple- and quintuple-ζ basis set levels (KS_{Q-5} and CBS_{Q-5}). However, the mean absolute deviation of 0.010 Å reported for CCSD(T)/aug-cc-pV5Z does not include results for GeH_4 and

CH_3Br, as optimizations were not performed at this level due to their computational requirements and nearness to a converged geometry as indicated by optimized structures obtained using lower level basis sets.

Table 3.1. Optimized geometries from B3LYP and CCSD(T) computations with the correlation consistent basis sets. Bond length (r) is reported in Å and angle (a) is in °.

	Basis Set	B3LYP		CCSD(T)		Expt.[a]
		cc-pV*n*Z	aug-cc-pV*n*Z	cc-pV*n*Z	aug-cc-pV*n*Z	
GeH_4						
r	*n*=D	1.542	1.541	1.543	1.546	1.514[b]
	T	1.534	1.534	1.542	1.542	
	Q	1.533	1.533	1.541	1.541	
	5[c]	1.533	1.533	1.541		
AsH						
r	D	1.545	1.543	1.542	1.544	1.535
	T	1.536	1.535	1.535	1.536	
	Q	1.534	1.534	1.533	1.534	
	5	1.534	1.534	1.533	1.534	
AsH^+						
r	D	1.547	1.547	1.538	1.541	
	T	1.539	1.539	1.534	1.535	
	Q	1.537	1.537	1.533	1.534	
	5	1.537	1.537	1.534	1.534	
AsH_2						
r	D	1.539	1.538	1.534	1.537	1.518[d]
	T	1.530	1.530	1.529	1.530	
	Q	1.528	1.528	1.528	1.528	
	5	1.528	1.528	1.528	1.528	
a	D	90.7	90.9	91.1	90.9	90.7[d]
	T	90.9	90.9	91.2	91.0	
	Q	90.9	90.9	91.1	91.1	
	5	91.0	91.0	91.2	91.1	
AsH_2^+						
r	D	1.541	1.542	1.532	1.536	
	T	1.533	1.533	1.529	1.530	
	Q	1.532	1.532	1.528	1.529	
	5	1.532	1.532	1.528	1.529	
a	D	91.0	90.9	91.9	91.6	
	T	90.9	90.9	91.8	91.7	
	Q	91.0	91.0	91.8	91.7	
	5	91.0	91.0	91.8	91.7	

(table continues on next page)

(Table 3.1 continued)

	Basis Set	B3LYP		CCSD(T)		Expt.[a]
		cc-pV*n*Z	aug-cc-pV*n*Z	cc-pV*n*Z	aug-cc-pV*n*Z	
AsH_3						
r	D	1.534	1.533	1.529	1.532	1.511[d]
	T	1.525	1.525	1.524	1.525	
	Q	1.523	1.523	1.523	1.524	
	5	1.523	1.523	1.523	1.524	
a	D	91.9	92.0	92.5	92.4	92.1[d]
	T	92.1	92.2	92.6	92.4	
	Q	92.2	92.2	92.5	92.5	
	5	92.2	92.2	92.5	92.6	
SeH						
r	D	1.484	1.483	1.478	1.481	1.475
	T	1.476	1.475	1.473	1.474	
	Q	1.474	1.474	1.472	1.473	
	5	1.474	1.474	1.472	1.472	
SeH^+						
r	D	1.503	1.504	1.496	1.499	
	T	1.496	1.496	1.491	1.492	
	Q	1.496	1.495	1.490	1.491	
	5	1.494	1.494	1.472	1.491	
SeH^-						
r	D	1.493	1.486	1.487	1.486	
	T	1.481	1.478	1.478	1.479	
	Q	1.479	1.477	1.477	1.478	
	5	1.477	1.477	1.477	1.468	
SeH_2						
r	D	1.479	1.479	1.473	1.476	1.460[d]
	T	1.471	1.471	1.468	1.469	
	Q	1.470	1.470	1.468	1.468	
	5	1.469	1.469	1.468	1.468	
a	D	91.1	91.2	91.3	91.3	90.6[d]
	T	91.3	91.3	91.3	91.1	
	Q	91.3	91.3	91.3	91.3	
	5	91.3	91.3	91.3	91.3	
SeH_2^+						
r	D	1.497	1.497	1.488	1.492	
	T	1.489	1.489	1.484	1.486	
	Q	1.488	1.488	1.484	1.484	
	5	1.488	1.488	1.484	1.484	

(table continues on next page)

(Table 3.1 continued)

	Basis Set	B3LYP		CCSD(T)		Expt.[a]
		cc-pV*n*Z	aug-cc-pV*n*Z	cc-pV*n*Z	aug-cc-pV*n*Z	
a	D	91.7	91.5	92.0	91.7	
	T	91.6	91.6	91.8	91.7	
	Q	91.6	91.6	91.8	91.8	
	5	91.6	91.6	91.8	91.8	
HBr						
r	D	1.433	1.432	1.426	1.429	1.414
	T	1.425	1.424	1.420	1.421	
	Q	1.424	1.424	1.420	1.421	
	5	1.423	1.423	1.421	1.421	
HBr^+						
r	D	1.468	1.469	1.457	1.460	1.448
	T	1.460	1.460	1.452	1.453	
	Q	1.459	1.459	1.452	1.453	
	5	1.459	1.459	1.453	1.453	
GaCl						
r	D	2.260	2.271	2.249	2.281	2.202
	T	2.243	2.246	2.255	2.265	
	Q	2.242	2.242	2.257	2.261	
	5	2.240	2.240	2.257	2.259	
GeO						
r	D	1.644	1.648	1.665	1.671	1.625
	T	1.630	1.632	1.649	1.653	
	Q	1.629	1.629	1.649	1.650	
	5	1.629	1.629	1.648	1.648	
As_2						
r	D	2.112	2.113	2.147	2.151	2.103
	T	2.105	2.105	2.135	2.135	
	Q	2.105	2.104	2.128	2.129	
	5	2.104	2.104	2.126	2.126	
GeS_2						
r	D	2.026	2.027	2.033	2.040	
	T	2.014	2.014	2.023	2.024	
	Q	2.011	2.010	2.016	2.017	
	5	2.010	2.010	2.013	2.014	
KrF_2						
r	D	1.921	1.911	2.012	1.921	1.875[d]
	T	1.891	1.893	1.885	1.886	
	Q	1.889	1.890	1.875	1.876	
	5	1.890	1.890	1.873	1.873	

(table continues on next page)

(Table 3.1 continued)

	Basis Set	B3LYP		CCSD(T)		Expt.[a]
		cc-pV*n*Z	aug-cc-pV*n*Z	cc-pV*n*Z	aug-cc-pV*n*Z	
BrCl						
r	D	2.194	2.191	2.200	2.205	2.136
	T	2.170	2.170	2.163	2.164	
	Q	2.166	2.166	2.150	2.151	
	5	2.163	2.163	2.144	2.144	
BrF						
r	D	1.804	1.796	1.819	1.801	1.759
	T	1.774	1.775	1.769	1.770	
	Q	1.771	1.772	1.762	1.762	
	5	1.771	1.771	1.760	1.760	
BrF^+						
r	D	1.726	1.717	1.740	1.724	
	T	1.691	1.692	1.686	1.688	
	Q	1.689	1.689	1.680	1.681	
	5	1.688	1.688	1.678	1.678	
BrO						
r	D	1.771	1.755	1.795	1.773	1.717
	T	1.732	1.729	1.735	1.731	
	Q	1.727	1.725	1.725	1.723	
	5	1.725	1.724	1.721	1.721	
BrO^-						
r	D	1.899	1.854	1.915	1.868	1.814[e]
	T	1.839	1.823	1.832	1.821	
	Q	1.826	1.819	1.817	1.812	
	5	1.822	1.817	1.811	1.809	
HOBr						
$r_{(Br-O)}$	D	1.873	1.864	1.888	1.874	1.834[f]
	T	1.844	1.844	1.840	1.840	
	Q	1.841	1.841	1.833	1.832	
	5	1.840	1.840	1.830	1.829	
$r_{(H-O)}$	D	0.975	0.971	0.974	0.973	0.961[f]
	T	0.966	0.967	0.965	0.967	
	Q	0.965	0.965	0.964	0.965	
	5	0.965	0.965	0.964	0.964	
a	D	101.7	103.4	100.8	102.7	102.3[f]
	T	103.2	103.7	102.3	103.1	
	Q	103.6	103.8	102.9	103.3	
	5	103.8	103.8	103.2	103.3	

(table continues on next page)

(Table 3.1 continued)

	Basis Set	B3LYP		CCSD(T)		Expt.[a]
		cc-pV*n*Z	aug-cc-pV*n*Z	cc-pV*n*Z	aug-cc-pV*n*Z	
$HOBr^+$						
$r_{(Br-O)}$	D	1.763	1.758	1.770	1.765	
	T	1.735	1.736	1.729	1.731	
	Q	1.733	1.733	1.724	1.724	
	5	1.732	1.732	1.721	1.721	
$r_{(H-O)}$	D	0.996	0.991	0.993	0.991	
	T	0.986	0.986	0.984	0.985	
	Q	0.985	0.985	0.983	0.983	
	5	0.985	0.985	0.983	0.983	
a	D	108.9	109.4	107.6	108.2	
	T	109.8	109.9	108.4	108.8	
	Q	110.0	110.0	108.8	109.0	
	5	110.0	110.0	109.1	109.1	
Br_2						
r	D	2.335	2.335	2.346	2.353	2.281
	T	2.315	2.316	2.311	2.313	
	Q	2.314	2.315	2.298	2.299	
	5	2.314	2.314	2.294	2.294	
Br_2^+						
r	D	2.240	2.242	2.252	2.259	
	T	2.222	2.224	2.220	2.223	
	Q	2.220	2.221	2.210	2.210	
	5	2.220	2.220	2.210	2.206	
BBr						
r	D	1.916	1.913	1.920	1.927	1.888
	T	1.903	1.901	1.906	1.907	
	Q	1.901	1.900	1.904	1.904	
	5	1.900	1.900	1.903	1.903	
NaBr						
r	D	2.519	2.526	2.554	2.580	2.502
	T	2.527	2.527	2.558	2.563	
	Q	2.522	2.523	2.556	2.558	
	5[g]	2.520		2.551		
$NaBr^+$						
r	D	2.979	2.979	3.046	3.028	
	T	2.928	2.926	2.983	2.997	
	Q	2.922	2.920	2.988	2.992	
	5	2.914		2.988		

(table continues on next page)

(Table 3.1 continued)

	Basis Set	B3LYP		CCSD(T)		Expt.[a]
		cc-pV*n*Z	aug-cc-pV*n*Z	cc-pV*n*Z	aug-cc-pV*n*Z	
CH_3Br						
$r_{(C-H)}$	D	1.097	1.093	1.084	1.099	1.082[h]
	T	1.084	1.084	1.085	1.086	
	Q	1.083	1.083	1.084	1.084	
	5[c]	1.083	1.083			
$r_{(C-Br)}$	D	1.957	1.960	1.947	1.963	1.934[h]
	T	1.954	1.954	1.948	1.948	
	Q	1.952	1.952	1.944	1.944	
	5[c]	1.952	1.952			
$a_{(H-C-H)}$	D	109.9	110.0	111.2	111.1	111.2[h]
	T	110.0	110.0	111.0	111.2	
	Q	110.0	110.0	111.1	111.1	
	5[c]	110.0	110.0			
CH_4Br^+						
$r_{(C-H)}$	D	1.097	1.094	1.099	1.098	
	T	1.085	1.085	1.084	1.085	
	Q[c]	1.084	1.084	1.086		
	5[c]	1.084	1.084			
$r_{(C-Br)}$	D	2.003	2.008	2.018	2.024	
	T	1.995	1.995	1.998	1.998	
	Q[c]	1.993	1.993	1.993		
	5[c]	1.992	1.992			
$r_{(Br-H)}$	D	1.452	1.451	1.443	1.446	
	T	1.444	1.444	1.438	1.439	
	Q[c]	1.443	1.443	1.439		
	5[c]	1.443	1.443			
$a_{(H-C-H)}$	D	109.6	109.7	113.5	113.6	
	T	109.6	109.6	113.3	113.4	
	Q[c]	109.6	109.6	113.3		
	5[c]	109.6	109.6			
$a_{(H-Br-C)}$	D	97.3	97.3	96.9	102.0	
	T	97.3	97.3	102.4	102.3	
	Q[c]	97.3	97.3	97.1		
	5[c]	97.3	97.3			

[a] From Ref. 92 unless otherwise noted.

[b] From Ref. 93.
[c] Due to computational requirements, optimization was not performed for all levels of the quadruple- and quintuple-ζ basis sets, particularly as the structural parameters are near convergence at the next lower-level basis set.
[d] From Ref. 94.
[e] From Ref. 95.
[f] From Ref. 96.
[g] No aug-cc-pV5Z basis set is available for Na at the time of this study.
[h] From Ref. 97.

Table 3.2. Mean absolute deviation of bond length (Å) and angle (º) from experiment. The two-point extrapolation scheme as presented in Eqn 3.1 has been used to determine the KS and CBS limits for the B3LYP and CCSD(T) bond lengths, respectively.

	Bond length (Å)				Angle (º)			
	B3LYP		CCSD(T)		B3LYP		CCSD(T)	
Basis Set	cc-pV*n*Z	aug-cc-pV*n*Z	cc-pVnZ	aug-cc-pV*n*Z	cc-pV*n*Z	aug-cc-pV*n*Z	cc-pVnZ	aug-cc-pV*n*Z
n = D	0.028	0.027	0.037	0.037	0.44	0.52	0.50	0.29
T	0.015	0.015	0.017	0.018	0.50	0.60	0.32	0.34
Q	0.013	0.013	0.014	0.014	0.60	0.64	0.39	0.42
5	0.012	0.012	0.014	0.011	0.65	0.66	0.50	0.64
KS/CBS Limit								
D-T[a]	0.010	0.010	0.016	0.013				
T-Q[a]	0.012	0.012	0.013	0.013				
Q-5[a]	0.011	0.011	0.013	0.010				

[a] The "D-T" scheme uses double- and triple-ζ results in the extrapolation; the "T-Q" scheme uses triple- and quadruple-ζ results; and the "Q-5" scheme uses quadruple- and quintuple-ζ results.

3.3.2. Atomization Energies

Atomization energies calculated with CCSD(T) and B3LYP for all of the G2 third-row test suite molecules are given in Table 3.3. Atomization energies calculated with CCSD(T) in combination with either the standard or augmented family of correlation consistent basis sets give smooth convergence behavior to the CBS limit for the energies, as is expected from these families of basis sets.[7,20,21,24] However, the convergence pattern for B3LYP in combination with

the series of basis sets was not smooth for all molecules, as there were some cases in which the cc-pVQZ results appeared to be either too high, or too low for smooth convergence to a limit. Examples include GeH_4, where there is a slight dip upon increasing the basis set from cc-pVQZ to cc-pV5Z, and SeH, where there is a slight dip upon increasing the basis set from cc-pVTZ to cc-pVQZ. Such dips are not observed when diffuse functions are included in the basis set. This unusual behavior has been investigated and further discussed by Wang and Wilson.[98-100] At the bottom of Table 2.3, the mean absolute deviation at each of the basis set levels has been computed, and it is apparent how little the deviation of B3LYP depends on the basis set in comparison to CCSD(T). For this test suite the mean absolute deviations for B3LYP are nearly converged at the triple-ζ level at ~3 kcal/mol. Also, at the double-ζ level there is a dramatic improvement in the atomization energy when using the augmented basis set, and overall the mean absolute deviations are diminished upon augmenting the basis sets.

The KS and CBS limits determined by several different methods – using three two-point extrapolations CBS_{D-T}, CBS_{T-Q}, CBS_{Q-5} and two exponential extrapolations CBS_{prop} and CBS_{total} – are provided in Table 3.4. Also included in Table 3.4 are the G2 and G3 energies obtained from earlier work, providing a comparison with the current results. It must be noted that the reported G2 results included spin orbit corrections for third-row atoms only while the reported G3 results included spin orbit corrections for all atoms. The present results contain corrections for spin orbit coupling only for second and third-row atoms.

The CBS_{T-Q} two-point extrapolation with the standard correlation consistent basis sets performed the best when compared with the other extrapolation schemes. However, for both the standard and the augmented correlation consistent basis set families, using this CBS_{T-Q} extrapolation scheme generates atomization energies that differ by more than 2.00 kcal/mol from

experiment for three molecules (GeH_4, GeS_2, and BBr). In comparing the exponential extrapolations for the 19 atomization energies, there are eight cases where the CBS_{prop} differs from the CBS_{total} by more than 1.00 kcal/mol for both the cc-pV*n*Z and aug-cc-pV*n*Z series. In every case, the CBS_{prop} value is greater than the CBS_{total} value. The greatest difference in these two extrapolations is from GeS_2, in which they differ by 3.15 kcal/mol. For this case, the CBS_{total} is much closer to experiment. The maximum deviation for the cc-pV*n*Z exponential CBS_{prop} limit is 2.92 kcal/mol from GeS_2, while the maximum deviation for the aug-cc-pV*n*Z exponential CBS_{prop} limit is 3.68 kcal/mol for GeH_4. As noted by Curtiss *et al.*,[68] the large deviation between the theoretically and experimentally based atomization energy for GeH_4, suggests that further experimental measurements of the enthalpy of formation for this species are needed, particularly as there has only been one such experiment to date.[101,102] However, as shown in Table 2.4, CCSD(T)/cc-pV*n*Z and the CBS_{total} extrapolation for GeH_4 is only 1.59 kcal/mol over the experimental value of 270.5 kcal/mol - just slightly outside of the experimental error bar of ±0.9 kcal/mol. The large deviation for BBr could be due to the fact that the atomization energy derived from experiment (103.5 kcal/mol) likely contains significant error, as discussed in earlier work.[103]

In Table 3.4 for B3LYP, there are several molecules that have errors of approximately 4.00 kcal/mol or larger, for both families of correlation consistent basis sets using the $KS_{Q\text{-}5}$ extrapolations. These molecules include AsH_2, AsH_3, GeS_2, BBr, KrF_2, and NaBr for standard sets and AsH_2, AsH_3, GeS_2, BBr, and KrF_2 for the augmented sets. The largest deviation in atomization energy for $KS_{Q\text{-}5}$ is for GeS_2 (6.49 kcal/mol), obtained using the standard correlation consistent basis sets. The B3LYP/aug-cc-pV*n*Z results in only four molecules with atomization energies within chemical accuracy (±1.00 kcal/mol). In comparison to Table 3.4, the

G2(B3LYP)[70] method has no atomization energies within chemical accuracy and there are eight molecules which have energy deviations greater than 3.0 kcal/mol from experiment. The inconsistencies of B3LYP in predicting accurate atomization energy for third-row molecules prohibits certitude when studying thermochemical properties for third-row systems that may have little or no experimental data.

Table 3.3. Atomization energies in kcal/mol computed with B3LYP and CCSD(T) and the correlation consistent basis sets.

	B3LYP		CCSD(T)		Expt.
	cc-pV*n*Z	aug-cc-pV*n*Z	cc-pV*n*Z	aug-cc-pV*n*Z	
$GeH_4 \rightarrow Ge + 4H$					
n=D	268.93	268.10	255.26	257.10	270.5[a]
T	272.21	272.41	267.45	268.75	
Q	273.21	273.38	271.27	272.86	
5	272.62	273.58	272.10	273.48	
$AsH \rightarrow As + H$					
D	66.10	66.03	53.05	56.99	64.6[b]
T	67.15	67.17	60.24	61.68	
Q	67.30	67.35	62.37	62.89	
5	67.33	67.37	62.96	63.21	
$AsH_2 \rightarrow As + 2H$					
D	134.85	134.62	118.27	121.02	131.1[b]
T	136.81	136.81	127.26	127.92	
Q	137.09	137.17	130.33	130.58	
5	137.13	137.20	131.19	131.17	
$AsH_3 \rightarrow As + 3H$					
D	206.66	206.15	183.79	189.42	206.0[b]
T	209.23	209.18	198.88	200.70	
Q	209.59	209.70	203.03	203.04	
5	209.63	209.73	204.16	203.84	
$SeH \rightarrow Se + H$					
D	74.56	75.18	67.47	68.79	74.3[c]
T	75.98	76.07	71.90	72.22	
Q	75.92	76.20	73.64	73.94	
5	76.24	76.30	74.11	74.27	
$SeH_2 \rightarrow Se + 2H$					
D	150.08	150.83	138.16	142.19	153.2[c]
T	152.30	152.40	146.74	148.34	
Q	152.36	152.65	150.34	151.18	
5	152.72	152.83	151.18	151.77	

(table continues on next page)

(Table 3.3 continued)

	B3LYP		CCSD(T)		Expt.
	cc-pV*n*Z	aug-cc-pV*n*Z	cc-pV*n*Z	aug-cc-pV*n*Z	
$HBr \rightarrow Br + H$					
D	83.42	84.30	79.34	81.73	86.5[d]
T	84.85	84.99	83.72	84.68	
Q	85.02	85.07	85.45	85.78	
5	85.10	85.17	85.91	86.10	
$GeO \rightarrow Ge + O$					
D	145.52	147.93	133.94	141.68	155.2[d]
T	152.28	152.90	148.12	150.78	
Q	153.66	153.73	152.73	153.98	
5	153.20	154.12	154.42	154.96	
$GeS_2 \rightarrow Ge + 2S$					
D	179.10	178.91	161.64	166.18	191.7[e]
T	183.56	183.97	180.00	182.19	
Q	184.88	184.92	188.22	189.37	
5	185.04	185.84	191.74	192.27	
$As_2 \rightarrow 2As$					
D	89.72	89.80	68.90	71.57	91.3[f]
T	92.07	92.22	80.67	82.40	
Q	92.24	92.41	85.99	86.91	
5	92.48	92.56	88.11	88.56	
$BrCl \rightarrow Br + Cl$					
D	43.88	44.25	35.46	38.43	51.5[d]
T	47.04	47.21	44.92	46.43	
Q	47.69	47.75	48.58	49.33	
5	48.10	48.38	50.28	50.67	
$BrF \rightarrow Br + F$					
D	52.05	55.82	40.75	51.79	58.9[d]
T	56.89	57.75	52.40	56.32	
Q	58.23	58.34	56.91	58.45	
5	58.33	58.44	58.40	59.04	
$BrO \rightarrow Br + O$					
D	50.67	54.21	34.62	44.21	55.3[d]
T	56.40	57.25	47.65	51.05	
Q	57.58	57.80	51.78	53.21	
5	57.80	57.92	53.40	54.00	
$BrB \rightarrow Br + B$					
D	97.08	96.88	92.56	93.07	103.5[f]
T	97.33	97.45	96.61	97.16	
Q	97.47	97.60	98.80	99.13	
5	97.59	97.65	99.63	99.80	

(table continues on next page)

(Table 3.3 continued)

	B3LYP		CCSD(T)		Expt.
	cc-pV*n*Z	aug-cc-pV*n*Z	cc-pV*n*Z	aug-cc-pV*n*Z	
$Br_2 \rightarrow 2Br$					
D	39.30	38.96	31.07	33.09	45.4[d]
T	41.80	41.90	39.21	40.51	
Q	42.23	42.26	42.63	43.28	
5	42.41	42.47	43.95	44.31	
$CH_3Br \rightarrow Br + C + 3H$					
D	348.87	349.32	329.23	334.33	358.2[g]
T	355.14	354.96	348.13	350.78	
Q	355.61	355.56	353.70	354.64	
5	355.61	355.70	355.43	355.85	
$GaCl \rightarrow Ga + Cl$					
D	104.51	105.10	98.36	101.76	109.9[d]
T	105.98	106.11	104.49	105.72	
Q	106.16	106.81	107.35	107.95	
5	106.72	106.98	108.51	108.82	
$KrF_2 \rightarrow Kr + 2F$					
D	10.66	22.99	-12.72	11.71	21.9[d]
T	22.50	25.83	8.57	18.08	
Q	25.96	26.68	16.44	20.24	
5	26.48	26.70	19.40	20.76	
$NaBr \rightarrow Na + Br$					
D	77.41	78.54	75.74	80.44	86.2[f]
T	79.80	80.07	81.89	83.21	
Q	80.30	80.40	85.22	85.82	
5[h]	80.74		86.49		
Mean absolute deviation					
D	5.48	4.29	17.08	12.10	
T	3.19	3.28	6.62	4.55	
Q	3.18	3.20	2.73	1.98	
5	3.12	2.93	1.47	1.32	

[a] From Refs. 101,102.
[b] From Ref. 104.
[c] From Ref. 105.
[d] From Ref. 106.
[e] From Ref. 107.
[f] From Ref. 92.
[g] From Ref. 108.
[h] No Peterson or Dunning aug-cc-pV5Z basis set is available for Na.

Table 3.4. Extrapolated KS and CBS limits for atomization energies in kcal/mol determined using B3LYP and CCSD(T) in combination with cc-pV*n*Z and aug-cc-pV*n*Z.

KS/CBS limit	B3LYP		CCSD(T)		G2[a]	G3[b]	Expt.
	cc-pV*n*Z	aug-cc-pV*n*Z	cc-pV*n*Z	aug-cc-pV*n*Z			
$GeH_4 \rightarrow Ge + 4H$							
D – T[c]	273.59	274.22	272.58	273.65	275.8	273.0	270.5[d]
T – Q[c]	273.95	274.09	274.06	275.86			
Q – 5[c]	272.00	273.79	272.98	274.13			
Property[e]	272.93	273.65	272.64	274.18			
Total[f]	272.91	273.55	272.09	273.57			
$AsH \rightarrow As + H$							
D – T	67.59	67.64	63.27	63.66	63.2	64.7	64.6[g]
T – Q	67.41	67.49	63.92	63.77			
Q – 5	67.36	67.40	63.58	63.54			
Property	67.33	67.38	63.22	63.31			
Total	67.32	67.38	62.90	63.16			
$AsH_2 \rightarrow As + 2H$							
D – T	137.63	137.73	131.05	130.83	131.8	131.9	131.1[g]
T – Q	137.29	137.43	132.57	132.52			
Q – 5	137.17	137.24	132.08	131.78			
Property	137.13	137.22	131.70	131.71			
Total	137.10	137.20	131.16	131.17			
$AsH_3 \rightarrow As + 3H$							
D – T	210.31	210.45	203.98	205.45	205.6	204.6	206.0[g]
T – Q	209.85	210.07	206.05	204.74			
Q – 5	209.67	209.76	205.35	204.67			
Property	209.64	209.76	204.15	203.90			
Total	209.60	209.73	204.86	203.67			
$SeH \rightarrow Se + H$							
D – T	76.58	76.44	73.76	73.66	74.2	75.4	74.3[h]
T – Q	75.88	76.30	74.91	75.19			
Q – 5	76.57	76.41	74.60	74.62			
Property	76.10	76.29	74.49	74.78			
Total	76.09	76.26	74.18	74.37			

(table continues on next page)

(Table 3.4 continued)

KS/CBS limit	B3LYP		CCSD(T)		G2[a]	G3[b]	Expt.
	cc-pV*n*Z	aug-cc-pV*n*Z	cc-pV*n*Z	aug-cc-pV*n*Z			
$SeH_2 \rightarrow Se + 2H$							
D – T	153.23	153.06	150.35	150.93	152.1	152.3	153.2[h]
T – Q	152.41	152.84	152.97	153.26			
Q – 5	153.10	153.01	152.05	152.39			
Property	152.58	152.81	152.03	152.54			
Total	152.55	152.76	151.41	151.94			
$HBr \rightarrow Br + H$							
D – T	85.46	85.28	85.56	85.93	85.9	86.7	86.5[i]
T – Q	85.14	85.13	86.71	86.58			
Q – 5	85.19	85.28	86.39	86.44			
Property	85.08	85.15	86.29	86.32			
Total	85.07	85.12	86.05	86.16			
$GeO \rightarrow Ge + O$							
D – T	155.13	154.99	154.09	154.62	155.7	156.8	155.2[i]
T – Q	154.66	154.34	156.10	156.31			
Q – 5	152.71	154.52	156.19	155.99			
Property	153.48	154.09	155.16	155.54			
Total	153.04	153.66	153.29	153.87			
$GeS_2 \rightarrow Ge + 2S$							
D – T	185.44	186.11	187.73	188.93	193.9	193.6	191.7[j]
T – Q	185.84	185.61	194.22	194.60			
Q – 5	185.21	186.80	195.43	194.39			
Property	185.22	188.74	194.62	194.70			
Total	183.95	183.95	191.47	191.87			
$As_2 \rightarrow 2As$							
D – T	93.06	93.24	85.62	86.95	91.2	91.7	91.3[k]
T – Q	92.36	92.55	89.87	90.20			
Q – 5	92.74	92.72	90.34	90.29			
Property	92.40	92.51	89.92	89.80			
Total	92.39	92.51	87.90	88.37			
$BrCl \rightarrow Br + Cl$							
D – T	48.38	48.46	48.90	49.80	50.0	51.2	51.5[i]
T – Q	48.17	48.14	51.25	51.44			
Q – 5	48.53	49.03	52.06	52.07			
Property	48.10	48.35	51.28	51.35			
Total	47.38	47.63	50.04	50.28			

(table continues on next page)

(Table 3.4 continued)

KS/CBS limit	B3LYP		CCSD(T)		G2[a]	G3[b]	Expt.
	cc-pV*n*Z	aug-cc-pV*n*Z	cc-pV*n*Z	aug-cc-pV*n*Z			
$BrF \rightarrow Br + F$							
D – T	58.92	58.56	57.30	58.23	59.1	58.6	58.9[i]
T – Q	59.20	58.77	60.20	60.00			
Q – 5	58.44	58.54	59.96	59.66			
Property	58.50	58.52	59.42	59.68			
Total	57.85	57.94	57.87	58.19			
$BrO \rightarrow Br + O$							
D – T	58.82	58.53	53.13	53.92	53.6	55.2	55.3[i]
T – Q	58.43	58.20	54.80	54.79			
Q – 5	58.03	58.05	55.10	54.83			
Property	57.86	57.94	54.04	54.33			
Total	57.34	57.52	53.05	53.44			
$BrB \rightarrow Br + B$							
D – T	97.44	97.69	98.32	98.87	101.2	102.8	103.5[j]
T – Q	97.58	97.70	100.40	100.56			
Q – 5	97.71	97.70	100.50	100.50			
Property	97.77	97.66	100.63	100.49			
Total	97.33	97.25	99.72	99.81			
$Br_2 \rightarrow 2Br$							
D – T	42.86	43.14	42.64	43.64	43.0	45.5	45.4[i]
T – Q	42.54	42.53	45.13	45.30			
Q – 5	42.60	42.69	45.34	45.40			
Property	42.40	42.43	44.94	44.93			
Total	42.37	42.41	44.16	44.43			
$CH_3Br \rightarrow Br + C + 3H$							
D – T	357.78	357.34	356.10	357.70	357.5	357.9	358.2[l]
T – Q	355.94	356.00	357.77	357.46			
Q – 5	355.61	355.84	357.25	357.12			
Property	355.63	355.68	356.12	356.09			
Total	355.30	355.33	355.65	355.75			
$GaCl \rightarrow Ga + Cl$							
D – T	106.59	106.53	107.08	107.39	110.1	111.4	109.9[i]
T – Q	106.29	107.32	109.43	109.57			
Q – 5	107.31	107.16	109.72	109.73			
Property	106.73	107.83	109.54	109.93			
Total	106.02	106.54	107.39	107.73			

(table continues on next page)

(Table 3.4 continued)

KS/CBS limit	B3LYP		CCSD(T)		G2[a]	G3[b]	Expt.
	cc-pV*n*Z	aug-cc-pV*n*Z	cc-pV*n*Z	aug-cc-pV*n*Z			
$KrF_2 \rightarrow Kr + 2F$							
D – T	27.49	27.03	17.54	20.76	23.8	22.5	21.9[i]
T – Q	28.48	27.30	22.19	21.81			
Q – 5	27.03	26.73	22.51	21.31			
Property	26.92	26.83	21.12	21.11			
Total	25.86	25.93	19.60	19.93			
$NaBr \rightarrow Na + Br$							
D – T	80.80	80.71	84.48	84.37	86.4	88.3	86.2[j]
T – Q	80.66	80.64	87.65	87.73			
Q – 5[m]	81.21		87.83				
Property[n]	80.75	80.49	88.02				
Total	80.39	78.68	86.77	86.77			

[a] Gaussian-2 values are from Ref. 68.

[b] Gaussian-3 values are from Ref. 72. Note G3 includes core-correlation effects and an expanded valence set, as opposed to this current work which does not.

[c] Two-point extrapolation is from Eqn. 3.1. "D-T" in table refers to the CBS_{D-T} extrapolation using results from double- and triple-ζ basis sets. "T-Q" refers to the CBS_{T-Q} extrapolation and "Q-5" refers to the CBS_{Q--5} extrapolation.

[d] From Refs. 101,102.

[e] CBS_{prop} extrapolation is from Eqn. 3.2.

[f] CBS_{total} extrapolation is from Eqn. 3.3.

[g] From Ref. 104.

[h] From Ref. 105.

[i] From Ref. 106.

[j] From Ref. 107.

[k] From Ref. 92.

[l] From Ref. 108.

[m] No Peterson or Dunning aug-cc-pV5Z basis set is available for Na.

[n] Due to the near-linearity of energies from the double- through quadruple-ζ basis sets, exponential extrapolation could not be performed for CCSD(T)/aug-cc-pV*n*Z.

3.3.3. Ionization Energies

Both CCSD(T) and B3LYP ionization energies can be found in Table 3.5. Overall, CCSD(T) performs well for ionization energies, with the largest difference between results at the quintuple-ζ level and experiment of 0.05 to 0.07 eV. Almost all of the energies converge toward

the experimental value from below. For B3LYP, the errors are greater, and are on the order of 0.1 to 0.2 eV at the quintuple-ζ level. Overall, the convergence in ionization energy for B3LYP with respect to increasing basis set level is not smooth. However, all of the fluctuations in convergence behavior are slight (~0.01 – 0.02 eV, at most), and convergence to a limit is nearly reached for B3LYP results at the triple-ζ level. Also in Table 3.5, the mean absolute deviation from experiment at each basis set level has been calculated. From this data it is obvious that B3LYP does not have convergent behavior towards some limit with neither the standard nor the augmented basis sets. The CCSD(T) deviations, however have the typical convergent behavior. When comparing the standard and augmented basis sets for both methods, there is a decrease in the mean absolute deviation, just as was found with regards to the atomization energy.

The KS and CBS limits for ionization energies can be found in Table 3.6, as well as comparisons to the G2 and G3 results from earlier work.[68,72] For the CCSD(T) ionization energy extrapolations, CBS_{prop} and CBS_{total} differ from experiment for only five cases by more than 0.04 eV (~1.0 kcal/mol). In contrast to extrapolation schemes for atomization energies, CBS_{prop} and CBS_{total} extrapolation schemes result in very similar ionization energy CBS limits. Even the CBS_{T-Q} two-point extrapolation does fairly well, with only one molecule, $NaBr^+$, that has an error greater than 0.07 eV. In comparing the G2 method, which has eight of fifteen ionization energy errors above 0.08 eV, CCSD(T) with the correlation consistent sets performs better for calculating ionization energies when using an extrapolation scheme of triple-ζ quality or better. There is also a slight improvement in energy as compared with experiment when using the augmented sets as compared to the standard correlation consistent sets.

For B3LYP, all but six molecules have KS limits greater than 0.08 eV as shown in Table 3.5, and only two molecules, Ge^+ and SeH_2^+, are within 0.04 eV of experiment. Approximately

half of the systems have ionization energies that are larger than those from experiment values, as shown for Ga, Se, Br, AsH_2, SeH, and NaBr.

Table 3.5. Ionization energies in eV computed with B3LYP and CCSD(T) coupled with cc-pV*n*Z and aug-cc-pV*n*Z.

	B3LYP		CCSD(T)		Expt.
	cc-pV*n*Z	aug-cc-pV*n*Z	cc-pV*n*Z	aug-cc-pV*n*Z	
$Ga \rightarrow Ga^+$					
D	6.080	6.094	5.822	5.848	5.999[a]
T	6.100	6.106	5.901	5.910	
Q	6.087	6.063	5.936	5.937	
5	6.076	6.076	5.945	5.945	
$Ge \rightarrow Ge^+$					
D	7.871	7.897	7.674	7.722	7.899[a]
T	7.867	7.853	7.798	7.810	
Q	7.869	7.869	7.822	7.827	
5	7.894	7.857	7.832	7.834	
$As \rightarrow As^+$					
D	9.630	9.671	9.510	9.584	9.788[a]
T	9.654	9.655	9.682	9.700	
Q	9.650	9.650	9.719	9.725	
5	9.653	9.654	9.730	9.733	
$Se \rightarrow Se^+$					
D	9.898	9.942	9.091	9.241	9.752[a]
T	9.938	9.943	9.507	9.558	
Q	9.953	9.944	9.648	9.665	
5	9.947	9.948	9.691	9.699	
$Br \rightarrow Br^+$					
D	11.888	11.955	11.285	11.437	11.814[a]
T	11.910	11.912	11.566	11.621	
Q	11.908	11.909	11.723	11.745	
5	11.909	11.910	11.773	11.782	
$Kr \rightarrow Kr^+$					
D	13.953	14.033	13.504	13.699	13.999[a]
T	13.948	13.946	13.701	13.752	
Q	13.939	13.939	13.868	13.893	
5	13.937	13.937	13.923	13.934	
$AsH \rightarrow AsH^+$					
D	9.530	9.613	9.352	9.419	9.641[b]
T	9.593	9.593	9.524	9.551	
Q	9.589	9.589	9.567	9.609	
5	9.593	9.593	9.581	9.617	

(table contiues on next page)

(Table 3.5 continued)

	B3LYP		CCSD(T)		Expt.
	cc-pV*n*Z	aug-cc-pV*n*Z	cc-pV*n*Z	aug-cc-pV*n*Z	
$AsH_2 \rightarrow AsH_2^+$					
D	9.468	9.504	9.138	9.242	9.443[b]
T	9.498	9.497	9.320	9.322	
Q	9.495	9.495	9.369	9.372	
5	9.498	9.499	9.385	9.379	
$SeH \rightarrow SeH^+$					
D	9.881	9.952	9.316	9.469	9.845[c]
T	9.951	9.958	9.688	9.724	
Q	9.956	9.959	9.812	9.812	
5	9.962	9.963	9.851	9.839	
$SeH_2 \rightarrow SeH_2^+$					
D	9.775	9.855	9.361	9.576	9.886[c]
T	9.851	9.858	9.736	9.801	
Q	9.855	9.859	9.804	9.840	
5	9.861	9.862	9.838	9.861	
$HBr \rightarrow HBr^+$					
D	11.544	11.647	11.159	11.354	11.660[d]
T	11.597	11.603	11.424	11.487	
Q	11.598	11.601	11.563	11.588	
5	11.600	11.602	11.607	11.618	
$BrF \rightarrow BrF^+$					
D	11.636	11.788	11.363	11.564	11.780[d]
T	11.616	11.675	11.497	11.614	
Q	11.637	11.662	11.655	11.702	
5	11.655	11.660	11.713	11.730	
$HOBr \rightarrow HOBr^+$					
D	10.435	10.620	10.300	10.559	10.638[e]
T	10.480	10.542	10.475	10.559	
Q	10.508	10.534	10.607	10.642	
5	10.528	10.534	10.661	10.667	
$Br_2 \rightarrow Br_2^+$					
D	10.378	10.437	10.199	10.341	10.520[d]
T	10.341	10.340	10.329	10.388	
Q	10.328	10.330	10.459	10.485	
5	10.330	10.331	10.502	10.514	

(table contiues on next page)

(Table 3.5 continued)

	B3LYP		CCSD(T)		Expt.
	cc-pV*n*Z	aug-cc-pV*n*Z	cc-pV*n*Z	aug-cc-pV*n*Z	
NaBr → $NaBr^+$					
D	8.465	8.509	7.908	8.143	8.310[d]
T	8.541	8.552	8.199	8.267	
Q	8.557	8.560	8.353	8.383	
5[f]	8.569		8.411		
Mean absolute deviation					
D	0.105	0.076	0.400	0.253	
T	0.109	0.104	0.175	0.129	
Q	0.109	0.104	0.077	0.061	
5	0.104	0.095	0.053	0.042	

[a] From Ref. 87.
[b] From Ref. 104.
[c] From Ref. 105.
[d] From Ref. 92.
[e] From Ref. 109.
[f] No Peterson or Dunning aug-cc-pV5Z basis set is available for Na.

Table 3.6. Extrapolated KS and CBS limits for ionization energies in eV determined using B3LYP and CCSD(T) in combination with cc-pV*n*Z and aug-cc-pV*n*Z.

KS/CBS limit	B3LYP		CCSD(T)		G2[a]	G3[b]	Expt.
	cc-pV*n*Z	aug-cc-pV*n*Z	cc-pV*n*Z	aug-cc-pV*n*Z			
Ga → Ga^+							
D – T[c]	6.108	6.111	5.934	5.936	5.93	6.00	5.999[d]
T – Q[c]	6.078	6.031	5.961	5.956			
Q – 5[c]	6.063	6.090	5.954	5.953			
Property[e,f]	5.879	-	5.954	5.952			
Total[g]	6.078	6.065	5.943	5.942			
Ge → Ge^+							
D – T	7.866	7.835	7.850	7.847	7.80	7.90	7.899[d]
T – Q	7.871	7.881	7.840	7.839			
Q – 5	7.920	7.844	7.841	7.841			
Property[f]	-	-	7.832	7.834			
Total	7.884	7.864	7.829	7.831			
As → As^+							
D – T	9.664	9.648	9.755	9.749	9.70	9.81	9.788[d]
T – Q	9.646	9.646	9.745	9.742			
Q – 5	9.657	9.658	9.742	9.741			
Property	9.657	9.652	9.732	9.734			
Total	9.651	9.652	9.728	9.728			

(table continues on next page)

(Table 3.6 continued)

KS/CBS limit	B3LYP		CCSD(T)		G2[a]	G3[b]	Expt.
	cc-pV*n*Z	aug-cc-pV*n*Z	cc-pV*n*Z	aug-cc-pV*n*Z			
$Se \rightarrow Se^+$							
D – T	9.955	9.944	9.682	9.691	9.64	9.71	9.752[d]
T – Q	9.963	9.944	9.751	9.744			
Q – 5	9.941	9.952	9.737	9.734			
Property[f]	9.951	-	9.693	9.718			
Total	9.951	9.946	9.690	9.697			
$Br \rightarrow Br^+$							
D – T	11.919	11.894	11.684	11.699	11.72	11.79	11.814[d]
T – Q	11.907	11.907	11.839	11.835			
Q – 5	11.910	11.910	11.824	11.822			
Property	11.910	11.909	11.840	11.852			
Total	11.909	11.909	11.782	11.789			
$Kr \rightarrow Kr^+$							
D – T	13.946	13.909	13.784	13.774	13.86	13.94	13.999[d]
T – Q	13.933	13.934	13.990	13.995			
Q – 5	13.935	13.935	13.981	13.978			
Property	13.936	13.938	13.988	14.112			
Total	13.937	13.938	13.944	13.954			
$AsH \rightarrow AsH^+$							
D – T	9.619	9.585	9.596	9.606	9.54	9.68	9.641[h]
T – Q	9.586	9.586	9.598	9.651			
Q – 5	9.597	9.598	9.595	9.625			
Property	9.594	9.591	9.584	9.630			
Total	9.590	9.592	9.580	9.619			
$AsH_2 \rightarrow AsH_2^+$							
D – T	9.511	9.494	9.397	9.355	9.34	9.48	9.443[h]
T – Q	9.492	9.493	9.405	9.408			
Q – 5	9.502	9.503	9.401	9.387			
Property	9.501	9.494	9.390	9.398			
Total	9.496	9.497	9.384	9.382			
$SeH \rightarrow SeH^+$							
D – T	9.980	9.960	9.845	9.831	9.80	9.84	9.845[i]
T – Q	9.959	9.959	9.902	9.876			
Q – 5	9.968	9.967	9.893	9.868			
Property	9.960	9.959	9.869	9.852			
Total	9.959	9.959	9.853	9.840			

(table continues on next page)

(Table 3.6 continued)

KS/CBS limit	B3LYP		CCSD(T)		G2[a]	G3[b]	Expt.
	cc-pV*n*Z	aug-cc-pV*n*Z	cc-pV*n*Z	aug-cc-pV*n*Z			
$SeH_2 \rightarrow SeH_2^+$							
D – T	9.883	9.859	9.894	9.896	9.85	9.90	9.886[i]
T – Q	9.858	9.859	9.854	9.868			
Q – 5	9.866	9.866	9.874	9.884			
Property	9.859	9.859	9.836	9.859			
Total	9.858	9.861	9.835	9.858			
$HBr \rightarrow HBr^+$							
D – T	11.619	11.584	11.536	11.543	11.58	11.63	11.660[j]
T – Q	11.598	11.599	11.664	11.661			
Q – 5	11.603	11.603	11.652	11.649			
Property	11.599	11.601	11.660	11.686			
Total	11.647	11.601	11.617	11.625			
$BrF \rightarrow BrF^+$							
D – T	11.608	11.627	11.553	11.634	11.71	11.75	11.780[j]
T – Q	11.652	11.653	11.771	11.767			
Q – 5	11.675	11.659	11.773	11.759			
Property[k]	11.794	11.660	11.745	11.742			
Total	11.654	11.660	11.750	11.751			
$HOBr \rightarrow HOBr^+$							
D – T	10.499	10.509	10.549	10.559	10.65	10.66	10.638[l]
T – Q	10.528	10.529	10.703	10.703			
Q – 5	10.549	10.533	10.718	10.693			
Property[k]	10.562	10.534	10.699	10.678			
Total	10.525	10.534	10.685	10.686			
$Br_2 \rightarrow Br_2^+$							
D – T	10.326	10.299	10.385	10.408	10.49	10.53	10.520[j]
T – Q	10.318	10.322	10.553	10.555			
Q – 5	10.333	10.331	10.548	10.544			
Property[k]	10.327	10.330	10.524	10.526			
Total	10.328	10.330	10.516	10.524			
$NaBr \rightarrow NaBr^+$							
D – T	8.573	8.571	8.322	8.319	8.41	8.52	8.310[j]
T – Q	8.569	8.566	8.465	8.467			
Q – 5[m]	8.581		8.471				
Property[n]	8.569	8.562	8.477				
Total	8.566	8.561	8.424	8.424			

[a] Gaussian-2 values are from Ref. 68.

[b] Gaussian-3 values are from Ref. 72. Note G3 includes core-correlation effects and an expanded valence set, as opposed to this current work which does not.

[c] Two-point extrapolation is from Eqn. 3.1 "D-T" in table refers to the CBS_{D-T} extrapolation using results from double- and triple-ζ basis sets. "T-Q" refers to the CBS_{T-Q} extrapolation and "Q-5" refers to the CBS_{Q-5} extrapolation.
[d] From Ref. 87.
[e] CBS_{prop} extrapolation is from Eqn 3.2.
[f] Not all B3LYP energies converge systematically as discussed in Ref. [99].
[g] CBS_{total} extrapolation is from Eqn 3.3.
[h] From Ref. 104.
[i] From Ref. 105.
[j] From Ref. 92.
[k] For aug-cc-pV*n*Z, only TZ, QZ and 5Z were used in the extrapolation.
[l] From Ref. 109.
[m] No Peterson or Dunning aug-cc-pV5Z basis set is available for Na.
[n] Due to the near-linearity of energies from the double- through quadruple-ζ basis sets, exponential extrapolation could not be performed for CCSD(T)/aug-cc-pV*n*Z.

3.3.4. Electron and Proton Affinity

The G2 third-row test suite includes only four electron affinities and two proton affinities. The electron affinities are provided in Table 3.7. The overall results for B3LYP are surprisingly comparable to CCSD(T), as the errors for the aug-cc-pV5Z range from 0.008 to 0.07 eV for B3LYP, and from 0.004 to 0.08 eV for CCSD(T). For B3LYP with the cc-pV*n*Z series, the energies converge toward a maximum as the basis set level is increased, while the opposite is true for the augmented sets, with the exception of bromine. In each case, except for the BrO^- electron affinity calculated with the aug-cc-pV*n*Z series, the B3LYP values converge toward the experimental values. For CCSD(T), calculated electron affinities smoothly converge toward a maximum value as the basis set size increases, when using either family of basis sets.

Proton affinities are also given in Table 3.7. Nearly all of the results are within 0.04 eV of experiment. In contrast to the observed electron affinity trends, the proton affinity of HBr determined using the cc-pV*n*Z series, converges towards a minimum, while the augmented sets converge towards a maximum. However, the limited number of molecules (two) makes it

impossible to identify general trends for the behavior of proton affinities with respect to increasing basis set size.

The KS and CBS limits for electron and proton affinities, as well as the corresponding G2 and G3 energies are given in Table 3.8. For electron affinities, the CBS/KS_{prop} extrapolations in combination with the standard basis set series provide results that are closer to experiment than those given by the CBS/KS_{total} extrapolations. The only exception to this is for BrO when CCSD(T)/cc-pV*n*Z is used, in which case the CBS_{total} result is nearer to experiment. Of the three two-point extrapolation schemes, overall, $CBS_{Q\text{-}5}$ provides energies nearest experiment. For the augmented sets, there is not a clear choice as to which extrapolation scheme works better for these four molecules. Both the CBS_{prop} and the CBS_{total} extrapolation schemes provide similar electron affinities when B3LYP or CCSD(T) are used.

The two proton affinities determined with the cc-pV*n*Z basis set series and the CBS/KS_{total} extrapolation scheme are nearer to experiment than those determined using the CBS/KS_{prop} extrapolation scheme, while both extrapolation schemes based upon the aug-cc-pV*n*Z basis set series result in nearly identical energies. For example, B3LYP coupled with aug-cc-pV*n*Z gives the same energy for CBS_{prop} and CBS_{total}, and in CCSD(T) the difference in the two schemes is 0.005 eV for HBr and 0.002 eV for CH_4Br^+.

Table 3.7. Electron and proton affinities in eV computed with B3LYP and CCSD(T) coupled with cc-pV*n*Z and aug-cc-pV*n*Z.

	B3LYP		CCSD(T)		Expt.
	cc-pV*n*Z	aug-cc-pV*n*Z	cc-pV*n*Z	aug-cc-pV*n*Z	
$Ge^- \rightarrow Ge$					
D	0.691	1.211	0.615	1.145	1.233[a]
T	0.956	1.228	0.996	1.237	
Q	1.109	1.226	1.159	1.252	
5	1.120	1.241	1.197	1.257	

(table continues on next page)

(Table 3.7 continued)

	B3LYP		CCSD(T)		Expt.
	cc-pV*n*Z	aug-cc-pV*n*Z	cc-pV*n*Z	aug-cc-pV*n*Z	
$Br^- \rightarrow Br$					
D	2.725	3.451	2.042	3.155	3.364[a]
T	3.217	3.406	2.858	3.230	
Q	3.329	3.401	3.203	3.338	
5	3.352	3.401	3.296	3.368	
$SeH^- \rightarrow SeH$					
D	1.537	2.248	1.130	2.005	2.213[b]
T	2.016	2.233	1.826	2.151	
Q	2.131	2.231	2.079	2.178	
5	2.166	2.232	2.153	2.198	
$BrO^- \rightarrow BrO$					
D	1.302	2.356	1.053	2.254	2.360[c]
T	1.831	2.306	1.743	2.342	
Q	2.049	2.296	2.135	2.418	
5	2.195	2.294	2.326	2.440	
$H^+ + Br^- \rightarrow HBr$					
D	14.532	13.856	14.716	13.977	14.000[b]
T	14.127	13.946	14.273	14.043	
Q	14.028	13.959	14.071	13.986	
5	14.010	13.964	14.017	13.972	
$H^+ + CH_3Br \rightarrow CH_4Br^+$					
D	6.816	6.757	6.951	6.847	6.820[d]
T	6.829	6.831	6.901	6.880	
Q	6.839	6.839	6.846	6.840	
5	6.842	6.842	6.825	6.827	

[a] From Ref. 87.
[b] From Ref. 110.
[c] From Ref. 95.
[d] From Ref. 111.

Table 3.8. Extrapolated KS and CBS limits for electron and proton affinities in eV determined using B3LYP and CCSD(T) in combination with cc-pV*n*Z and aug-cc-pV*n*Z.

KS/CBS limit	B3LYP		CCSD(T)		G2[a]	G3[b]	Expt.
	cc-pV*n*Z	aug-cc-pV*n*Z	cc-pV*n*Z	aug-cc-pV*n*Z			
$Ge \rightarrow Ge^-$							
D – T[c]	1.067	1.236	1.156	1.276	1.22	1.25	1.233[d]
T – Q[c]	1.221	1.225	1.278	1.263			
Q – 5[c]	1.132	1.257	1.236	1.261			
Property[e]	1.168	1.246	1.237	1.257			
Total[f]	1.136	1.235	1.199	1.256			
$Br \rightarrow Br^-$							
D – T	3.424	3.388	3.201	3.262	3.32	3.39	3.364[d]
T – Q	3.410	3.396	3.455	3.416			
Q – 5	3.377	3.396	3.394	3.399			
Property	3.360	3.401	3.383	3.379			
Total	3.353	3.401	3.332	3.381			
$SeH \rightarrow SeH^-$							
D – T	2.217	2.226	2.119	2.213	2.21	2.23	2.213[g]
T – Q	2.215	2.229	2.263	2.198			
Q – 5	2.204	2.233	2.232	2.219			
Property	2.176	2.234	2.205	2.199			
Total	2.164	2.231	2.171	2.194			
$BrO \rightarrow BrO^-$							
D – T	2.054	2.284	2.034	2.380	2.45	2.42	2.360[h]
T – Q	2.209	2.289	2.421	2.473			
Q – 5	2.347	2.293	2.526	2.464			
Property	2.294	2.294	2.442	2.501			
Total	2.193	2.294	2.402	2.454			
$H^+ + Br^- \rightarrow HBr$							
D – T	13.957	13.984	14.087	14.070	14.01	13.98	14.000[g]
T – Q	13.955	13.968	13.923	13.945			
Q – 5	13.991	13.969	13.961	13.956			
Property	14.001	13.963	13.960	13.967			
Total	14.008	13.963	13.992	13.962			

(table continues on next page)

$H^+ + CH_3Br \rightarrow CH_4Br^+$							
D – T	6.834	6.862	6.880	6.894	6.83	6.84	6.820[i]
T – Q	6.847	6.845	6.805	6.810			
Q – 5	6.844	6.844	6.803	6.814			
Property	6.848	6.841	6.812	6.822			
Total	6.842	6.841	6.816	6.820			

[a] Gaussian-2 values are from Ref. 68.

[b] Gaussian-3 values are from Ref. 72. Note G3 includes core-correlation effects and an expanded valence set, as opposed to this current work which does not.

[c] Two-point extrapolation is from Eqn 3.1. "D-T" in table refers to the CBS_{D-T} extrapolation using results from double- and triple-ζ basis sets. "T-Q" refers to the CBS_{T-Q} extrapolation and "Q-5" refers to the CBS_{Q-5} extrapolation.
[d] From Ref. 87.
[e] CBS_{prop} extrapolation is from Eqn. 3.2.
[f] CBS_{total} extrapolation is from Eqn. 3.3.
[g] From Ref. 110.
[h] From Ref. 95.
[I] From Ref. 111.

3.3.5. Energy Summary

In Table 3.9, the total mean absolute deviation from experiment for atomization energies, ionization energies, and electron affinities are summarized for CCSD(T) and B3LYP for each type of CBS and KS fit used. For B3LYP, the current results do not point to one obvious best extrapolation scheme to use for all energies. Overall, the two-point KS_{Q-5} extrapolation for B3LYP with quadruple- and quintuple-ζ basis sets provides the best extrapolation scheme for B3LYP and was consistently nearer to experiment than the other schemes. In general, the augmented correlation consistent basis sets provided extrapolated results nearer to experiment with B3LYP in comparison to results from using the standard basis sets. However, this is not the case for CCSD(T), as the deviation for atomization energy is actually smaller for the standard sets (CBS_{T-Q}=1.04 and CBS_{prop} =1.14 kcal/mol, respectively) than for the augmented basis sets (CBS_{T-Q}=1.18 and CBS_{prop} =1.24 kcal/mol, respectively).

Nevertheless, for both the ionization energy and electron affinity calculations, there is significant improvement using the augmented sets with each of the extrapolations schemes over using the standard basis sets. However, for the electron affinities, the data set is too small to provide conclusive statements for an overall trend. Proton affinities have not been included in the summary of energies tables since there are only two in the test set, but are included in the

"Third-row total" section. One important note is that the ability to extrapolate the CCSD(T) results when using the correlation consistent basis sets allows for great improvement over a single basis sets level. For example, if an cc-pVTZ basis sets was the most expensive calculation that could be run for ionization energies, the average deviation for atomization energy would be 4.55 kcal/mol, as shown in the bottom of Table 3.3, but a simple two-point extrapolation would enable this error to drop to 1.71 kcal/mol. This is nearly a three-fold decrease in the error from using only a single basis set.

In comparison to the previous G2 results, the smallest mean absolute deviations were from the CCSD(T) extrapolated ionization energies, in cases where the extrapolation scheme included at least two basis sets of triple-ζ or higher quality, whereas the G2 deviation is nearly double this difference. The overall G3 mean absolute deviation from experiment for all of the energies (0.94 kcal/mol) is much nearer to that seen for the CCSD(T) extrapolated results (e.g., $CBS_{Q\text{-}5}$/aug-cc-pV*n*Z = 0.87 kcal/mol).

In comparing the current calculations to G3, it must be noted that in all of the G3 calculations involving the 6-31G(d) basis set[112] for third-row atoms, the 3*d* orbitals are included as part of the valence set, while the work in this chapter utilized the correlation consistent basis sets and did not contain the 3*d* orbitals in the valence space. Additionally, G3 theory adds the effect of core-correlation via a MP2(full) calculation in combination with the G3Large[63] basis set. In this chapter, core-correlation effects and an expanded valence space have not been included in the calculations, and as a result, the G3 results appear comparable to the CCSD(T) results that are reported. Additionally, G3 uses a four-parameter "high level correction" that is known to contribute largely to its success.

Table 3.9. Total mean absolute deviation of from experimental AE, IE, and EA determined using B3LYP and CCSD(T) in combination with cc-pV*n*Z and aug-cc-pV*n*Z.

	KS/CBS limit[a]	B3LYP cc-pV*n*Z	B3LYP aug-cc-pV*n*Z	G2 (B3LYP)[b]	CCSD(T) cc-pV*n*Z	CCSD(T) aug-cc-pV*n*Z	G2[c]	G3[d]
AE	D – T	2.92	2.66	3.32	2.44	1.71	1.24	1.01
(kcal/mol)	T – Q	3.05	2.71		1.04	1.18		
	Q – 5	2.91	2.53		1.11	1.06		
	Property[e]	3.12	2.90		1.14	1.24		
	Total[f]	3.29	3.37		1.62	1.52		
IE	D – T	0.111	0.101	0.104	0.084	0.078	0.078	0.039
(eV)	T – Q	0.108	0.104		0.041	0.037		
	Q – 5	0.101	0.108		0.041	0.028		
	Property	0.082	0.093		0.048	0.040		
	Total	0.085	0.094		0.050	0.044		
EA	D – T	0.134	0.029	0.040	0.163	0.043	0.054	0.046
(eV)	T – Q	0.053	0.032		0.064	0.054		
	Q – 5	0.034	0.036		0.057	0.045		
	Property	0.043	0.034		0.030	0.050		
	Total	0.081	0.031		0.039	0.040		
Third-row	D – T	2.69	2.24	2.63	2.34	1.66	1.41	0.94
total for	T – Q	2.55	2.29		1.05	1.05		
AE, IE,	Q – 5	2.36	2.25		1.05	0.87		
EA, PA	Property	2.31	2.29		1.03	1.07		
(kcal/mol)	Total	2.50	2.52		1.32	1.22		

[a] Two-point extrapolation is from Eqn. 3.1. "D-T" in table refers to the CBS_{D-T} extrapolation using results from double- and triple-ζ basis sets. "T-Q" refers to the CBS_{T-Q} extrapolation and "Q-5" refers to the CBS_{Q-5} extrapolation.

[b] Modified Gaussian-2 values are from Ref. 70.

[c] Gaussian-2 values are from Ref. 68.

[d] Gaussian-3 values are from Ref. 72. Note G3 includes core-correlation effects and an expanded valence set, as opposed to this current work which does not.

[e] CBS_{prop} extrapolation is from Eqn 3.2.

[f] CBS_{total} extrapolation is from Eqn 3.3.

3.4. Conclusions

This study included 40 energy calculations (19 atomization energies, 15 ionization energies, 4 electron affinities, and 2 proton affinities), 2 electron correlation methods, 8 basis sets, and 5 different extrapolation schemes for molecules containing third-row atoms Ga-Kr. The B3LYP method inconsistently describes ionization energy for these third-row systems when

using the correlation consistent sets and extrapolating to the KS limit. The deviation for atomization energies is 2-3 kcal/mol depending on which method of extrapolation is used. For the four electron affinity calculations, B3LYP does perform well.

Using CCSD(T) in combination with the correlation consistent basis sets and extrapolating to the CBS limit proves to be a viable method and basis set combination for obtaining accurate results for these third-row systems. For the 40 energies calculated, the total mean absolute deviation from experiment is 1.03 kcal/mol when using the exponential CBS_{prop} limit from the cc-pV*n*Z for atomization energy and aug-cc-pV*n*Z for ionization energy and electron affinity. When using the two-point CBS_{T-Q} limit and the same basis set combination, the total deviation is 0.98 kcal/mol from experiment. The best agreement with experiment for any single extrapolation procedures examined is for the CBS_{Q-5} scheme used for the augmented correlation consistent basis sets, resulting in a mean absolute error in all energies of only 0.87 kcal/mol.

Using B3LYP coupled with the correlation consistent basis sets does provide an inexpensive approach to accurate optimal geometries, but the description of energetic properties have inconsistent deviations from experiment, especially for ionization energies. The results from the CCSD(T) calculations in combination with the correlation consistent basis sets, do however, provide a reliable means to predict molecular properties on molecules containing third-row atoms, without the use of empirical correction factors, which can be substantially large.[113] The performance of the correlation consistent basis sets with CCSD(T) allows for great confidence in future calculation containing third-row molecules, even if little or no experimental data are available for comparison.

CHAPTER 4

THE SIGNIFICANCE OF RELATIVISTIC EFFECTS ON THE STRUCTURE AND ENERGTICS OF THIRD-ROW MOLECULES[§]

4.1. Introduction

The previous chapter described a benchmark study of the performance of the correlation consistent basis sets in the prediction of structural and energetic properties of third-row atoms and molecules. This study showed that B3LYP could attain atomization energies, ionization energies, and electron and proton affinities at the Kohn-Sham limit that were within 2-3 kcal/mol from established experimental data. For CCSD(T), energies with an average error of ~1.0 kcal/mol from experiment were possible at the CBS limit. The non-relativistic Hamiltonian (which was discussed in Chapter 2), was employed in this earlier work. As an account of relativistic effects has been shown to be important for even some first-row species, (REF) this chapter will evaluate the impact of a relativistic Hamiltonian upon the structural and energetic properties of the same test suite of third-row molecules examined in the last chapter.

The use of a non-relativistic computational approach is no longer adequate when the speed of the core electrons becomes a substantial fraction of the speed of light. In systems containing heavy metals, such as gold or mercury, even a qualitative description of the electronic structure may not be possible unless relativistic effects are included. In relativistic theory, the

[§] This chapter has been adapted from the publication of *J. Chem. Phys.*, Vol. 122, Scott Yockel and Angela K. Wilson, "Relativistic effects determined using the Douglas-Kroll contracted basis sets and correlation consistent basis sets with small-core relativistic pseudopotentials", Page 174310/1-14, Copyright (2005), with permission from American Institute of Physics.

Dirac equation is analogous to the Schrödinger equation and includes the speed of light and change in mass due to relativity, which when solved yields the relativistic total energy. Accounting for the change in energy due to relativity is expected to enable a better description of the electronic structure of atoms and molecules. To account for relativistic effects completely, the full four-component Dirac Hamiltonian[114] would need to be solved. However, solving the four-component Dirac Hamiltonian is even more computationally demanding than the Schrödinger equation, significantly limiting the size of chemical system which could be studied. Because of this, many different methods have been developed to incorporate relativistic effects into electronic structure calculations more efficiently, as noted below. Generally in quantum chemical calculations, adequate relativistic treatment includes only a two-component formalism, which only involves electronic effects. This scheme is commonly referred to as the "large-component" formalism for having the largest impact on the energy.

There are two general types of relativistic effects that stem from the large-component formalism. The first type of effect is referred to as "spin-dependent," and is caused when the spin (s) and orbital (l) angular momentum quantum numbers are strongly connected, leading to spin-orbit coupling (L-S coupling). Spin-orbit coupling is most prevalent, when spin (*s*) and spatial (*l*) states are degenerate. In this case the total angular quantum number ($j = s + l$) must be used in the description of electronic states instead of the individual *s* and *l* quantum numbers. The second type of relativistic effect is referred to as "spin-independent". Such effects are important when the speed of the electrons in the core region becomes a significant fraction of the speed of light. This phenomenon causes the relativistic mass of the electrons to increase, thereby altering the electronic energy and is known as the scalar relativistic effect. The scalar relativistic effect is mainly observed for the inner *s*-orbitals, and causes the contraction of these orbitals

towards the nucleus, while indirectly causing the *p*-orbitals to contract slightly. These contracted orbitals, furthermore shield the outer *d*- and *f*- orbitals from the nuclear charge allowing for the *d*- and *f*- orbitals to expand. This expansion and contraction of orbitals has a direct effect on the electronic structure of the system.

Inclusion of spin-orbit effects in quantum chemistry calculations is not trivial for molecular systems, because the determination of orbitals for inclusion in the spin-orbit coupling part of the calculation is not always clear. The general approach used is to calculate spin-orbit splitting from experimental atomic spectra so that comparisons of calculated properties can be made with experimentally derived properties. Spin-orbit effects are typically small (<0.5 kcal/mol) for first- and second-row atoms (Li-Ne and Na-Ar), but can become large (>1.0 kcal/mol) in third-row atoms. For example, the lowering in energy due to the spin-orbit splitting for Kr^+ is ~5.0 kcal/mol.[88] Thus, the inclusion of spin-orbit corrections is needed to describe chemical properties correctly for molecules containing third-row atoms.

Accounting for the scalar relativistic effect can be done within the basis set or by modifications to the Hamiltonian. In the basis set approach, corrections for the scalar relativistic contraction of the *s*- and *p*-orbitals are made by incorporating this effect into a relativistic effective core potential (RECP), which is also referred to as a pseudopotential (PP). The RECP essentially "removes" the core electrons and replaces them by a pseudopotential that was determined using a relativistic method, such as Dirac-Hartree-Fock. Using an RECP is the most widely used approach to account for scalar relativistic effects, due to its efficiency and ease of implementation in many software codes.[26,115-119] However, using a RECP is limited only to electronic structure calculations involving valence orbitals and is not applicable to studies that

involve correlating the core electrons, because the core orbitals have been replaced by the pseudopotential and are no longer defined explicitly.

Modification to the Hamiltonian is another approach used to account for relativistic effects. However, because the Dirac Hamiltonian is only applicable to small systems, as mentioned above, a number of approximate, less computationally expensive approaches to account for relativistic effects are available. These approaches include the zeroth-order regular approximation (ZORA),[120] the Breit-Pauli Hamiltonian,[121] the modified Dirac method of Dyall,[122,123] stationary direct perturbation theory (SDPT),[124] and the Douglas-Kroll-Hess approach (DK).[125-127] The Douglas-Kroll-Hess approach is known to account for most of the scalar relativistic effects,[28] and the first-order DK implementation includes only the correction to the spin-free one-electron terms, which is an efficient means to include the effects of scalar relativity in electronic structure calculations. (More detailed descriptions of these methods and the virtues of the methods can be found in Refs. 120-127.)

Scalar relativistic effects are well known for atoms and have been shown to result from the increased attraction of the inner s-orbitals to the nucleus with increasing atomic charge. This attraction causes the magnitude of the scalar relativistic effect in atoms to increase with increasing atomic number. However, less is known about scalar relativistic effects on molecular properties, such as atomization energies. There have been numerous earlier studies that have attempted to describe the effects due to scalar relativity on molecular properties, which have used several of the approximations mentioned previously. Pople and co-workers have used both the Dirac-Coulomb-Hartree Fock method for their G2/97 test suite, as well as the SDPT method for the G3/99 test suite in order to describe the scalar relativistic contribution to the atomization energies. Feller and Peterson have used the one-electron Darwin and mass-velocity terms in the

Breit-Pauli Hamiltonian to re-examine energies of the G2/97 suite.[24] More recently, the Douglas-Kroll-Hess Hamiltonian has been used by Dixon and co-workers to describe the impact of relativistic corrections upon energies and frequencies for a range of molecules.[21,22,28] In these studies it was shown that the magnitude of the scalar relativistic corrections can be significant, even for first-row molecules, particularly for species which contain multiple halogen atoms. Using the Douglas-Kroll approach, Bauschlicher noted scalar relativistic effects upon atomization energies of ~0.7 and ~1.0 kcal/mol on BF_3 and CF_4, respectively.[128,129] Feller and Peterson have shown that the impact can be important on first-row non-halogenated species as well, with an effect of –0.6 kcal/mol upon the atomization energy of CO_2.[24] Table 4.1 includes selected data from previous studies to demonstrate the impact that scalar relativistic effects have on the atomization energy of lighter main-group compounds.

For second-row systems, scalar relativistic effects become more pronounced, particularly for multi-halogenated species. Feller and Dixon have determined a scalar relativistic effect of –1.62 kcal/mol for $SiCl_4$.[21] Again, the scalar effect can be important for non-halogenated species such as SO_2, where the effect is –0.9 kcal/mol.[24] Most calculations on first- and second-row atoms neglect the scalar relativistic effects. However, as can be seen from the prior studies in Table 4.1, for some molecules this effect can become quite significant when trying to achieve an accuracy of 1.0 kcal/mol in the atomization energy. Bauschlicher found an effect of –7.88 kcal/mol for the atomization energy of GaF_3.[130] In a study by Ricca and Bauschlicher, an effect of –3.58 kcal/mol upon GeH_4 was noted.[131] As shown by Table 4.1, there is a large increase in the scalar relativistic effect on the atomization energy of molecules containing third-row atoms in comparison to the change from first- to second-row systems. This suggests the possible

significance of scalar relativistic corrections on calculated molecular properties involving third-row atoms.

Comprehensive studies including scalar relativistic corrections on larger test suites of molecules have focused on molecules with first- and second-row atoms.[21,24,132,133] To date, few broad studies of third-row systems have analyzed the effect that scalar relativistic corrections have on the prediction of structural and chemical properties. Thus, the focus of this chapter is to compare and contrast the performance of two families (cc-pV*n*Z-DK and cc-pV*n*Z-PP) of correlation consistent basis sets used in combination with the CCSD(T) method in the description of scalar relativistic effects, and to examine the impact of these effects upon molecular properties of third-row molecules in the G2 test suite. These calculations will be directly compared to the energies and structures reported in Chapter 3.[134]

Table 4.1. A comparison of the scalar relativistic effect (SR) on atomization energies (kcal/mol) selected from previous studies.

Molecule	SR	Reference
BF_3	-0.7	Bauschlicher[129]
CF_4	-1.0	Bauschlicher[129]
CO_2	-0.6	Feller and Peterson[24]
$SiCl_4$	-1.62	Feller and Dixon[21]
SO_2	-0.9	Feller and Peterson[24]
GaF_3	-7.88	Bauschlicher[130]
GeH_4	-3.58	Ricca and Bauschlicher[131]

4.2. Methodolgy

The scalar relativistic effects in this study were obtained by two different approaches. In the first approach, the scalar relativistic effects were determined by taking the difference in the energies computed with a nonrelativistic Hamiltonian and DK Hamiltonian, [127,135,136] as implemented in the MOLPRO quantum chemistry code.[85] The electron correlated method used throughout this study was the coupled cluster approximation [CCSD(T)],[50-52] which includes single, double and quasiperturbative triple excitations of the ground state wave function. This

method was used in combination with the correlation consistent basis set families (cc-pV*n*Z). These sets are constructed systematically to recover more correlation energy with each increase in basis set size.

In correlated calculations that involve Gaussian basis sets (such as cc-pV*n*Z), contracted basis functions are generally used to describe the core regions, which reduce the total number of basis functions thereby reducing the cost of the calculation. Contracting these core basis function leads to inflexibility in the basis set, which is normally not problematic. However, using the DK Hamiltonian causes a contraction of the inner *s*- and *p*-orbitals that changes their radial distributions, and this change leads to erroneous results when using basis sets that have generally contracted primitive *s*- and *p*- basis functions. In a study by de Jong, *et al.*,[28] on properties of diatomics containing F, Cl, and Br, they compare the difference between four different results obtained using two types of basis sets (non-relativistic contracted and uncontracted basis sets) with both the DK Hamiltonian and the standard Hamiltonian. For the non-relativistic Hamiltonian there is little difference in the dissociation energies calculated with the two different basis sets (non-relativistic contracted vs. uncontracted). However, while using the DK Hamiltonian the energies obtained with the two different basis sets become significantly different (> 1.0 kcal/mol) for Br containing systems. When using the standard contracted basis sets in a DK Hamiltonian calculation for Br_2, the scalar relativistic contribution to the dissociation energy is not even qualitatively correct; it has the wrong sign and is more than four times the magnitude (4.13 kcal/mol) as compared to the uncontracted basis set (-1.06 kcal/mol). It can be seen from that study that erroneous results from DK calculations with the standard contracted basis set result from the inflexibility of the basis set to compensate for the radial distribution changes in the wave function (the *s*,*p* contraction and *d*,*f* expansion of the orbitals).

To remedy this problem, de Jong and co-workers recontracted the standard correlation consistent basis sets for use with the one-electron DK Hamiltonian, producing the cc-pV*n*Z-DK basis sets. In this study, the geometries and atomization energies have been obtained using the cc-pV*n*Z-DK sets with the DK Hamiltonian in CCSD(T), and are directly compared to the non-relativistic calculations from Chapter 3 with CCSD(T) and the standard cc-pV*n*Z basis sets.[134] The scalar relativistic effect on molecular properties has been computed as the difference between the previous non-relativistic computations in Chapter 3 and the relativistic computations of this chapter.

Another way to evaluate the effect of scalar relativity on chemical properties is to use the newly developed correlation consistent basis sets by Peterson,[26,27] which contain a RECP. These new families of basis sets are denoted cc-pV*n*Z-PP and aug-cc-pV*n*Z-PP. Like the all-electron correlation consistent sets (cc-pV*n*Z), it has been shown that the total energy and other properties computed with these new sets also have a smooth convergent behavior toward the CBS limit.[26,27] Unlike other RECP's the cc-pV*n*Z-PP basis sets provide a better interplay between the basis set and the pseudopotential and do not suffer artificial interactions between the pseudopotential and the electrons.[137-139] This improvement stems from the use of a small-core (10 electron) multiconfiguration-Dirac-Hartree-Fock (MCDHF)-adjusted pseudopotentials from Stoll, Dolg, and co-workers,[118,140] which allows the outer core orbitals to be described with basis functions. The accuracy obtainable with the cc-pV*n*Z-PP basis sets and a correlated method, such as CCSD(T), is very similar to the accuracy obtained using the DK Hamiltonian and CCSD(T) with the cc-pV*n*Z-DK basis sets. The cc-pV*n*Z-PP sets have been used for third-row atoms, while the cc-pV*n*Z and aug-cc-pV*n*Z sets[1,2,4] were used for the first- and second-row atoms.

Optimized structures and frequencies were obtained using the CCSD(T) method at each basis set level. From the frequency calculations, the zero point energy (ZPE) corrections were obtained and applied to the total energy of each molecule in order to calculate the atomization energy, ionization energy, electron affinity and proton affinity of 36 third-row systems. In each of the computations, the standard frozen core approximation was used, which did not include the *3d* orbitals in the correlation space. In comparison to the G3 calculations from the previous study, the *3d* orbital were included in the correlation space.[72] Spin-orbit corrections were made to the total energy for both atoms and molecules. However, as the magnitude of the spin-orbit effects on first-row atoms are below one millihartree,[141] these were not included. This enabled an appropriate comparison to results from Chapter 3 as well as to prior G2 and CBS-*n* benchmark studies, where the first-order spin orbit corrections were not included. It must be noted, however, that the spin-orbit correction for the fluorine atom is 0.58 kcal/mol, which is the largest of the first-row atoms. In the KrF_2 molecule included in this study, the overall spin-orbit correction would have been 1.16 kcal/mol if the first-row correction was utilized. For systems containing second row atoms, the corrections were determined using the Moore Tables.[87] For third-row atoms and molecules, first-order spin-orbit corrections were obtained from configuration interaction calculations done by Blaudeau and Curtiss.[88]

The convergent behavior of energetics calculated with the correlation consistent basis sets allows for extrapolation to the CBS limit. At this limit, the error associated with an incomplete one-particle basis has been eliminated and the remaining error arises from the computational method. Since the development of the correlation consistent basis sets, many extrapolation procedures have been created for use in the determination of molecular properties at the CBS limit. This study utilizes two different numerical approaches to obtain the CBS limit

of energies and geometries, as was done in Chapter 3. The first approach, is a two-point extrapolation utilizing Eqn. 3.1.[89] The second approach is an exponential fit by Feller and was implemented in two ways as described in Chapter 3, Eqn. 3.2 and Eqn. 3.3.[19] In total, the five different CBS limit extrapolations used are denoted $CBS_{D\text{-}T}$, $CBS_{T\text{-}Q}$, $CBS_{Q\text{-}5}$, CBS_{prop}, and CBS_{total}.

4.3. Results and Discussion

4.3.1. Geometry

The inclusion of scalar relativistic corrections results in little change (<0.01 Å) in the calculated non-relativistic bond lengths and angles when using CCSD(T), as shown in Table 4.2. Most of the bond lengths decrease slightly (<0.003 Å) when scalar relativistic corrections are applied. There are, however, a few exceptions (GaCl, BrF, BrF^+, BrO, BrO^-, HOBr, and $HOBr^+$) in which the bond distances are lengthened. For GaCl, the increase at the CCSD(T)/cc-pV5Z-DK level is 0.013 Å, whereas the increases are much smaller (0.001-0.005 Å) for the other species. The most notable changes in decreasing bond lengths are for GeH_4, As_2, Br_2^+ and BBr, where the relativistic effect results in a decrease of ~0.006-0.007Å in bond length at the highest basis set level as compared with the non-relativistic bond lengths. In comparing the relativistic bond lengths obtained using the Douglas-Kroll and pseudopotential approaches, the bond lengths obtained using the Douglas-Kroll approach are generally slightly longer (0.001 Å) than those obtained using the pseudopotentials.

The molecule test set only includes five molecules that are not linear. The bond angles for four of these species decrease slightly when the scalar relativistic corrections are applied,

while the bond angle for CH_3Br is slightly (0.1°) larger than the angle determined when the effect has not been applied.

In Table 4.3, the total mean absolute deviations from experimentally determined bond lengths have been tabulated at each basis set level and CBS limits from Eqns. 3.1, 3.2, and 3.3. When including the scalar relativistic effect, the overall change in bond lengths is minimal and is nearly identical at the quintuple-ζ level. At the CBS limit, the changes in bond length using the DK approach are on average 0.001 Å shorter in comparison to the cc-pV*n*Z values, while the bond lengths from the pseudopotential approach are only slightly shorter (~0.003Å) at the CBS limit. Because the bond lengths of third-row containing molecules change only slightly with the inclusion of scalar relativity; in the future DK CCSD(T) energy calculations at the non-relativistic CCSD(T) geometry would be advantageous and expected to provide nearly the same total energy as the optimized structures.

Table 4.2. Geometries using CCSD(T) in combination with cc-pV*n*Z-DK, cc-pV*n*Z-PP, and aug-cc-pV*n*Z. The bond lengths (r) are given in Å and the angles (a) are given in °.

	Basis Set	cc-pV*n*Z[a]	aug-cc-pV*n*Z[a]	cc-pV*n*Z-DK	cc-pV*n*Z-PP	aug-cc-pV*n*Z-PP	Expt.[b]
GeH_4							
$r_{(Ge-H)}$	*n*=D	1.543	1.546	1.538	1.539	1.541	1.514[c]
	T	1.542	1.542	1.535	1.535	1.535	
	Q	1.541	1.541	1.534	1.534	1.534	
	5	1.541	-----	1.534	1.534	1.534	
AsH							
$r_{(As-H)}$	D	1.542	1.544	1.542	1.542	1.544	1.535
	T	1.535	1.536	1.533	1.533	1.533	
	Q	1.533	1.534	1.531	1.531	1.531	
	5	1.533	1.534	1.531	1.531	1.531	
AsH^+							
$r_{(As-H)}$	D	1.538	1.541	1.538	1.537	1.540	
	T	1.534	1.535	1.532	1.531	1.532	
	Q	1.533	1.534	1.531	1.530	1.531	
	5	1.534	1.534	1.531	1.530	1.531	

(table continues on next page)

(Table 4.2 contiuned)

	Basis Set	cc-pV*n*Z[a]	aug-cc-pV*n*Z[a]	cc-pV*n*Z-DK	cc-pV*n*Z-PP	aug-cc-pV*n*Z-PP	Expt.[b]
AsH_2							
$r_{(As-H)}$	D	1.534	1.537	1.534	1.534	1.536	1.518[e]
	T	1.529	1.530	1.527	1.526	1.527	
	Q	1.528	1.528	1.525	1.525	1.525	
	5	1.528	1.528	1.526	1.525	1.525	
$a_{(H-As-H)}$	D	91.1	90.9	90.9	90.9	90.7	90.7[e]
	T	91.2	91.0	90.9	90.9	90.8	
	Q	91.1	91.1	90.9	90.9	90.8	
	5	91.2	91.1	90.9	90.9	90.9	
AsH_2^+							
$r_{(As-H)}$	D	1.532	1.536	1.532	1.532	1.535	
	T	1.529	1.530	1.527	1.526	1.527	
	Q	1.528	1.529	1.526	1.525	1.525	
	5	1.528	1.529	1.526	1.525	1.525	
$a_{(H-As-H)}$	D	91.9	91.6	91.6	91.6	91.2	
	T	91.8	91.7	91.5	91.5	91.4	
	Q	91.8	91.7	91.5	91.5	91.4	
	5	91.8	91.7	91.5	91.5	91.5	
AsH_3							
$r_{(As-H)}$	D	1.529	1.532	1.528	1.528	1.531	1.511[e]
	T	1.524	1.525	1.522	1.521	1.522	
	Q	1.523	1.524	1.521	1.520	1.521	
	5	1.523	1.524	1.521	1.520	1.520	
$a_{(H-As-H)}$	D	92.5	92.4	92.2	92.2	92.1	92.1[e]
	T	92.6	92.4	92.2	92.2	92.1	
	Q	92.5	92.5	92.2	92.2	92.1	
	5	92.5	92.6	92.2	92.2	92.2	
SeH							
$r_{(Se-H)}$	D	1.478	1.481	1.478	1.479	1.481	1.475
	T	1.473	1.474	1.471	1.470	1.471	
	Q	1.472	1.473	1.470	1.469	1.470	
	5	1.472	1.472	1.470	1.469	1.470	

(table continues on next page)

(Table 4.2 contiuned)

	Basis Set	cc-pV*n*Z[a]	aug-cc-pV*n*Z[a]	cc-pV*n*Z-DK	cc-pV*n*Z-PP	aug-cc-pV*n*Z-PP	Expt.[b]
SeH^+							
$r_{(Se-H)}$	D	1.496	1.499	1.495	1.495	1.498	
	T	1.491	1.492	1.489	1.489	1.489	
	Q	1.490	1.491	1.488	1.487	1.488	
	5	1.491	1.491	1.488	1.487	1.488	
SeH^-							
$r_{(Se-H)}$	D	1.487	1.486	1.487	1.487	1.486	
	T	1.478	1.479	1.477	1.476	1.476	
	Q	1.477	1.478	1.475	1.474	1.475	
	5	1.477	1.468	1.475	1.474	1.475	
SeH_2							
$r_{(Se-H)}$	D	1.473	1.476	1.472	1.473	1.476	1.460[e]
	T	1.468	1.469	1.466	1.466	1.467	
	Q	1.468	1.468	1.466	1.465	1.465	
	5	1.468	1.468	1.466	1.465	1.465	
$a_{(H-Se-H)}$	D	91.3	91.3	91.1	91.1	91.0	90.6[e]
	T	91.3	91.1	91.0	90.9	90.8	
	Q	91.3	91.3	91.0	90.9	90.9	
	5	91.3	91.3	91.0	91.0	90.9	
SeH_2^+							
$r_{(Se-H)}$	D	1.488	1.492	1.487	1.488	1.491	
	T	1.484	1.486	1.483	1.482	1.483	
	Q	1.484	1.484	1.482	1.481	1.481	
	5	1.484	1.484	1.482	1.481	1.481	
$a_{(H-Se-H)}$	D	92.0	91.7	91.7	91.7	91.4	
	T	91.8	91.7	91.5	91.5	91.3	
	Q	91.8	91.8	91.5	91.5	91.4	
	5	91.8	91.8	91.5	91.5	91.5	
HBr							
$r_{(H-Br)}$	D	1.426	1.429	1.425	1.426	1.429	1.414
	T	1.420	1.421	1.418	1.418	1.419	
	Q	1.420	1.421	1.418	1.418	1.419	
	5	1.421	1.421	1.419	1.419	1.419	

(table continues on next page)

(Table 4.2 contiuned)

	Basis Set	cc-pV*n*Z[a]	aug-cc-pV*n*Z[a]	cc-pV*n*Z-DK	cc-pV*n*Z-PP	aug-cc-pV*n*Z-PP	Expt.[b]
HBr^+							
$r_{(H-Br)}$	D	1.457	1.460	1.456	1.456	1.460	1.448
	T	1.452	1.453	1.450	1.451	1.452	
	Q	1.452	1.453	1.451	1.451	1.451	
	5	1.453	1.453	1.451	1.451	1.451	
GaCl							
$r_{(Ga-Cl)}$	D	2.249	2.281	2.260	2.265	2.296	2.202
	T	2.255	2.265	2.266	2.260	2.287	
	Q	2.257	2.261	2.270	2.265	2.269	
	5	2.257	2.259	2.270	2.265	2.267	
GeO							
$r_{(Ge-O)}$	D	1.665	1.671	1.665	1.666	1.672	1.625
	T	1.649	1.653	1.648	1.647	1.652	
	Q	1.649	1.650	1.648	1.646	1.647	
	5	1.648	1.648	1.647	1.646	1.646	
As_2							
$r_{(As-As)}$	D	2.147	2.151	2.143	2.145	2.147	2.103
	T	2.135	2.135	2.128	2.126	2.127	
	Q	2.128	2.129	2.121	2.119	2.120	
	5	2.126	2.126	2.119	2.117	2.118	
GeS_2							
$r_{(Ge-S)}$	D	2.033	2.040	2.031	2.033	2.038	
	T	2.023	2.024	2.019	2.017	2.019	
	Q	2.016	2.017	2.012	2.011	2.011	
	5[f]	2.013	2.014	-----	2.008	-----	
KrF_2							
$r_{(Kr-F)}$	D	2.012	1.921	2.006	1.986	1.922	1.875[e]
	T	1.885	1.886	1.885	1.882	1.884	
	Q	1.875	1.876	1.875	1.873	1.875	
	5	1.873	1.873	1.874	1.872	1.871	
BrCl							
$r_{(Br-Cl)}$	D	2.200	2.205	2.201	2.199	2.204	2.136
	T	2.163	2.164	2.163	2.162	2.163	
	Q	2.150	2.151	2.150	2.150	2.150	
	5	2.144	2.144	2.144	2.143	2.144	

(table continues on next page)

(Table 4.2 contiuned)

	Basis Set	cc-pV*n*Z[a]	aug-cc-pV*n*Z[a]	cc-pV*n*Z-DK	cc-pV*n*Z-PP	aug-cc-pV*n*Z-PP	Expt.[b]
BrF							
$r_{(Br-F)}$	D	1.819	1.801	1.820	1.821	1.806	1.759
	T	1.769	1.770	1.770	1.769	1.771	
	Q	1.762	1.762	1.764	1.763	1.764	
	5	1.760	1.760	1.762	1.761	1.761	
BrF^+							
$r_{(Br-F)}$	D	1.740	1.724	1.741	1.741	1.728	
	T	1.686	1.688	1.687	1.686	1.689	
	Q	1.680	1.681	1.682	1.681	1.681	
	5	1.678	1.678	1.679	1.679	1.679	
BrO							
$r_{(Br-O)}$	D	1.795	1.773	1.799	1.798	1.777	1.717
	T	1.735	1.731	1.737	1.738	1.733	
	Q	1.725	1.723	1.728	1.727	1.726	
	5	1.721	1.721	1.724	1.723	1.723	
BrO^-							
$r_{(Br-O)}$	D	1.915	1.868	1.920	1.927	1.876	1.814[e]
	T	1.832	1.821	1.837	1.835	1.826	
	Q	1.817	1.812	1.822	1.821	1.817	
	5	1.811	1.809	1.816	1.815	1.813	
HOBr							
$r_{(Br-O)}$	D	1.888	1.874	1.890	1.891	1.879	1.834[g]
	T	1.840	1.840	1.842	1.842	1.842	
	Q	1.833	1.832	1.835	1.834	1.834	
	5	1.830	1.829	1.832	1.831	1.831	
$r_{(H-O)}$	D	0.974	0.973	0.974	0.974	0.973	0.961[g]
	T	0.965	0.967	0.965	0.965	0.967	
	Q	0.964	0.965	0.964	0.964	0.965	
	5	0.964	0.964	0.964	0.964	0.964	
$a_{(H-O-Br)}$	D	100.8	102.7	100.6	100.6	102.4	102.3[g]
	T	102.3	103.1	102.0	102.1	102.9	
	Q	102.9	103.3	102.7	102.8	103.1	
	5	103.2	103.3	102.9	103.0	103.1	

(table continues on next page)

(Table 4.2 contiuned)

	Basis Set	cc-pV*n*Z[a]	aug-cc-pV*n*Z[a]	cc-pV*n*Z-DK	cc-pV*n*Z-PP	aug-cc-pV*n*Z-PP	Expt.[b]
$HOBr^+$							
$r_{(Br-O)}$	D	1.770	1.765	1.772	1.771	1.768	
	T	1.729	1.731	1.730	1.730	1.731	
	Q	1.724	1.724	1.725	1.725	1.725	
	5	1.721	1.721	1.722	1.722	1.722	
$r_{(H-O)}$	D	0.993	0.991	0.993	0.993	0.991	
	T	0.984	0.985	0.984	0.984	0.985	
	Q	0.983	0.983	0.983	0.983	0.983	
	5	0.983	0.983	0.983	0.983	0.983	
$a_{(H-O-Br)}$	D	107.6	108.2	107.4	107.4	108.0	
	T	108.4	108.8	108.2	108.2	108.7	
	Q	108.8	109.0	108.7	108.8	108.9	
	5	109.1	109.1	108.8	108.8	108.9	
Br_2							
$r_{(Br-Br)}$	D	2.346	2.353	2.345	2.340	2.346	2.281
	T	2.311	2.313	2.308	2.308	2.310	
	Q	2.298	2.299	2.296	2.295	2.296	
	5	2.294	2.294	2.292	2.292	2.292	
Br_2^+							
$r_{(Br-Br)}$	D	2.252	2.259	2.251	2.245	2.252	
	T	2.220	2.223	2.217	2.217	2.219	
	Q	2.210	2.210	2.207	2.206	2.207	
	5	2.210	2.206	2.204	2.203	2.203	
BBr							
$r_{(B-Br)}$	D	1.920	1.927	1.916	1.917	1.923	1.888
	T	1.906	1.907	1.901	1.901	1.902	
	Q	1.904	1.904	1.898	1.898	1.898	
	5	1.903	1.903	1.897	1.897	1.897	
CH_3Br							
$r_{(C-H)}$	D	1.084	1.099	1.100	1.101	1.099	1.082[h]
	T	1.085	1.086	1.085	1.085	1.086	
	Q	1.084	1.084	1.084	1.084	1.084	
	5[f]	-----	-----	-----	-----	-----	

(table continues on next page)

(Table 4.2 contiuned)

	Basis Set	cc-pV*n*Z[a]	aug-cc-pV*n*Z[a]	cc-pV*n*Z-DK	cc-pV*n*Z-PP	aug-cc-pV*n*Z-PP	Expt.[b]
$r_{(C-Br)}$	D	1.947	1.963	1.957	1.956	1.965	1.934[h]
	T	1.948	1.948	1.946	1.946	1.947	
	Q	1.944	1.944	1.943	1.943	1.943	
	5[f]	-----	-----	-----	-----	-----	
$a_{(H-C-H)}$	D	111.2	111.1	110.9	110.9	111.2	111.2[h]
	T	111.0	111.2	111.0	111.0	111.2	
	Q	111.1	111.1	111.1	111.1	111.2	
	5[f]	-----	-----	-----	-----	-----	
CH_4Br^+	D	1.099	1.098	1.101	1.101	1.100	
$r_{(C-H)}$	T	1.084	1.085	1.087	1.087	1.087	
	Q[i]	1.086	-----	1.086	1.086	-----	
	5[f]	-----	-----	-----	-----	-----	
	D	2.018	2.024	2.020	2.015	2.025	
$r_{(C-Br)}$	T	1.998	1.998	1.999	1.998	1.999	
	Q[i]	1.993	-----	1.994	1.994	-----	
	5[f]	-----	-----			-----	
	D	1.443	1.446	1.442	1.443	1.445	
$r_{(Br-H)}$	T	1.438	1.439	1.436	1.437	1.438	
	Q[i]	1.439	-----	1.436	1.437	-----	
	5[f]	-----	-----	-----	-----	-----	
	D	113.5	113.6	113.6	113.4	113.6	
$a_{(H-C-H)}$	T	113.3	113.4	113.4	113.4	113.5	
	Q[i]	113.3	-----	113.4	113.4	-----	
	5[f]	-----	-----	-----	-----	-----	
	D	96.9	102.0	96.7	96.6	96.4	
$a_{(H-Br-C)}$	T	102.4	102.3	96.7	96.8	96.6	
	Q[i]	97.1	-----	96.8	96.8	-----	
	5[f]	-----	-----	-----	-----	-----	

[a] cc-pV*n*Z and aug-cc-pV*n*Z results are from Ref. 134.
[b] From Ref. 92 unless otherwise noted.
[c] From Ref. 93.
[d] From Ref. 94.
[e] From Ref. 95.

[f] Due to computational requirements, optimization was not performed for all types of the quintuple-ζ basis sets.
[g] From Ref. 96.
[h] From Ref. 97.
[i] The aug-cc-pVQZ-PP optimization was not performed due to the computational requirements.

Table 4.3. Total mean absolute deviation of bond lengths (Å) computed with CCSD(T) and cc-pV*n*Z-DK, cc-pV*n*Z-PP, and aug-cc-pV*n*Z-PP.

Basis Set	cc-pV*n*Z	aug-cc-pV*n*Z	cc-pV*n*Z-DK	cc-pV*n*Z -PP	aug-cc-V*n*Z -PP
n=D	0.037	0.037	0.039	0.039	0.035
T	0.017	0.018	0.014	0.013	0.016
Q	0.014	0.014	0.014	0.011	0.011
5	0.014	0.011	0.015	0.011	0.011
CBS limit					
D - T	0.016	0.013	0.015	0.013	0.011
T - Q	0.013	0.013	0.014	0.010	0.010
Q - 5	0.013	0.010	0.014	0.011	0.011

4.3.2. Atomization Energy

The atomization energy has been calculated for 18 molecules from the G2 third-row test suite in order to assess the magnitude of the scalar relativistic effect. These energies were determined using CCSD(T) with the cc-pV*n*Z-PP and aug-cc-pV*n*Z-PP basis sets and using CCSD(T) with both the DK Hamiltonian and the cc-pV*n*Z-DK basis sets, which are reported in Table 4.4. The values in parentheses in Table 4.4 represent the change in atomization energy due to the scalar relativistic correction. The results from the five different CBS extrapolations are provided in Table 4.5.

To determine the magnitude of the scalar relativistic correction, the differences in the non-relativistic and relativistic atomization energies were compared between: (a) previous CCSD(T)/cc-pV*n*Z calculations and CCSD(T)/cc-pV*n*Z-DK calculations with the one-electron DK terms; (b) previous CCSD(T)/cc-pV*n*Z calculations and CCSD(T)/cc-pV*n*Z-PP calculations; and (c) previous CCSD(T)/aug-cc-pV*n*Z calculations and CCSD(T)/aug-cc-pV*n*Z-PP calculations. In a earlier study by Feller and Dixon,[21] on a set of 37 molecules from the G2/97

test suite that contain first- and second-row atoms, the scalar relativistic correction to the atomization energy was on average –0.7 kcal/mol. From that study, it can be seen that typically the atomization energy is lowered when scalar relativistic effects are included.

A few general trends can be observed from the scalar relativistic correction in Table 4.4. The magnitude of the scalar relativistic correction is lower at higher basis set levels. This is consistent with previous work,[128] which noted that calculations which account for more of the electron correlation results in a reduced scalar relativistic correction to the atomization energy. In comparing the scalar relativistic correction from cc-pV5Z-DK and cc-pV5Z-PP, using the DK method always yields a lower (more negative) scalar relativistic effect. As shown at the bottom of Table 4.4, the total mean absolute deviation for cc-pV*n*Z-DK is lower than that for cc-pV*n*Z-PP at all basis set levels but the double ζ-level. For the 18 molecules studied, the overall atomization energy is lowered by slightly less than 1.0 kcal/mol, which is slightly larger the change in atomization energy for molecules containing first- and second-row atoms. There are however, some exceptions when the scalar relativistic correction is larger than 1.0 kcal/mol. This is important since the target accuracy for calculating atomization energy is 1.0 kcal/mol.

The largest correction for scalar relativity for atomization energy was found for GeH_4, GeS_2, and KrF_2. At the quintuple-ζ level, the atomization energy of GeH_4 is lowered by 2.37, 2.04, and 3.18 kcal/mol when using the cc-pV5Z-DK, cc-pV5Z-PP, and aug-cc-pV5Z-PP basis sets, respectively. The scalar relativistic correction for GeS_2 is slightly lower, but still between 2-3 kcal/mol. KrF_2 has the largest spread (~1 kcal/mol) of scalar relativistic corrections when comparing cc-pV5Z-PP to aug-cc-pV5Z-PP. Generally at higher ζ-levels, the difference in the scalar relativistic correction when using the cc-pV*n*Z-PP and aug-cc-pV*n*Z-PP basis sets is closer to 0.01-0.02 kcal/mol. This large difference in values can also be seen in the non-relativistic

atomization energies of KrF_2, which also converge much faster when using the aug-cc-pV*n*Z basis sets. It must also be noted that at lower levels of electron correlation calculations (CCSD(T)/cc-pVDZ), the atomization energy of KrF_2 is negative, which represents an unstable system. A further study of krypton containing compounds is contained in later chapters of this manuscript.

There are only a handful of other studies that have incorporated scalar relativistic effects in atomization energy calculations for the molecules included in this study. In comparing to the previously calculated scalar relativistic corrections using the Douglas-Kroll approach, the calculated corrections in this chapter are of similar sign and magnitude. The benchmark calculations that were preformed by de Jong *et al.*, after they created the cc-pV*n*Z-DK basis sets, included CISD/cc-pVTZ-DK calculations to estimate the scalar relativistic correction. They predicted the scalar relativistic corrections for dissociation energies to be –1.06, –1.05, and –0.74 kcal/mol for Br_2, BrF, and BrCl, respectively. The CCSD(T)/cc-pVTZ-DK corrections for these molecules, as found in this study, were approximately half of the size from the previous study, and are –0.44, –0.60, and –0.35 kcal/mol for Br_2, BrF, and BrCl, respectively. This is expected because the inclusion of the triples in CCSD(T) significantly increase the correlation energy recovered as compared with CISD and is consistent with the idea that at higher levels of electron correlation, the effects due to scalar relativity diminish. The change in scalar relativistic corrections to the atomization energy was found to be the largest for GeH_4, when compared to Ricca and Bauschlicher's previous studies.[131]

The magnitude of their scalar relativistic prediction was based upon a B3LYP/6-311++G(2df,2p) geometry and used the Douglas-Kroll approach with the modified coupled pair

functional (MCPF) and a triple-ζ basis to predict a scalar relativistic correction of -3.58 kcal/mol for the atomization energy. This correction is 1.24 kcal/mol larger than the predicted CCSD(T)/cc-pVTZ-DK correction in Table 4.4 for GeH_4 and is ~1.7 kcal/mol larger than the pseudopotential corrections determined using a triple-ζ basis set. Also, in light of findings by de Jong and co-workers on the use of non-relativistic contracted basis sets with the Douglas-Kroll approach, there should be considerable error in the scalar relativistic correction estimated by Ricca and Bauschlicher on GeH_4 because their calculations use a non-relativistic contracted basis set with a relativistic method.

In more recent work by Feller and co-workers,[22] CCSD(T)/aug-cc-pVQZ geometries were used and scalar relativistic corrections were then determined using CCSD(T)/cc-pVQZ-DK for a group of small halogens. Their bromine systems (HBr, Br_2, BrF, BrCl, CH_3Br) have very similar (<0.1 kcal/mol) scalar relativistic corrections to all of the quadruple-ζ values reported in Table 4.4, with the exception of the CH_3Br pseudopotential calculations that are 0.3 kcal/mol smaller than their correction. These differences in scalar relativistic corrections reflect the slight change when using the aug-cc-pVQZ geometry for the cc-pVQZ-DK relativistic calculations. The PP methodology was utilized as introduced by Peterson, and the relativistic atomization energies for several species (As_2, Br_2, HBr, GaCl, GeO, Ge^-, Br^-) are nearly identical to his results.[26,27] (There is a slight difference of <0.2 kcal/mol at the quintuple zeta basis set level, which can be accounted for due to the different means used for the calculation of the spin effects in the two studies.)

At the bottom of Table 4.4, the total mean absolute deviation of the atomization energies as compared with experiment is given. As noted in prior studies[24,133] the scalar relativistic corrections do not result in a large change in the mean absolute deviation of the atomization

energies from experiment. Rather, in all cases (cc-pV*n*Z-DK, cc-pV*n*Z-PP, and aug-cc-pV*n*Z-PP), the scalar relativistic correction results in an increase in the mean absolute deviation from experiment by ~1.0 kcal/mol, or less. Exceptions to this overall increase in the deviation of the atomization energy upon the inclusion of scalar relativistic effects include GeH_4 and KrF_2.

The mean absolute deviation in atomization energy has been tabulated for each of the five-extrapolation schemes, which can be found in Table 4.5. At each basis set level, the deviation from experiment slightly increases as compared to the previous results. However, the inclusion of scalar relativity improves the convergence of the atomization energy to the CBS limit. This can be seen at the higher basis set levels, where the deviation from experiment at the individual ζ-levels increase and the two-point CBS limits decrease. For example, when comparing the total mean absolute values from Table 4.4 at the triple and quadruple ζ-levels for aug-cc-pV*n*Z (4.55 and 1.98 kcal/mol) and aug-cc-pV*n*Z-PP (5.15 and 2.49 kcal/mol) there is an increase in the deviation from experiment, while the $CBS_{T\text{-}Q}$ listed in Table 4.10 for these basis set decrease from 1.18 (aug-cc-pV*n*Z) to 0.98 kcal/mol (aug-cc-pV*n*Z-PP) kcal/mol. Because the error in the individual data points increase and the CBS limit values decrease, this indicates that when including the scalar relativistic corrections the individual data points define a better convergence to the CBS limit.

Table 4.4. Atomization energies in kcal/mol determined using CCSD(T) in combination with the cc-pV*n*Z, aug-cc-pV*n*Z, cc-pV*n*Z-DK, cc-pV*n*Z-PP, and aug-cc-pV*n*Z basis sets. The scalar relativistic effects are noted in parenthesis.

	cc-pV*n*Z[a]	aug-cc-pV*n*Z[a]	cc-pV*n*Z-DK	cc-pV*n*Z-PP	aug-cc-pV*n*Z-PP	Expt.
$GeH_4 \rightarrow Ge + 4H$						
n=D	255.26	257.10	252.53(-2.73)	252.28(-2.98)	255.29(-1.82)	270.5[b]
T	267.45	268.75	265.10(-2.34)	265.53(-1.91)	266.78(-1.97)	
Q	271.27	272.86	268.90(-2.37)	269.22(-2.05)	269.64(-3.22)	
5	272.10	273.48	269.73(-2.37)	270.06(-2.04)	270.30(-3.18)	

(table continues on next page)

(Table 4.4 continued)

	cc-pV*n*Z[a]	aug-cc-pV*n*Z[a]	cc-pV*n*Z-DK	cc-pV*n*Z-PP	aug-cc-pV*n*Z-PP	Expt.
$AsH \rightarrow As + H$						
D	56.00	56.99	55.46(-0.55)	55.42(-0.59)	56.98(-0.01)	64.6[c]
T	60.92	61.68	60.46(-0.46)	60.54(-0.38)	61.28(-0.41)	
Q	62.59	62.89	62.12(-0.48)	62.21(-0.38)	62.48(-0.41)	
5	63.06	63.21	62.58(-0.48)	62.68(-0.39)	62.81(-0.40)	
$AsH_2 \rightarrow As + 2H$						
D	118.27	121.02	117.06(-1.20)	116.99(-1.28)	119.83(-1.19)	131.1[c]
T	127.26	127.92	126.24(-1.02)	126.42(-0.84)	127.74(-0.18)	
Q	130.33	130.58	129.30(-1.04)	129.49(-0.84)	129.97(-0.61)	
5	131.19	131.17	130.15(-1.04)	130.34(-0.85)	130.57(-0.60)	
$AsH_3 \rightarrow As + 3H$						
D	186.79	189.42	184.86(-1.93)	184.75(-2.04)	188.30(-1.13)	206.0[c]
T	198.88	200.70	197.24(-1.65)	197.53(-1.36)	199.19(-1.51)	
Q	203.03	203.04	201.36(-1.66)	201.67(-1.36)	202.27(-0.77)	
5	204.16	203.84	202.49(-1.67)	202.78(-1.37)	203.10(-0.74)	
$SeH \rightarrow Se + H$						
D	67.47	68.79	66.84(-0.62)	66.80(-0.67)	68.64(-0.15)	74.3[d]
T	71.90	72.22	71.38(-0.52)	71.47(-0.42)	72.29(+0.07)	
Q	73.64	73.94	73.11(-0.53)	73.22(-0.43)	73.49(-0.44)	
5	74.11	74.27	73.57(-0.54)	73.68(-0.43)	73.83(-0.44)	
$SeH_2 \rightarrow Se + 2H$						
D	138.16	142.19	138.18(+0.02)	138.10(-0.06)	141.54(-0.65)	153.2[d]
T	146.74	148.34	146.38(-0.35)	146.57(-0.17)	148.10(-0.24)	
Q	150.34	151.18	149.52(-0.82)	149.74(-0.60)	150.25(-0.93)	
5	151.18	151.77	150.36(-0.82)	150.58(-0.60)	150.85(-0.93)	
$HBr \rightarrow Br + H$						
D	79.34	81.73	78.69(-0.65)	78.64(-0.70)	80.90(-0.83)	86.5[e]
T	83.72	84.68	83.16(-0.56)	83.12(-0.60)	84.05(-0.63)	
Q	85.45	85.78	84.88(-0.57)	84.88(-0.57)	85.18(-0.60)	
5	85.91	86.10	85.34(-0.57)	85.34(-0.57)	85.51(-0.59)	
$GeO \rightarrow Ge + O$						
D	133.94	141.68	132.82(-1.12)	132.61(-1.33)	140.53(-1.15)	155.2[e]
T	148.12	150.78	147.23(-0.90)	147.72(-0.40)	150.28(-0.50)	
Q	152.73	153.98	151.76(-0.97)	152.32(-0.41)	153.53(-0.45)	
5	154.42	154.96	153.42(-1.00)	153.97(-0.45)	154.50(-0.46)	
$GeS_2 \rightarrow Ge + 2S$						
D	161.64	166.18	158.68(-2.97)	158.65(-2.99)	163.28(-2.89)	191.7[f]
T	180.00	182.19	177.49(-2.51)	177.49(-2.51)	180.15(-2.04)	
Q	188.22	189.37	185.32(-2.90)	186.20(-2.01)	187.32(-2.04)	
5	191.74	192.27	188.78(-2.96)	189.72(-2.02)	190.09(-2.18)	

(table continues on next page)

(Table 4.4 continued)

	cc-pV*n*Z[a]	aug-cc-pV*n*Z[a]	cc-pV*n*Z-DK	cc-pV*n*Z-PP	aug-cc-pV*n*Z-PP	Expt.
$As_2 \rightarrow 2As$						
D	68.90	71.57	68.00(-0.90)	67.94(-0.96)	70.84(-0.73)	91.3[g]
T	80.67	82.40	80.05(-0.62)	80.38(-0.29)	81.90(-0.49)	
Q	85.99	86.91	85.30(-0.68)	85.56(-0.43)	86.40(-0.51)	
5	88.11	88.56	87.37(-0.74)	87.65(-0.46)	88.08(-0.48)	
$BrCl \rightarrow Br + Cl$						
D	35.46	38.43	35.26(-0.20)	35.22(-0.24)	38.52(+0.09)	51.5[e]
T	44.92	46.43	44.56(-0.35)	44.65(-0.26)	46.16(-0.26)	
Q	48.58	49.33	48.17(-0.40)	48.29(-0.29)	49.01(-0.32)	
5	50.28	50.67	49.84(-0.44)	49.95(-0.33)	50.34(-0.33)	
$BrF \rightarrow Br + F$						
D	40.75	51.79	40.34(-0.42)	40.27(-0.49)	51.12(-0.67)	58.9[e]
T	52.40	56.32	51.80(-0.60)	52.01(-0.39)	55.87(-0.45)	
Q	56.91	58.45	56.27(-0.64)	56.42(-0.49)	57.93(-0.52)	
5	58.40	59.04	57.74(-0.66)	57.88(-0.51)	58.51(-0.53)	
$BrO \rightarrow Br + O$						
D	34.62	44.21	34.13(-0.49)	34.05(-0.57)	43.41(-0.81)	55.3[e]
T	47.65	51.05	46.96(-0.69)	47.12(-0.52)	50.40(-0.64)	
Q	51.78	53.21	51.02(-0.76)	51.18(-0.60)	52.56(-0.65)	
5	53.40	54.00	52.61(-0.79)	52.74(-0.66)	53.33(-0.67)	
$BrB \rightarrow Br + B$						
D	92.56	93.07	92.45(-0.11)	92.34(-0.22)	93.01(-0.06)	103.5[g]
T	96.61	97.16	96.60(-0.01)	96.62(+0.01)	97.14(-0.01)	
Q	98.80	99.13	98.79(-0.01)	98.81(+0.01)	99.12(0.00)	
5	99.63	99.80	99.62(-0.02)	99.65(+0.01)	99.80(0.00)	
$Br_2 \rightarrow 2Br$						
D	31.07	33.09	30.80(-0.27)	30.66(-0.40)	33.02(-0.07)	45.4[e]
T	39.21	40.51	38.77(-0.44)	38.70(-0.51)	40.02(-0.49)	
Q	42.63	43.28	42.12(-0.51)	42.13(-0.50)	42.73(-0.55)	
5	43.95	44.31	43.40(-0.55)	43.41(-0.54)	43.75(-0.56)	
$CH_3Br \rightarrow Br + C + 3H$						
D	329.23	334.33	328.50(-0.73)	328.89(-0.34)	333.61(-0.71)	358.2[h]
T	348.13	350.78	347.51(-0.62)	347.67(-0.47)	350.21(-0.57)	
Q	353.70	354.64	352.98(-0.72)	353.19(-0.51)	354.12(-0.52)	
5	355.43	355.85	354.70(-0.73)	354.91(-0.52)	355.31(-0.54)	
$GaCl \rightarrow Ga + Cl$						
D	98.36	101.76	97.47(-0.90)	97.32(-1.04)	100.91(-0.85)	109.9[e]
T	104.49	105.72	103.61(-0.89)	103.90(-0.59)	105.12(-0.61)	
Q	107.35	107.95	106.40(-0.95)	106.82(-0.53)	107.45(-0.50)	
5	108.51	108.82	107.57(-0.94)	108.00(-0.51)	108.29(-0.53)	

(table continues on next page)

(Table 4.4 continued)

	cc-pV*n*Z[a]	aug-cc-pV*n*Z[a]	cc-pV*n*Z-DK	cc-pV*n*Z-PP	aug-cc-pV*n*Z-PP	Expt.
$KrF_2 \rightarrow Kr + 2F$						
D	-12.72	11.71	-11.96(+0.77)	-11.52(+1.20)	12.88(+1.18)	21.9[e]
T	8.57	18.08	8.93(+0.36)	8.83(+0.26)	19.86(+1.78)	
Q	16.44	20.24	17.73(+1.29)	18.24(+1.79)	20.97(+0.73)	
5	19.40	20.76	20.67(+1.27)	21.10(+1.70)	21.49(+0.73)	
Total mean absolute deviation						
D	17.08	12.10	18.28	18.32	13.14	
T	6.62	4.55	7.54	7.38	5.15	
Q	2.73	1.98	3.56	3.31	2.49	
5	1.47	1.32	2.18	1.93	1.60	

[a] cc-pV*n*Z and aug-cc-pV*n*Z results are from Ref. 134.
[b] From Refs. 101,102.
[c] From Ref. 104.
[d] From Ref. 105.
[e] From Ref. 106.
[f] From Ref. 107.
[g] From Ref. 92.
[h] From Ref. 108.

Table 4.5. Extrapolated CBS limits for atomization energies in kcal/mol using CCSD(T) in combination with cc-pV*n*Z, aug-cc-pV*n*Z, cc-pV*n*Z-DK, cc-pV*n*Z-PP, and aug-cc-pV*n*Z.

CBS Limit	cc-pV*n*Z[a]	aug-cc-pV*n*Z[a]	cc-pV*n*Z-DK	cc-pV*n*Z-PP	aug-cc-pV*n*Z-PP	G2[b]	G3[c]	Expt.
$GeH_4 \rightarrow Ge + 4H$								
D–T[d]	272.58	273.65	270.40	271.11	271.62	275.8	273.0	270.5[d]
T–Q[d]	274.06	275.86	271.66	271.91	271.73			
Q–5[d]	272.98	274.13	270.61	270.95	270.99			
Total[f]	272.09	273.57	269.77	270.37	270.48			
Property[f]	272.64	274.18	270.23	270.47	270.54			
$AsH \rightarrow As + H$								
D–T	62.99	63.66	62.56	62.70	63.09	63.2	64.7	64.6[g]
T–Q	63.81	63.77	63.33	63.42	63.35			
Q–5	63.56	63.54	63.07	63.16	63.15			
Total	63.03	63.16	62.57	62.83	62.89			
Property	63.34	63.31	62.84	62.94	62.94			
$AsH_2 \rightarrow As + 2H$								
D–T	131.05	130.83	130.11	130.39	131.08	131.8	131.9	131.1[g]
T–Q	132.57	132.52	131.52	131.73	131.59			
Q–5	132.08	131.78	131.04	131.23	131.21			
Total	131.16	131.17	130.15	130.65	130.74			
Property	131.70	131.71	130.64	130.81	130.82			
$AsH_3 \rightarrow As + 3H$								
D–T	203.98	205.45	202.45	202.91	203.78	205.6	204.6	206.0[g]
T–Q	206.05	204.74	204.38	204.69	204.52			
Q–5	205.35	204.67	203.67	203.95	203.96			
Total	204.15	203.67	202.53	203.23	203.34			
Property	204.86	203.90	203.15	203.41	203.44			

(table continues on next page)

(Table 4.5 continued)

CBS Limit	cc-pV*n*Z[a]	aug-cc-pV*n*Z[a]	cc-pV*n*Z-DK	cc-pV*n*Z-PP	aug-cc-pV*n*Z-PP	G2[b]	G3[c]	Expt.
$SeH \rightarrow Se + H$								
D–T	73.76	73.66	73.29	73.44	73.83	74.2	75.4	74.3[h]
T–Q	74.91	75.19	74.37	74.49	74.37			
Q–5	74.60	74.62	74.06	74.18	74.19			
Total	74.18	74.37	73.64	73.94	73.97			
Property	74.49	74.78	73.93	74.03	74.02			
$SeH_2 \rightarrow Se + 2H$								
D–T	150.35	150.93	149.84	150.14	150.87	152.1	152.3	153.2[h]
T–Q	152.97	153.26	151.81	152.05	151.81			
Q–5	152.05	152.39	151.23	151.46	151.47			
Total	151.41	151.94	150.51	151.06	151.10			
Property	152.03	152.54	151.02	151.21	151.18			
$HBr \rightarrow Br + H$								
D–T	85.56	85.93	85.04	85.01	85.38	85.9	86.7	86.5[i]
T–Q	86.71	86.58	86.13	86.16	86.01			
Q–5	86.39	86.44	85.82	85.82	85.85			
Total	86.05	86.16	85.47	85.66	85.69			
Property	86.29	86.32	85.70	85.72	85.72			
$GeO \rightarrow Ge + O$								
D–T	154.09	154.62	153.29	154.08	154.39	155.7	156.8	155.2[i]
T–Q	156.10	156.31	155.07	155.68	155.90			
Q–5	156.19	155.99	155.16	155.70	155.53			
Total	153.29	153.87	152.28	154.27	154.71			
Property	155.16	155.54	154.09	154.60	155.03			

(table continues on next page)

(Table 4.5 continued)

CBS Limit	cc-pV*n*Z[a]	aug-cc-pV*n*Z[a]	cc-pV*n*Z-DK	cc-pV*n*Z-PP	aug-cc-pV*n*Z-PP	G2[b]	G3[c]	Expt.
$GeS_2 \rightarrow Ge + 2S$								
D–T	187.73	188.93	185.42	185.42	187.26	193.9	193.6	191.7[j]
T–Q	194.22	194.60	191.03	192.56	192.55			
Q–5	195.43	194.39	192.41	193.41	192.99			
Total	191.47	191.87	188.36	191.38	191.30			
Property	194.62	194.70	191.20	192.84	192.21			
$As_2 \rightarrow 2As$								
D–T	85.62	86.95	85.12	85.62	86.56	91.2	91.7	91.3[k]
T–Q	89.87	90.20	89.14	89.33	89.68			
Q–5	90.34	90.29	89.54	89.85	89.85			
Total	87.90	88.37	87.23	88.25	88.57			
Property	89.92	89.80	89.02	89.16	89.28			
$BrCl \rightarrow Br + Cl$								
D–T	48.90	49.80	48.48	48.63	49.38	50.0	51.2	51.5[i]
T–Q	51.25	51.44	50.81	50.94	51.08			
Q–5	52.06	52.07	51.58	51.69	51.73			
Total	50.04	50.28	49.47	50.63	50.80			
Property	51.28	51.35	50.82	50.93	51.06			
$BrF \rightarrow Br + F$								
D–T	57.30	58.23	56.63	56.95	57.86	59.1	58.6	58.9[i]
T–Q	60.20	60.00	59.52	59.64	59.43			
Q–5	59.96	59.66	59.28	59.42	59.11			
Total	57.87	58.19	57.00	58.62	58.80			
Property	59.42	59.68	58.77	58.83	59.06			

(table continues on next page)

(Table 4.5 continued)

CBS Limit	cc-pV*n*Z[a]	aug-cc-pV*n*Z[a]	cc-pV*n*Z-DK	cc-pV*n*Z-PP	aug-cc-pV*n*Z-PP	G2[b]	G3[c]	Expt.
$BrO \rightarrow Br + O$								
D–T	53.13	53.92	52.36	52.63	53.35	53.6	55.2	55.3[i]
T–Q	54.80	54.79	53.99	54.14	54.13			
Q–5	55.10	54.83	54.28	54.38	54.14			
Total	53.05	53.44	52.13	53.25	53.54			
Property	54.04	54.33	53.24	53.33	53.63			
$BrB \rightarrow Br + B$								
D–T	98.32	98.87	98.35	98.43	98.88	101.2	102.8	103.5[j]
T–Q	100.40	100.56	100.39	100.41	100.57			
Q–5	100.50	100.50	100.48	100.52	100.50			
Total	99.72	99.81	99.67	100.16	100.21			
Property	100.63	100.49	100.57	100.56	100.49			
$Br_2 \rightarrow 2Br$								
D–T	42.64	43.64	42.13	42.08	42.97	43.0	45.5	45.4[i]
T–Q	45.13	45.30	44.57	44.64	44.71			
Q–5	45.34	45.40	44.75	44.76	44.82			
Total	44.16	44.43	43.59	44.11	44.21			
Property	44.94	44.93	44.37	44.41	44.40			
$CH_3Br \rightarrow Br + C + 3H$								
D–T	356.10	357.70	355.52	355.57	357.20	357.5	357.9	358.2[l]
T–Q	357.77	357.46	356.97	357.22	356.98			
Q–5	357.25	357.12	356.51	356.72	356.57			
Total	355.65	355.75	354.85	355.57	355.53			
Property	356.12	356.09	355.33	355.59	355.54			

(table continues on next page)

(Table 4.5 continued)

CBS Limit	cc-pV*n*Z[a]	aug-cc-pV*n*Z[a]	cc-pV*n*Z-DK	cc-pV*n*Z-PP	aug-cc-pV*n*Z-PP	G2[b]	G3[c]	Expt.
$GaCl \rightarrow Ga + Cl$								
D–T	107.08	107.39	106.20	106.67	106.89	110.1	111.4	109.9[i]
T–Q	109.43	109.57	108.44	108.95	109.16			
Q–5	109.72	109.73	108.79	109.24	109.16			
Total	107.39	107.73	106.37	108.36	108.62			
Property	109.54	109.93	108.56	108.97	109.36			
$KrF_2 \rightarrow Kr + 2F$								
D–T	17.54	20.76	17.73	17.40	22.80	23.8	22.5	21.9[i]
T–Q	22.19	21.81	24.16	25.10	21.78			
Q–5	22.51	21.31	23.75	24.10	22.04			
Total	19.60	19.93	20.83	23.54	21.25			
Property	21.12	21.11	23.04	23.97	21.43			

[a] cc-pV*n*Z and aug-cc-pV*n*Z results are from Ref. 134.
[b] Gaussian-2 values are from Ref. 68.
[c] Gaussian-3 values are from Ref.72.
[d] Two-point extrapolation is from Eqn 3.1. "D–T" in table refers to the $CBS_{D\text{-}T}$ extrapolation using results from double-ζ and triple-ζ basis sets. "T–Q" refers to the $CBS_{T\text{-}Q}$ extrapolation and "Q–5" refers to the $CBS_{Q\text{-}5}$ extrapolation.
[e] From Refs. 101,102.
[f] Where Total=CBS_{total} and Property=CBS_{prop} from Eqn 3.2 and 3.3, respectively.
[g] From Ref. 104.
[h] From Ref. 105.
[i] From Ref. 106.
[j] From Ref. 107.
[k] From Ref. 92.
[l] From Ref. 108.

4.3.3. Ionization Energy

In Table 4.6, relativistic CCSD(T) ionization energies for molecules of the third-row G2 test suite are reported, and additionally, the signs and magnitudes of the scalar relativistic effects are provided. Typically, the scalar relativistic corrections for ionization energies are approximately half of the size of those determined for atomization energies. As shown in Table 4.6, the molecule with the largest scalar relativistic correction is SeH^+ with a correction of ~0.05 eV for both the cc-pV5Z-DK and cc-pV5Z-PP basis sets. Kedziora *et al.*,[133] report ionization energy scalar relativistic corrections for Al-Cl, and compared to their corrections, the third-row corrections are approximately two to three times larger than the values for second-row species. This increase in the magnitude of scalar relativistic correction from second- to third-row species was expected.

Again, the results from the use of the cc-pV*n*Z-DK and the cc-pV*n*Z-PP basis sets are almost indistinguishable when comparing the error at each ζ-level. Only a slightly smaller mean absolute deviation is obtained with the pseudopotential basis set, as is shown at the bottom of Table 4.6. On the other hand, there is a more substantial decrease in the mean absolute deviation when using the aug-cc-pV*n*Z-PP sets as compared with the cc-pV*n*Z-PP or cc-pV*n*Z-DK sets for ionization energy.

Table 4.6. Ionization energies in eV using CCSD(T) in combination with cc-pV*n*Z, aug-cc-pV*n*Z, cc-pV*n*Z-DK, cc-pV*n*Z-PP, and aug-cc-pV*n*Z. The scalar relativistic effects are noted in parenthesis.

	cc-pV*n*Z[a]	aug-cc-pV*n*Z[a]	cc-pV*n*Z-DK	cc-pV*n*Z-PP	aug-cc-pV*n*Z-PP	Expt.
$Ga \rightarrow Ga^+$						
n=D	5.822	5.848	5.785(-0.037)	5.804(-0.018)	5.817(-0.031)	5.999[b]
T	5.901	5.910	5.867(-0.034)	5.883(-0.017)	5.890(-0.021)	
Q	5.936	5.937	5.901(-0.035)	5.902(-0.034)	5.904(-0.032)	
5	5.945	5.945	5.908(-0.036)	5.910(-0.035)	5.911(-0.034)	

(table continues on next page)

(Table 4.6 continued)

	cc-pV*n*Z[a]	aug-cc-pV*n*Z[a]	cc-pV*n*Z-DK	cc-pV*n*Z-PP	aug-cc-pV*n*Z-PP	Expt.
$Ge \rightarrow Ge^+$						
D	7.674	7.722	7.640(-0.034)	7.655(-0.019)	7.690(-0.032)	7.899[b]
T	7.798	7.810	7.766(-0.032)	7.771(-0.027)	7.779(-0.031)	
Q	7.822	7.827	7.791(-0.032)	7.792(-0.030)	7.796(-0.030)	
5	7.832	7.834	7.800(-0.032)	7.801(-0.030)	7.803(-0.030)	
$As \rightarrow As^+$						
D	9.510	9.584	9.482(-0.028)	9.497(-0.013)	9.554(-0.030)	9.788[b]
T	9.682	9.700	9.656(-0.026)	9.667(-0.016)	9.677(-0.023)	
Q	9.719	9.725	9.692(-0.027)	9.694(-0.025)	9.700(-0.024)	
5	9.730	9.733	9.703(-0.027)	9.706(-0.025)	9.708(-0.025)	
$Se \rightarrow Se^+$						
D	9.091	9.241	9.060(-0.031)	9.069(-0.023)	9.191(-0.050)	9.752[b]
T	9.507	9.558	9.475(-0.032)	9.489(-0.018)	9.526(-0.031)	
Q	9.648	9.665	9.614(-0.034)	9.611(-0.037)	9.628(-0.037)	
5	9.691	9.699	9.657(-0.034)	9.655(-0.036)	9.663(-0.036)	
$Br \rightarrow Br^+$						
D	11.285	11.437	11.257(-0.028)	11.239(-0.046)	11.378(-0.060)	11.814[b]
T	11.566	11.621	11.540(-0.026)	11.563(-0.002)	11.595(-0.027)	
Q	11.723	11.745	11.695(-0.028)	11.689(-0.034)	11.711(-0.034)	
5	11.773	11.782	11.744(-0.029)	11.739(-0.034)	11.749(-0.034)	
$Kr \rightarrow Kr^+$						
D	13.504	13.699	13.482(-0.022)	13.498(-0.007)	13.652(-0.048)	13.999[b]
T	13.701	13.752	13.683(-0.018)	13.727(+0.026)	13.744(-0.008)	
Q	13.868	13.893	13.847(-0.020)	13.850(-0.018)	13.875(-0.017)	
5	13.923	13.934	13.902(-0.021)	13.906(-0.017)	13.917(-0.018)	
$AsH \rightarrow AsH^+$						
D	9.352	9.419	9.327(-0.025)	9.337(-0.015)	9.412(-0.006)	9.641[c]
T	9.524	9.551	9.501(-0.023)	9.511(-0.013)	9.531(-0.020)	
Q	9.567	9.609	9.543(-0.024)	9.545(-0.022)	9.555(-0.053)	
5	9.581	9.617	9.557(-0.024)	9.559(-0.022)	9.563(-0.053)	
$AsH_2 \rightarrow AsH_2^+$						
D	9.138	9.242	9.116(-0.022)	9.120(-0.018)	9.212(-0.029)	9.443[c]
T	9.320	9.322	9.299(-0.021)	9.309(-0.011)	9.337(+0.015)	
Q	9.369	9.372	9.347(-0.022)	9.349(-0.021)	9.363(-0.009)	
5	9.385	9.379	9.363(-0.022)	9.364(-0.021)	9.370(-0.009)	
$SeH \rightarrow SeH^+$						
D	9.316	9.469	9.266(-0.051)	9.276(-0.041)	9.421(-0.048)	9.845[d]
T	9.688	9.724	9.635(-0.053)	9.648(-0.041)	9.695(-0.029)	
Q	9.812	9.812	9.760(-0.052)	9.759(-0.053)	9.779(-0.032)	
5	9.851	9.839	9.799(-0.052)	9.798(-0.053)	9.807(-0.032)	

(table continues on next page)

(Table 4.6 continued)

	cc-pV*n*Z[a]	aug-cc-pV*n*Z[a]	cc-pV*n*Z-DK	cc-pV*n*Z-PP	aug-cc-pV*n*Z-PP	Expt.
$SeH_2 \rightarrow SeH_2^+$						
D	9.361	9.576	9.360(-0.001)	9.370(+0.009)	9.535(-0.041)	9.886[d]
T	9.736	9.801	9.681(-0.055)	9.693(-0.043)	9.746(-0.055)	
Q	9.804	9.840	9.790(-0.014)	9.790(-0.015)	9.812(-0.028)	
5	9.838	9.861	9.824(-0.015)	9.824(-0.014)	9.835(-0.026)	
$HBr \rightarrow HBr^+$						
D	11.159	11.354	11.132(-0.027)	11.126(-0.033)	11.298(-0.056)	11.660[e]
T	11.424	11.487	11.400(-0.024)	11.418(-0.007)	11.461(-0.026)	
Q	11.563	11.588	11.537(-0.026)	11.533(-0.030)	11.557(-0.031)	
5	11.607	11.618	11.580(-0.027)	11.576(-0.030)	11.587(-0.031)	
$BrF \rightarrow BrF^+$						
D	11.363	11.564	11.340(-0.024)	11.359(-0.005)	11.526(-0.038)	11.780[e]
T	11.497	11.614	11.481(-0.016)	11.519(+0.022)	11.600(-0.013)	
Q	11.655	11.702	11.639(-0.016)	11.645(-0.010)	11.684(-0.018)	
5	11.713	11.730	11.696(-0.016)	11.703(-0.009)	11.712(-0.018)	
$HOBr \rightarrow HOBr^+$						
D	10.300	10.559	10.248(-0.052)	10.219(-0.081)	10.469(-0.090)	10.638[f]
T	10.475	10.559	10.430(-0.045)	10.448(-0.027)	10.563(+0.004)	
Q	10.607	10.642	10.579(-0.028)	10.594(-0.013)	10.624(-0.019)	
5	10.661	10.667	10.633(-0.028)	10.639(-0.023)	10.649(-0.019)	
$Br_2 \rightarrow Br_2^+$						
D	10.199	10.341	10.161(-0.037)	10.148(-0.050)	10.268(-0.073)	10.520[e]
T	10.329	10.388	10.297(-0.032)	10.322(-0.008)	10.354(-0.034)	
Q	10.459	10.485	10.425(-0.034)	10.420(-0.039)	10.445(-0.040)	
5	10.502	10.514	10.468(-0.035)	10.462(-0.040)	10.473(-0.040)	
Total mean absolute deviation						
D	0.400	0.253	0.429	0.425	0.291	
T	0.175	0.129	0.211	0.193	0.153	
Q	0.077	0.061	0.108	0.107	0.075	
5	0.053	0.042	0.074	0.073	0.055	

[a] cc-pV*n*Z and aug-cc-pV*n*Z results are from Ref. 134.
[b] From Ref. 87.
[c] From Ref. 104.
[d] From Ref. 105.
[e] From Ref. 92.
[f] From Ref. 109.

Table 4.7. Extrapolated CBS limits for ionization energies in eV using CCSD(T) in combination with cc-pV*n*Z, aug-cc-pV*n*Z, cc-pV*n*Z-DK, cc-pV*n*Z-PP, and aug-cc-pV*n*Z.

CBS Limit	cc-pV*n*Z[a]	aug-cc-pV*n*Z[a]	cc-pV*n*Z-DK	cc-pV*n*Z-PP	aug-cc-pV*n*Z-PP	G2[b]	G3[c]	Expt.
$Ga \rightarrow Ga^+$								
D–T[d]	5.934	5.936	5.901	5.917	5.920	5.93	6.00	5.999[e]
T–Q[d]	5.961	5.956	5.926	5.915	5.915			
Q–5[d]	5.954	5.953	5.917	5.918	5.918			
Total[f]	5.943	5.942	5.907	5.909	5.910			
Property[f]	5.954	5.952	5.916	5.911	5.911			
$Ge \rightarrow Ge^+$								
D–T	7.850	7.847	7.819	7.819	7.816	7.80	7.90	7.899[e]
T–Q	7.840	7.839	7.809	7.808	7.809			
Q–5	7.841	7.841	7.809	7.811	7.810			
Total	7.829	7.831	7.798	7.801	7.803			
Property	7.832	7.834	7.800	7.801	7.803			
$As \rightarrow As^+$								
D–T	9.755	9.749	9.729	9.738	9.729	9.70	9.81	9.788[e]
T–Q	9.745	9.742	9.718	9.714	9.717			
Q–5	9.742	9.741	9.715	9.718	9.717			
Total	9.728	9.728	9.701	9.607	9.708			
Property	9.732	9.734	9.704	9.705	9.708			
$Se \rightarrow Se^+$								
D–T	9.682	9.691	9.649	9.666	9.668	9.64	9.71	9.752[e]
T–Q	9.751	9.744	9.716	9.701	9.703			
Q–5	9.737	9.734	9.702	9.701	9.699			
Total	9.690	9.697	9.657	9.665	9.671			
Property	9.693	9.718	9.680	9.670	9.676			

(table continues on next page)

(Table 4.7 continued)

CBS Limit	cc-pV*n*Z[a]	aug-cc-pV*n*Z[a]	cc-pV*n*Z-DK	cc-pV*n*Z-PP	aug-cc-pV*n*Z-PP	G2[b]	G3[c]	Expt.
$Br \rightarrow Br^+$								
D–T	11.684	11.699	11.659	11.700	11.686	11.72	11.79	11.814[e]
T–Q	11.839	11.835	11.809	11.781	11.796			
Q–5	11.824	11.822	11.795	11.791	11.788			
Total	11.782	11.789	11.752	11.759	11.770			
Property	11.840	11.852	11.808	11.770	11.796			
$Kr \rightarrow Kr^+$								
D–T	13.784	13.774	13.768	13.823	13.783	13.86	13.94	13.999[e]
T–Q	13.990	13.995	13.967	13.940	13.971			
Q–5	13.981	13.978	13.958	13.964	13.960			
Total	13.944	13.954	13.920	13.938	13.960			
Property	13.988	14.112	14.037	13.970	14.187			
$AsH \rightarrow AsH^+$								
D–T	9.596	9.606	9.574	9.584	9.581	9.54	9.68	9.641[g]
T–Q	9.598	9.651	9.574	9.570	9.573			
Q–5	9.595	9.625	9.571	9.573	9.571			
Total	9.580	9.619	9.556	9.559	9.564			
Property	9.584	9.630	9.562	9.558	9.564			
$AsH_2 \rightarrow AsH_2^+$								
D–T	9.397	9.355	9.377	9.389	9.389	9.34	9.48	9.443[g]
T–Q	9.405	9.408	9.383	9.377	9.381			
Q–5	9.401	9.387	9.379	9.381	9.378			
Total	9.384	9.382	9.363	9.365	9.371			
Property	9.390	9.398	9.366	9.362	9.371			

(table continues on next page)

(Table 4.7 continued)

CBS Limit	cc-pV*n*Z[a]	aug-cc-pV*n*Z[a]	cc-pV*n*Z-DK	cc-pV*n*Z-PP	aug-cc-pV*n*Z-PP	G2[b]	G3[c]	Expt.
$SeH \rightarrow SeH^+$								
D–T	9.845	9.831	9.790	9.804	9.811	9.80	9.84	9.845[h]
T–Q	9.902	9.876	9.852	9.840	9.841			
Q–5	9.893	9.868	9.840	9.840	9.836			
Total	9.853	9.840	9.802	9.810	9.815			
Property	9.869	9.852	9.825	9.812	9.818			
$SeH_2 \rightarrow SeH_2^+$								
D–T	9.894	9.896	9.816	9.829	9.835	9.85	9.90	9.886[h]
T–Q	9.854	9.868	9.869	9.860	9.860			
Q–5	9.874	9.884	9.859	9.860	9.859			
Total	9.835	9.858	9.828	9.835	9.841			
Property	9.836	9.859	9.839	9.834	9.837			
$HBr \rightarrow HBr^+$								
D–T	11.536	11.543	11.513	11.540	11.529	11.58	11.63	11.660[i]
T–Q	11.664	11.661	11.637	11.617	11.627			
Q–5	11.652	11.649	11.625	11.622	11.618			
Total	11.617	11.625	11.589	11.596	11.607			
Property	11.660	11.686	11.630	11.608	11.640			
$BrF \rightarrow BrF^+$								
D–T	11.553	11.634	11.540	11.587	11.632	11.71	11.75	11.780[i]
T–Q	11.771	11.767	11.755	11.737	11.746			
Q–5	11.773	11.759	11.756	11.764	11.741			
Total	11.750	11.751	11.731	11.745	11.742			
Property	11.745	11.742	11.943	11.822	11.846			

(table continues on next page)

(Table 4.7 continued)

CBS Limit	cc-pV*n*Z[a]	aug-cc-pV*n*Z[a]	cc-pV*n*Z-DK	cc-pV*n*Z-PP	aug-cc-pV*n*Z-PP	G2[b]	G3[c]	Expt.
$HOBr \rightarrow HOBr^+$								
D–T	10.549	10.559	10.507	10.544	10.602	10.65	10.66	10.638[j]
T–Q	10.703	10.703	10.688	10.701	10.668			
Q–5	10.718	10.693	10.690	10.685	10.675			
Total	10.685	10.686	10.659	10.679	10.665			
Property	10.699	10.678	10.767	10.715	10.702			
$Br_2 \rightarrow Br_2^+$								
D–T	10.385	10.408	10.355	10.395	10.390	10.49	10.53	10.520[i]
T–Q	10.553	10.555	10.518	10.491	10.511			
Q–5	10.548	10.544	10.512	10.506	10.503			
Total	10.516	10.524	10.480	10.486	10.499			
Property	10.524	10.526	10.600	10.515	10.598			

[a] cc-pV*n*Z and aug-cc-pV*n*Z results are from Ref. 134.
[b] Gaussian-2 values are from Ref. 68.
[c] Gaussian-3 values are from Ref. 72.
[d] Two-point extrapolation is from Eqn. 3.1. "D–T" in table refers to the $CBS_{D\text{-}T}$ extrapolation using results from double-ζ and triple-ζ basis sets. "T–Q" refers to the $CBS_{T\text{-}Q}$ extrapolation and "Q–5" refers to the $CBS_{Q\text{-}5}$ extrapolation.
[e] From Ref. 141.
[f] Where Total=CBS_{total} and Property=CBS_{prop} from Eqn. 3.2 and 3.3, respectively.
[g] From Ref. 104.
[h] From Ref. 105.
[i] From Ref. 92.
[j] From Ref. 109.

4.3.4. Electron and Proton Affinity

The electron affinities and proton affinities calculated using CCSD(T) are provided in Table 4.8. The magnitude of the scalar relativistic correction for electron and proton affinities is comparable to that of the ionization energies. For the four systems studied, the scalar relativistic corrections to the electron affinities were all very similar at the quintuple-ζ level, and range between –0.025 and –0.044 eV as determined using the cc-pV5Z-DK and aug-cc-pV5Z-PP basis sets. For Ge and Br, cc-pV5Z-PP results in corrections of slightly smaller magnitude, of –0.013 and –0.011 eV, respectively. For the HBr proton affinity, the scalar relativistic corrections are positive, which is contrary to the usual energy change. Mean absolute deviations are not reported for electron affinities and proton affinities due to the very small size of the G2 third-row test suite, with only four electron affinities and two proton affinities.

Table 4.8. Electron and proton affinities in eV using CCSD(T) in combination with cc-pV*n*Z, aug-cc-pV*n*Z, cc-pV*n*Z-DK, cc-pV*n*Z-PP, and aug-cc-pV*n*Z-PP. The scalar relativistic effects are noted in parenthesis.

	cc-pV*n*Z[a]	aug-cc-pV*n*Z[a]	cc-pV*n*Z-DK	cc-pV*n*Z-PP	aug-cc-pV*n*Z-PP	Expt.
$Ge^- \rightarrow Ge$						
D	0.615	1.145	0.580(-0.035)	0.647(+0.031)	1.115(-0.030)	1.233[b]
T	0.996	1.237	0.957(-0.039)	0.992(-0.004)	1.199(-0.038)	
Q	1.159	1.252	1.121(-0.039)	1.140(-0.019)	1.215(-0.037)	
5	1.197	1.257	1.158(-0.039)	1.184(-0.013)	1.219(-0.037)	
$Br^- \rightarrow Br$						
D	2.042	3.155	2.268(+0.226)	2.427(+0.385)	3.115(-0.040)	3.364[b]
T	2.858	3.230	2.920(+0.062)	2.837(-0.020)	3.188(-0.043)	
Q	3.203	3.338	3.198(-0.005)	3.207(+0.004)	3.294(-0.044)	
5	3.296	3.368	3.271(-0.025)	3.285(-0.011)	3.324(-0.044)	
$SeH^- \rightarrow SeH$						
D	1.130	2.005	1.091(-0.038)	1.212(-0.033)	1.968(-0.056)	2.213[c]
T	1.826	2.151	1.790(-0.036)	1.749(-0.007)	2.089(-0.026)	
Q	2.079	2.178	2.041(-0.038)	2.059(-0.030)	2.161(-0.031)	
5	2.153	2.198	2.114(-0.039)	2.136(-0.030)	2.180(-0.031)	

(table continues on next page)

(Table 4.8 continued)

	cc-pV*n*Z[a]	aug-cc-pV*n*Z[a]	cc-pV*n*Z-DK	cc-pV*n*Z-PP	aug-cc-pV*n*Z-PP	Expt.
$BrO^- \rightarrow BrO$						
D	1.053	2.254	1.023(-0.030)	1.046(-0.006)	2.233(-0.021)	2.360[d]
T	1.743	2.342	1.713(-0.030)	1.713(-0.030)	2.315(-0.027)	
Q	2.135	2.418	2.104(-0.031)	2.111(-0.024)	2.389(-0.029)	
5	2.326	2.440	2.294(-0.031)	2.300(-0.026)	2.411(-0.029)	
$H^+ + Br^- \rightarrow HBr$						
D	14.716	13.977	14.730(+0.014)	14.569(-0.147)	13.981(+0.004)	14.000[c]
T	14.273	14.043	14.287(+0.014)	14.368(+0.094)	14.058(+0.016)	
Q	14.071	13.986	14.087(+0.016)	14.078(+0.007)	14.004(+0.018)	
5	14.017	13.972	14.035(+0.018)	14.021(+0.004)	13.990(+0.018)	
$H^+ + CH_3Br \rightarrow CH_4Br^+$						
D	6.951	6.847	6.940(-0.011)	6.930(-0.021)	6.854(+0.007)	6.820[e]
T	6.901	6.880	6.885(-0.017)	6.875(-0.027)	6.858(-0.022)	
Q	6.846	6.840	6.834(-0.012)	6.834(-0.011)	6.821(-0.019)	
5	6.825	6.827	6.814(-0.011)	6.814(-0.011)	6.808(-0.019)	

[a] cc-pV*n*Z and aug-cc-pV*n*Z results are from Ref. 134.
[b] From Ref. 87.
[c] From Ref. 110.
[d] From Ref. 95.
[e] From Ref. 111.

Table 4.9. Extrapolated CBS limits for electron and proton affinities using CCSD(T) in combination with cc-pV*n*Z, aug-cc-pV*n*Z, cc-pV*n*Z-DK, cc-pV*n*Z-PP, and aug-cc-pV*n*Z.

CBS Limit	cc-pV*n*Z[a]	aug-cc-pV*n*Z[a]	cc-pV*n*Z-DK	cc-pV*n*Z-PP	aug-cc-pV*n*Z-PP	G2[b]	G3[c]	Expt.
$Ge^- \rightarrow Ge$								
D–T[d]	1.156	1.276	1.116	1.138	1.235	1.22	1.25	1.233[e]
T–Q[d]	1.278	1.263	1.240	1.248	1.226			
Q–5[d]	1.236	1.261	1.197	1.230	1.224			
Total[f]	1.199	1.256	1.162	1.205	1.220			
Property[f]	1.237	1.257	1.198	1.223	1.220			
$Br^- \rightarrow Br$								
D–T	3.201	3.262	3.194	3.010	3.218	3.32	3.39	3.364[e]
T–Q	3.455	3.416	3.401	3.476	3.372			
Q–5	3.394	3.399	3.348	3.368	3.355			
Total	3.332	3.381	3.300	3.417	3.360			
Property	3.383	3.379	3.341	3.547	3.524			
$SeH^- \rightarrow SeH$								
D–T	2.119	2.213	2.084	1.975	2.140	2.21	2.23	2.213[g]
T–Q	2.263	2.198	2.223	2.285	2.213			
Q–5	2.232	2.219	2.191	2.217	2.201			
Total	2.171	2.194	2.130	2.214	2.195			
Property	2.205	2.199	2.156	2.260	2.211			
$BrO^- \rightarrow BrO$								
D–T	2.034	2.380	2.003	1.993	2.349	2.45	2.42	2.360[h]
T–Q	2.421	2.473	2.389	2.402	2.443			
Q–5	2.526	2.464	2.495	2.498	2.434			
Total	2.402	2.454	2.363	2.429	2.435			
Property	2.442	2.501	2.538	2.575	2.458			

(table continues on next page)

(Table 4.9 continued)

CBS Limit	cc-pV*n*Z[a]	aug-cc-pV*n*Z[a]	cc-pV*n*Z-DK	cc-pV*n*Z-PP	aug-cc-pV*n*Z-PP	G2[b]	G3[c]	Expt.
$H^+ + Br^- \rightarrow HBr$								
D–T	14.087	14.070	14.101	14.283	14.091	14.01	13.98	14.000[g]
T–Q	13.923	13.945	13.941	13.867	13.964			
Q–5	13.961	13.956	13.981	13.961	13.975			
Total	13.992	13.962	14.013	13.903	13.962			
Property	13.960	13.967	13.980	13.637	13.985			
$H^+ + CH_3Br \rightarrow CH_4Br^+$								
D–T	6.880	6.894	6.861	6.851	6.860	6.83	6.84	6.820[i]
T–Q	6.805	6.810	6.797	6.805	6.794			
Q–5	6.803	6.814	6.792	6.792	6.795			
Total	6.816	6.820	6.808	6.803	6.796			
Property	6.812	6.822	6.759	6.775	6.807			

[a] cc-pV*n*Z and aug-cc-pV*n*Z results are from Ref. 134.
[b] Gaussian-2 values are from Ref. 68.
[c] Gaussian-3 values are from Ref.72.
[d] Two-point extrapolation is from Eqn 3.1. "D–T" in table refers to the $CBS_{D\text{-}T}$ extrapolation using results from double-ζ and triple-ζ basis sets. "T–Q" refers to the $CBS_{T\text{-}Q}$ extrapolation and "Q–5" refers to the $CBS_{Q\text{-}5}$ extrapolation.
[e] From Ref. 141.
[f] Where Total=CBS_{total} and Property=CBS_{prop} from Eqn. 3.1 and 3.2, respectively.
[g] From Ref. 110.
[h] From Ref. 95.
[i] From Ref. 111.

4.3.5. Energy Summary

In Table 4.10, the mean absolute deviations from experiment for the atomization energies, ionization energies, and electron affinities are reported at the CBS limit. Five different means have been used to determine the CBS limit as was discussed in the methodology section (Sec 4.2). In general, there are only slight variances in the extrapolated CBS values when comparing the mean absolute deviation obtained when scalar relativistic corrections are included in the calculations with that obtained from the non-relativistic calculations.

For the atomization energies, the mean absolute deviation using the $CBS_{D\text{-}T}$ extrapolation scheme increases when the scalar relativistic effect is applied. The $CBS_{T\text{-}Q}$ and $CBS_{Q\text{-}5}$ schemes result in slightly lower mean absolute deviations for the non-relativistic calculations as compared with those that include the scalar correction. The exception to this is the cc-pV*n*Z-DK $CBS_{T\text{-}Q}$ extrapolation. In all of these cases, the mean absolute deviations deviate from one another by no more than 0.20 kcal/mol for any type of calculation done, provided the two-point extrapolation scheme is used with a basis set of at least triple-zeta quality. This is also true when the CBS_{prop} scheme is used. However, a large difference occurs for the CBS_{total} scheme.

For the ionization energies, the mean absolute deviation increases slightly when the scalar relativistic effect is included in the calculations. This difference is generally no more than 0.025 eV. For the electron affinities, the mean absolute deviations for the CBS extrapolations of the scalar relativistic calculations are similar to those of the non-relativistic calculations when a basis set of at least triple-zeta quality is used for the two-point extrapolation scheme. The mean absolute deviation is larger for the scalar relativistic calculations when the CBS_{prop} scheme is used.

Table 4.10. Total mean absolute deviation in atomization energy (kcal/mol), ionization energy (eV), and electron affinity (eV), and combined energies total (kcal/mol) using CCSD(T) and cc-pV*n*Z, aug-cc-pV*n*Z, cc-pV*n*Z-DK, cc-pV*n*Z-PP, and aug-cc-pV*n*Z-PP.

	CBS Limit	cc-pV*n*Z[a]	aug-cc-pV*n*Z[a]	cc-pV*n*Z-DK	cc-pV*n*Z-PP	aug-cc-pV*n*Z-PP	G2[b]	G3[c]
Σ AE	D–T[d]	2.44	1.71	3.02	2.85	2.00	1.24	1.01
(kcal/mol)	T–Q[d]	1.04	1.18	1.17	1.17	0.98		
	Q–5[d]	1.11	1.06	1.07	1.10	0.96		
	Total[e]	1.62	1.52	2.38	1.48	1.30		
	Property[e]	1.14	1.24	1.39	1.33	1.14		
Σ IE	D–T	0.084	0.078	0.119	0.095	0.094	0.078	0.039
(eV)	T–Q	0.041	0.037	0.040	0.052	0.044		
	Q–5	0.041	0.028	0.046	0.044	0.048		
	Total	0.050	0.044	0.069	0.071	0.057		
	Property	0.048	0.040	0.072	0.060	0.072		
Σ EA	D–T	0.163	0.043	0.191	0.262	0.165	0.054	0.046
(eV)	T–Q	0.064	0.054	0.023	0.062	0.048		
	Q–5	0.057	0.045	0.054	0.039	0.055		
	Total	0.039	0.040	0.057	0.040	0.040		
	Property	0.030	0.050	0.075	0.116	0.088		
Total	D–T	2.34	1.66	2.99	2.98	2.22	1.41	0.94
(kcal/mol)	T–Q	1.05	1.05	0.99	1.24	0.99		
	Q–5	1.05	0.87	1.05	1.04	1.03		
	Total	1.32	1.22	1.86	1.47	1.24		
	Property	1.03	1.07	1.49	1.67	1.38		

[a] cc-pV*n*Z and aug-cc-pV*n*Z results are from Ref. 134.

[b] Gaussian-2 values are from Ref. 68.

[c] Gaussian-3 values are from Ref. 72.

[d] Two-point extrapolation is from Eqn. 3.1. "D–T" in table refers to the $CBS_{D\text{-}T}$ extrapolation using results from double-ζ and triple-ζ basis sets. "T–Q" refers to the $CBS_{T\text{-}Q}$ extrapolation and "Q–5" refers to the $CBS_{Q\text{-}5}$ extrapolation.

[e] Where Total=CBS_{total} and Property=CBS_{prop} from Eqn. 3.2 and 3.3, respectively.

4.4. Conclusions

The impact of scalar relativistic corrections determined by three different means upon energetic and structural properties of third-row molecules from the G2-extended test suite has been investigated. Overall, the effects determined by the Douglas-Kroll approach and those determined by small-core relativistic pseudopotentials combined with two different families of correlation consistent basis sets are similar. On average, the scalar relativistic corrections have a magnitude of 1.0 kcal/mol for atomization energies and 0.03 eV for ionization energies. The largest scalar relativistic correction was found to be –3.18 kcal/mol for the atomization energy of GeH_4 when using the aug-cc-pV5Z-PP basis sets. In comparing the three different basis sets used, cc-pV*n*Z-DK, cc-pV*n*Z-PP, and aug-cc-pV*n*Z-PP, the augmented sets usually predict properties nearest to the experimental value.

CHAPTER 5

THE DEVELOPMENT OF THE CORE-VALENCE CORRELATION CONSISTENT BASIS SETS FOR SECOND-ROW ATOMS Al-Ar REVISITED

5.1. Introduction

As discussed in the previous chapters, the popularity of the correlation consistent basis sets stems from their unique construction, which entails a "consistent" improvement in the description of electron correlation with each subsequent basis set in the series.[142] This behavior, in part, is a reason these sets[1-3] have seen widespread utility in thousands of studies. Using correlation consistent basis sets and extrapolating molecular properties to the complete basis set (CBS) limit, as done in Chapters 3 and 4, have enabled a well-developed hierarchy of the performance of *ab initio* methods to evolve. For example, the combination of a method such as coupled cluster [CCSD(T)] with the correlation consistent basis sets has allowed the prediction of molecular properties to "chemical accuracy" (e.g., dissociation energies within 1.0 kcal/mol of reliable, well-established results from experiment).[7,8,10-13,19-22,24,60,75,76,134]

There are, however, cases where extrapolations of molecular properties to the CBS limit, while using method like CCSD(T), does not provide properties near chemical accuracy. For example, in 1995, Bauschlicher and Partridge observed an unusually large (~6 kcal/mol) deviation from the experimentally established dissociation energy (D_e) of SO_2 in comparison to their CCSD(T) calculated value at the CBS limit.[29] They noted that the energy computed using the aug-cc-pVTZ basis set was much poorer (~10 kcal/mol) than that obtained using the 6-311+G(3df,2p) basis set. One noticeable difference in these basis sets is the value of the largest

d-exponent (aug-cc-pVTZ is 0.819, 6-311+G(3df,2p) 2.6). This lack of high (tight) exponent *d*-functions in the aug-cc-pVTZ basis set is responsible for the large error in the D_e of SO_2 as noted by Bauschlicher and Partridge. They later explored the addition of polarization functions to the aug-cc-pV*n*Z basis sets. This study was the first to show that an additional tight-*d* function significantly impacted the dissociation energy of SO_2, and suggested that additional high exponent functions would further improve the dissociation energy. Following this work, Martin noticed a significant deviation from experiment in the atomization energy of SO, and investigated the impact of the addition of a series of high exponent higher angular momentum functions to the correlation consistent basis sets.[31] In a later study, Martin and Uzan observed that such deviations also occurred for other second-row species, such as SiO and Cl_2, and, again, noted that these deviations could be remedied by the inclusion of additional tight basis functions.[31] They recommended one additional high exponent *d*-function for the triple- and quadruple-ζ basis sets to form the cc-pVTZ+1 and cc-pVQZ+1 basis sets. (It should be noted that the extrapolations utilized in these earlier studies did not include cc-pVDZ results. As a result of this omission, the error at the CBS limit was exacerbated. Much smaller errors would have been obtained if the cc-pVDZ results had been included in the extrapolation schemes.[22] However, this extreme sensitivity of the CBS limit to the inclusion or exclusion of the cc-pVDZ results did further exemplify a convergence issue in the cc-pV*n*Z sets for the second-row atoms.[15])

Dunning *et al.* have cautioned that the addition of any new functions to a basis set, however arbitrary, will result in improvements to the total energy, and likely to the dissociation energy, as the effects of correlation are larger in molecules than in atoms.[15] In light of this, and the obvious deficiencies noted in the basis sets, Dunning, Peterson, and Wilson re-evaluated the

construction of the standard cc-pV*n*Z basis sets for second-row atoms.[15] Comparison of the D_e of O_2 to SO, led them to believe there were two possible problems in the construction of the valence *d*-sets, which could effect the convergence behavior in second-row systems: (1) a near duplication of exponents in the (3*d*) and (4*d*) sets; and (2) a deficiency in the early members of the *d* sets needed for the description of core polarization effects and valence orbital correlation effects. The best remedy to these problems was found by making modifications to the cc-pV*n*Z basis sets that included the addition of a single tight-*d* basis function at each basis set level and a re-optimization of all of the *d*-functions in order to provide a systematic expansion of the valence and outer core regions. During the optimization of the new sets of *d* functions, it was also noted that the even-tempered expansion for the *d*-sets was no longer adequate.

The modified basis sets, known as the cc-pV(*n*+*d*)Z and aug-cc-pV(*n*+*d*)Z series of basis sets, successfully addressed the differences in the convergence behavior of the D_e for O_2 and SO. Further benchmarks, on Si_2, PN, and AlCl in Dunning's initial study, also demonstrated that calculated molecular properties, such as D_e, converge more quickly to the CBS limit. Wilson *et al.*, have shown that the augmented tight-*d* basis sets have significant impact on the structure and energetics of SO_2.[17] In fact, the r_e(SO) in SO_2 at the cc-pV(T+*d*)Z level is comparable to the bond distance determined using cc-pV5Z (1.4398 Å and 1.4348 Å, respectively). The improvement of the convergence behavior in the dissociation energy of SO_2 resulted in a reduction of the error in the three-point CBS limit (TZ, QZ, 5Z) from 6.0 kcal/mol for the cc-pV*n*Z set to less than 1.0 kcal/mol for the cc-pV(*n*+*d*)Z sets when the zero-point energy (ZPE) correction was included. Also, in a study of SO_3,[143,144] the effect of a single tight-*d* function on atomization energy was an astounding 25.27 kcal/mol at the double-ζ level and 14.32 kcal/mol at the triple-ζ level. These benchmark studies, as well as others,[18,25,145] have illustrated the

importance in using the cc-pV(n+d)Z and aug-cc-pV(n+d)Z sets in calculations of molecular properties containing second-row atoms.

In the majority of electronic structure calculations, the frozen-core approximation is utilized, due both to computational efficiency and to interest in the chemistry largely associated with the valence electrons. However, often for accurate descriptions of structural (<0.01 Å) and energetic (<1.0 kcal/mol) properties, the inclusion of core-core and core-valence correlation is necessary.[10,21,24] It is, however, not advised to perform all-electron calculations utilizing basis sets optimized for valence-only correlated calculations, as they do not provide a balanced description of the core orbitals.[146] Woon and Dunning developed the correlation consistent polarized core valence *n-zeta* (cc-pCVnZ) basis sets, which was the first systematically constructed series of basis sets designed for describing the core and core-valence contribution to the total correlation energy.[9] In the development of the core functions for first-row atoms (B-Ne), the exponents of the core functions were optimized in the presence of the valence sets to minimize the core-core and the core-valence correlation energy, using the configuration interaction with single and double excitations (CISD) method. Peterson and Dunning later developed cc-pCVnZ sets for second-row atoms (Al-Ar)[16] in a manner akin to that utilized for the development of basis sets for first-row atoms, thereby adding (1s1p1d) to cc-pVDZ, (2s2p2d1f) to cc-pVTZ, (3s3p3d2f1g) to cc-pVQZ, and (4d3f2g1h) to cc-pV5Z. (For cc-pCV5Z, new core s and p functions were not optimized; rather, the (20s12p) primitive HF sets were recontracted to [11s10p], see Ref. 16 for further discussion.) Peterson and Dunning found that the convergence of the core-valence contribution to the total correlation energy was slower than that of core-core correlation when the cc-pCVnZ basis sets were used. As a result of this observation, they also developed the w*eighted* core-valence correlation consistent basis sets (cc-

p*w*CV*n*Z) for first- and second-row atoms. For these sets, the exponents of the core functions were optimized to favor the core-valence contribution by weighting the core-core correlation term, in order to increase the rate of convergence of the core-valence correlation. Peterson and Dunning discovered that the inclusion of a small fraction of the core-core correlation must be used in order to maintain systematic convergence behavior.

As discussed, the valence correlation consistent basis sets serve as the foundation for the development of the core-valence basis sets. However, for the augmented tight-*d* basis sets, there are no corresponding core-valence sets. Rather, for second-row atoms, the standard core-valence basis sets are still used. There are deficiencies which arise from this, however, which suggest the need for modified core-valence basis sets that are compatible with the augmented tight-*d* valence sets. First, there are two *d*-functions in both the cc-pV(D+*d*)Z and cc-pCVDZ sets. Core-valence sets systematically build upon valence basis sets at all angular momentum levels, thus, this equivalent number of *d*-functions suggests that the core-valence sets may be deficient in their number of *d*-functions at each basis set level. Second, it is expected that the D_e from valence-only correlated calculations with the cc-pV(*n*+*d*)Z basis sets would be smaller than the D_e determined from all-electron calculations with the cc-pCV*n*Z basis sets. However, as discussed further in Sec. 5.3, this does not occur in all cases for these two series of basis sets.

Because of the superiority and recommended use of the cc-pV(*n*+*d*)Z basis sets rather than the cc-pV*n*Z sets for frozen-core calculations, the aim of this chapter is to develop core-valence basis sets built upon the cc-pV(*n*+*d*)Z valence sets for use in all-electron calculations. Using the modified sets developed in the present study, benchmark calculations have been performed to predict the D_e and bond lengths of SO, SO_2, S_2, AlCl, PN, and Si_2 and to illustrate the utility of these basis sets.

5.2. Methodology

The subsequent subsections outline two schemes for the construction of core-valence sets based upon the cc-pV(n+d)Z valence sets for second-row atoms. In order to maintain consistency with the development of the original correlation consistent core-valence sets for second-row atoms, the total number of core-d functions beyond the cc-pV(n+d)Z valence-d sets in the new cc-pCV(n+d)Z sets should be 1d (for n=D), 2d (for n=T), 3d (for n=Q), and 4d (for n=5). The optimization of these new core-d functions should also provide a systematic improvement upon the electron correlation energy and prediction of molecular properties computed with cc-pV(n+d)Z. Amending the cc-pV(n+d)Z set with core functions is expected to provide improvement similar to using the cc-pCVnZ sets for all-electron calculations as compared with the cc-pVnZ sets for valence-only calculations. For the optimization of the d-exponents, the CISD method was used. The reference wavefunction for the CISD calculations was obtained by state-averaging any degenerate ground state for the atoms. In the all-electron calculations, only the 1s (K shell) was frozen for the second-row atoms, which is generally not of chemical interest and contributes very little to the total electron correlation. This was also the procedure used in the original development of the cc-pCVnZ sets for the second-row atoms. The MOLPRO 2002.6 quantum chemistry software suite was used throughout this study.[85]

5.2.1. General Basis Set Considerations

As mentioned previously, relative to the cc-pV(n+d)Z basis sets, the cc-pCVnZ basis sets are deficient by one core-d function at each basis set level. Thus, in the revision of the core-valence sets, an additional core-d function was included in the sets, and all of the core-d functions were optimized for each ζ-level. In order to maintain consistency with the previous

core-valence correlation consistent basis sets the new core-*d* set was optimized so that the sum of the core-core (LL) and core-valence (LM) correlation was minimized (i.e. provides the largest contribution to the total correlation energy). In other words,

$$\Delta E_{corr} = E_{CISD}(LL+LM+MM) - E_{CISD}(MM). \quad (5.1)$$

The difference between the all-electron and valence-only correlated calculations is equal to the sum of the core-core and core-valence correlation energies. Throughout this study, the exponents were generated by optimizing α and β parameters in an even-tempered expansion,

$$\zeta_i = \alpha\beta^{i-1} \quad (5.2)$$

where ζ is the basis set exponent and *i* represents the number of basis functions. Therefore, the exponent of the lowest value core function (*i*=1) is equal to α and the second function (*i*=2) is αβ, and so forth. The parameter, β, is also referred to as the "spacing" between exponents, since each exponent is separated by a factor of β. The other remaining (*s,p,f,g,h)* core functions were unaltered and were obtained from the cc-pCV*n*Z basis sets. Spherical basis functions were used throughout. These considerations were used throughout the process of determining a new set of core-*d* functions for the cc-pCV(*n*+*d*)Z basis set.

5.2.2. Optimization Scheme 1

An additional core-*d* function, which is needed to create revised core-valence basis sets, should not simply be added to each of the existing cc-pCV*n*Z sets. Such an approach in itself would not provide optimal *d* functions because the core-*d* functions are optimal for the standard cc-pV*n*Z basis sets, not for the cc-pV(*n*+*d*)Z sets, which should serve as the base for the revised core-valence sets. Therefore, in the presence of the valence functions from the cc-pV(*n*+*d*)Z sets

(including the tight-*d* function which are referred to as ζ_0), all of the core-*d* functions (herein referred to as ζ_1, ζ_2, ζ_3 …) were reoptimized including the additional core-*d* function. Overall, for the double-, triple-, and quadruple-ζ basis sets, the optimization resulted in core-*d* functions that had higher exponents than the tight-*d* function, ζ_0. These functions (denoted S1-CV+d) are shown in Fig. 5.1(a) for sulfur and are the open circles to the right of the solid circles.

Generally, augmenting the valence basis sets with core functions produces exponents with higher values than those of the valence sets. At the quintuple-ζ level, however, the optimal ΔE_{corr} resulted in a smaller ζ_1 exponent than the ζ_0 exponent. This arises, in part, to the saturation of the *d*-space at the quintuple-ζ level when nine *d*-functions are present, and to the large ζ_0 function (6.510), which is significantly in the core region. To circumvent a linear dependence problem (two exponents with values nearly degenerate) that occurred during the optimization of the core-*d* functions for the ζ_2 and ζ_0 exponents, the common β spacing between exponents was redefined. Thus, for the quintuple-ζ set, the β spacing was redefined as the spacing between the ζ_1 and the ζ_0 exponent, while the tight-*d* exponent (ζ_0) from the cc-pV(5+d)Z set remains fixed as before. The first core-*d* exponent (ζ_1) was optimized so that it was smaller than the ζ_0 function, and the second core-*d* exponent (ζ_2) was redefined as $\alpha\beta^2$. This strategy allows the ζ_1 and ζ_2 exponents to straddle the fixed ζ_0 tight-*d* function. Furthermore, the value of the third core-*d* function (ζ_3) was $\alpha\beta^3$, and the value of the ζ_4 function was $\alpha\beta^4$. This scheme was chosen for all of the quintuple-ζ core-*d* sets in scheme 1.

The cc-pV(*n*+*d*)Z valence-*d* were used as the base to build core-*d* functions and the valence tight-*d* set used a non-even-tempered spacing of the *d*-functions, which was needed to expand both the valence and outer core regions.[15] Some difficulties occurred during the

optimization of core-*d* functions using scheme 1, which was due the location of the tight-*d* exponent from using a non-even-tempered expansion. The non-even-tempered approach used in the determination of the valence-*d* and tight-*d* exponents in the cc-pV(*n*+*d*)Z basis sets led to difficulties in the optimization of core-*d* functions using scheme 1. For the quintuple-ζ level, this was discussed previously and can be seen in Fig. 5.1(a), where ζ_1 and ζ_2 straddle ζ_0. Another difficulty was also encountered in optimizing core-*d* functions in the presence of the valence-*d* set from cc-pV(*n*+*d*)Z for argon, as shown in Fig. 5.1(b). In this case, scheme 1 optimization resulted in a linear dependency problem for the ζ_0 and ζ_1 exponents at the quadruple-ζ level. An attempt at straddling the ζ_0 function was made by changing the normal β spacing, similar to the strategy used at the quintuple-ζ level. However, this attempt was unsuccessful as well, which was again due to the linear dependency of the ζ_1 and ζ_0 exponents. These inconsistencies in the construction of the core-*d* exponents led to a second optimization approach (scheme 2).

Figure 5.1. Optimized core-*d* exponents for (a) sulfur and (b) argon using scheme 1 are plotted as open circles. Valence-*d* exponents from cc-pV*n*Z and cc-pV(*n*+*d*)Z and core-*d* exponents from cc-pCV*n*Z and cc-p*w*CV*n*Z are plotted with solid symbols for comparison.

(a)

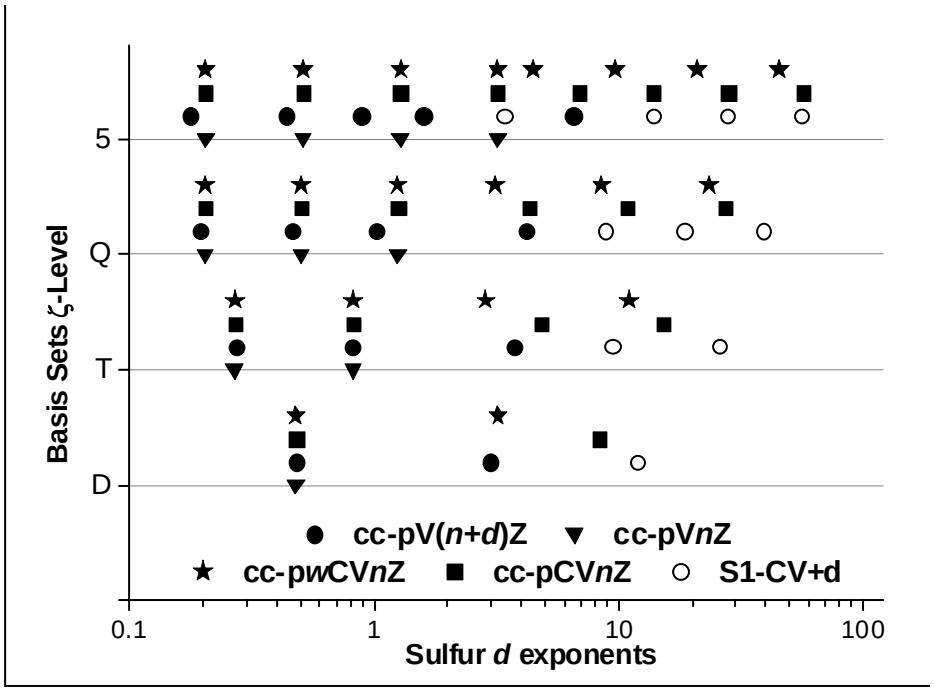

(b)

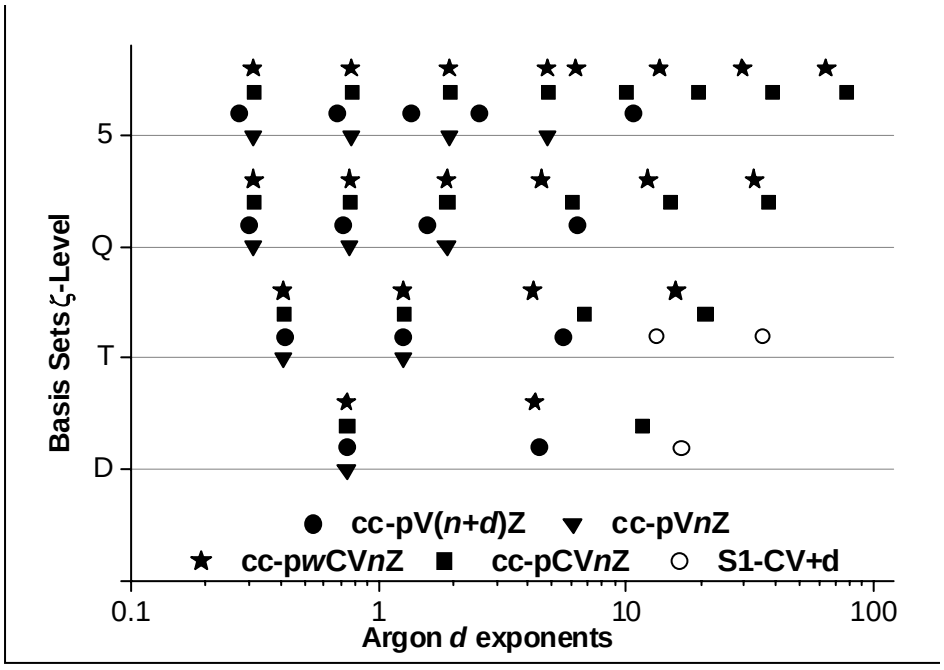

5.2.3. Optimization Scheme 2

Due to the complications arising from the scheme 1 optimization of the core-*d* functions in the previous section, the focus of this scheme was to re-establish an even-tempered expansion throughout the valence and core regions. This entailed a reoptimization of the tight-*d* exponent along with the set of core-*d* functions. It must be noted that during the optimization of the cc-pV(*n*+*d*)Z set, a few issues were encountered while optimizing the tight-*d* function at the double- and triple-ζ levels. As discussed in Ref. 15, the initial optimization of the 3*d* set exponents for cc-pV(T+*d*)Z, resulted in all of the *d* exponents in the valence space without the needed tight-*d* function. Therefore, in the final approach used in Ref. 15, only the tight-*d* function was optimized. At the cc-pV(D+*d*)Z level, the optimized tight-*d* exponent was much smaller than the corresponding triple- or quadruple-ζ tight-*d* functions. This large change in the tight-*d* exponent at the cc-pV(D+d)Z level is thought to be due to the small number of *d*-functions present for the description of both the valence and outer core regions. Subsequently, the tight-*d* function in the cc-pV(D+*d*)Z basis set was estimated from a ratio of the triple- and quadruple-ζ tight-*d* functions. (See Ref. 15 for further details on optimization of tight-*d* exponents in cc-pV(*n*+*d*)Z). It is thought that the challenges faced during the optimization of the original tight-*d* function should not arise while optimizing the tight-*d* exponent together with the core-*d* functions.

In light of the problems encountered in scheme 1, in scheme 2 the original cc-pV*n*Z sets were used as the base for constructing new ζ_0 and core-*d* sets, since they contain an even-tempered set of *d* functions. A simple analysis of Fig. 5.1 shows that ζ_0 from cc-pV(*n*+*d*)Z is generally located in the region between the ζ_1 core-*d* exponents of cc-p*w*CV*n*Z and cc-pCV*n*Z. Optimizing the ζ_0 function with the core-*d* functions allowed more flexibility in the description of the core region, which lowered the ΔE_{corr} as compared to scheme 1. For argon at the double-ζ

level, scheme 2 results in a lower ΔE_{corr} by 1.829 mE_h in comparison to the ΔE_{corr} obtained from optimization scheme 1. Optimization of the ζ_0 exponent and the set of core-*d* functions (ζ_1, ζ_2, ζ_3, ζ_4) with scheme 2 did not lead to any inconsistencies at the various basis set levels. Furthermore, at the double-ζ level the addition of a core-*d* function caused the ζ_0 exponent to optimize in the core region without estimating the exponent, as discussed previously.

Figure 5.2. Optimized core-*d* exponents for (a) sulfur and (b) argon using scheme 2 are plotted as open triangles. Valence-*d* exponents from cc-pV*n*Z and cc-pV(*n*+*d*)Z and core-*d* exponents from cc-pCV*n*Z and cc-p*w*CV*n*Z are plotted with solid symbols for comparison.

(a)

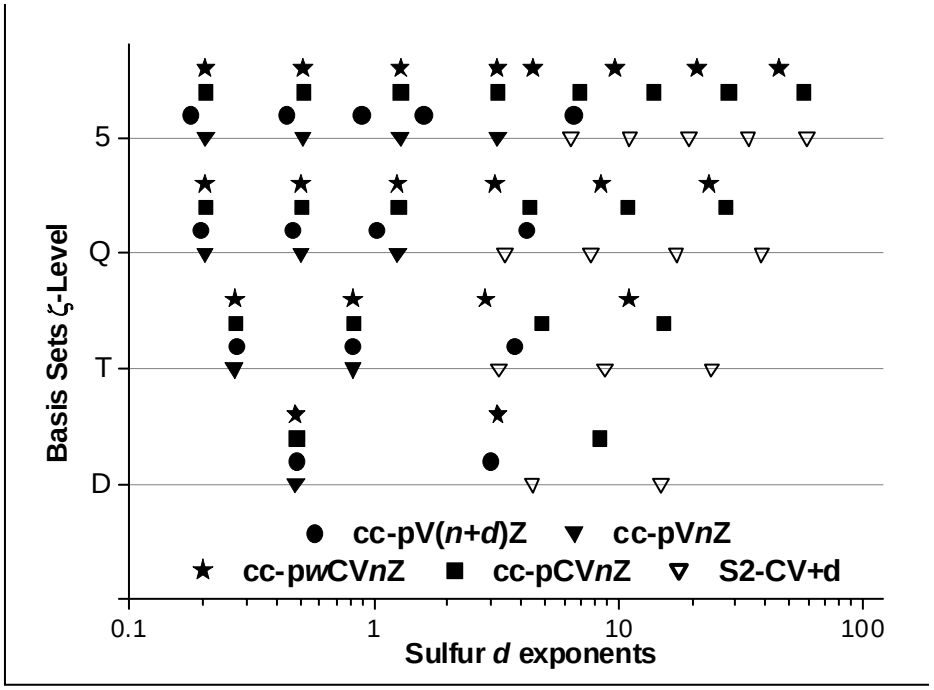

(b)

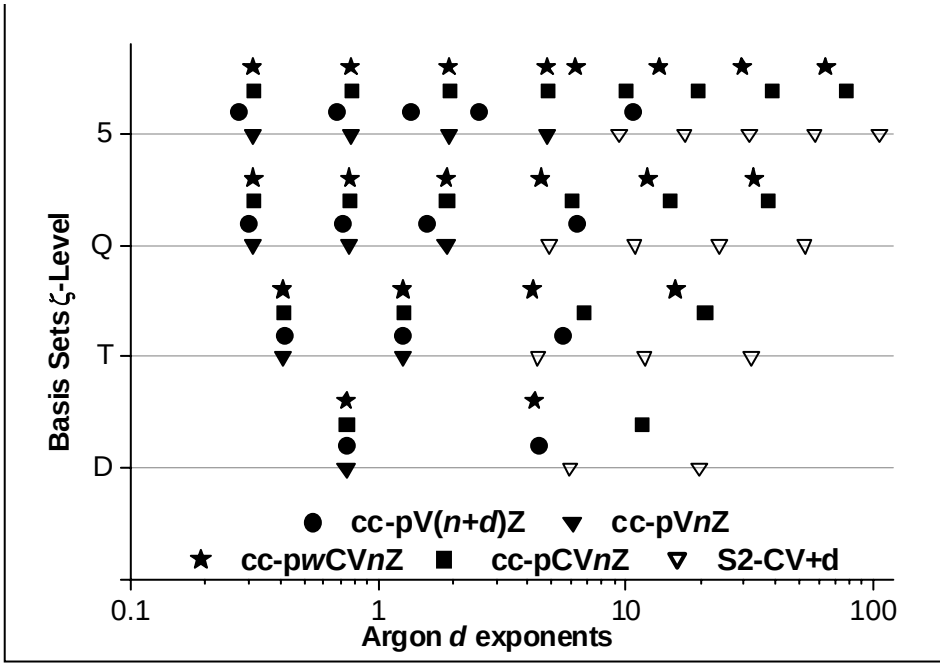

5.2.4. Mixed Approach – Optimization Scheme 3

Further analysis of scheme 2 during the molecular benchmark studies (discussed in Sec. 5.3) suggested deficiencies in the scheme. In particular, the D_e computed while using cc-pCV(D+*d*)Z did not improve upon the cc-pV(D+*d*)Z valence-only values for all of the molecules tested. Closer inspection of the ζ_0 functions in scheme 2 revealed that at the double-ζ level, the ζ_0 exponent does not follow the general trend in which the exponents become more diffuse as the basis set size is decreased. To illustrate, for sulfur the exponents are 6.386, 3.434, and 3.239 for quintuple- quadruple- and triple-ζ, respectively, whereas for double-ζ, the exponent is 4.435. At the double-ζ level the ζ_0 exponent was too far in the core region. This was not surprising when considering the small number of *d* functions present at the double-ζ level. As mentioned previously, problems were also encountered in the optimization of the tight-*d* (ζ_0) exponent during the development of the cc-pV(D+d)Z sets.[15] For scheme 2, this inconsistency in the description of the valence and core regions only occurred at the double-ζ level. Even though the cc-pCV(D+d)Z basis set from scheme 2 was an improvement over the cc-pCVDZ set, it was still not adequate for the description of molecular properties in all-electron calculations, as it did not improve over the cc-pV(D+d)Z valence-only calculations. Therefore, a mixed scheme of scheme 1 and 2 (referred to as scheme 3) was chosen, since scheme 1 did improve upon the cc-pV(D+*d*)Z valence-only calculated molecular properties and the ΔE_{corr} as compared to cc-pCVDZ. Scheme 3 used the optimization approach from scheme 1 for the double-ζ basis set which is comprised of the newly optimized ζ_1 core-*d* function and the valence-*d* set from cc-pV(D+*d*)Z. The triple-, quadruple-, and quintuple-ζ *d*-exponents were optimized as in scheme 2.

The exponents for the new *d*-functions in cc-pCV(*n*+*d*)Z are listed in Table 5.1. For each atom, the cc-pCV(*n*+*d*)Z sets resulted in a lowering of the ΔE_{corr} as compared with the cc-

pCV*n*Z sets. This is shown in Fig. 5.3 for sulfur and argon. Also, the convergent behavior of the core-valence correlation energy of the atoms was improved with the inclusion of the additional *d*-function, and is similar to the improvement seen in using cc-pV(*n*+*d*)Z valence sets as opposed to the standard cc-pV*n*Z sets.

Table 5.1. Optimized tight-*d* (ζ_0) and core-*d* (ζ_1, ζ_2, ζ_3, ζ_4) exponents for the second-row atoms (Al-Ar).

Atom	Set	ζ_0	ζ_1	ζ_2	ζ_3	ζ_4
Al	D[a]	0.190	5.938			
	T	1.795	4.992	13.883		
	Q	1.665	3.893	9.100	21.273	
	5	2.897	5.579	10.744	20.690	39.845
Si	D	0.275	7.867			
	T	2.251	6.186	16.999		
	Q	2.266	5.165	11.773	26.833	
	5	4.289	7.958	14.768	27.403	50.849
P	D	0.374	10.056			
	T	2.750	7.504	20.479		
	Q	2.904	6.515	14.618	32.800	
	5	5.429	10.017	18.481	34.097	62.909
S	D	0.481	11.880			
	T	3.239	8.818	24.005		
	Q	3.434	7.681	17.183	38.439	
	5	6.504	12.039	22.284	41.247	76.348
Cl	D	0.603	14.099			
	T	3.846	10.395	28.095		
	Q	4.136	9.185	20.399	45.304	
	5	7.599	14.046	25.964	47.995	88.719
Ar	D	0.739	16.523			
	T	4.424	11.938	32.214		
	Q	4.882	10.784	23.819	52.612	
	5	9.377	17.195	31.531	57.819	106.022

[a] All ζ_0 values at the double-ζ level are from Ref. 15.

Figure 5.3. Comparison of the ΔE_{corr} from the cc-pCV(n+d)Z and cc-pCVnZ basis sets for (a) sulfur and (b) argon using CCSD(T).

(a)

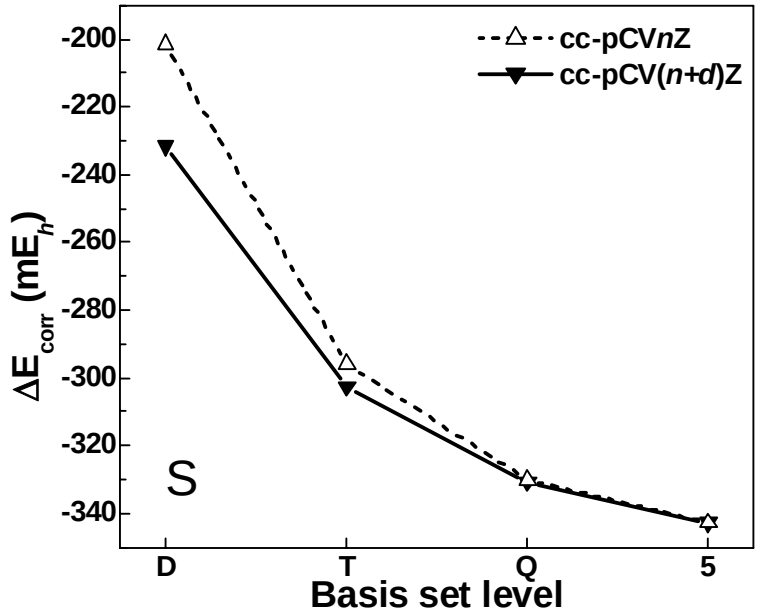

(b)

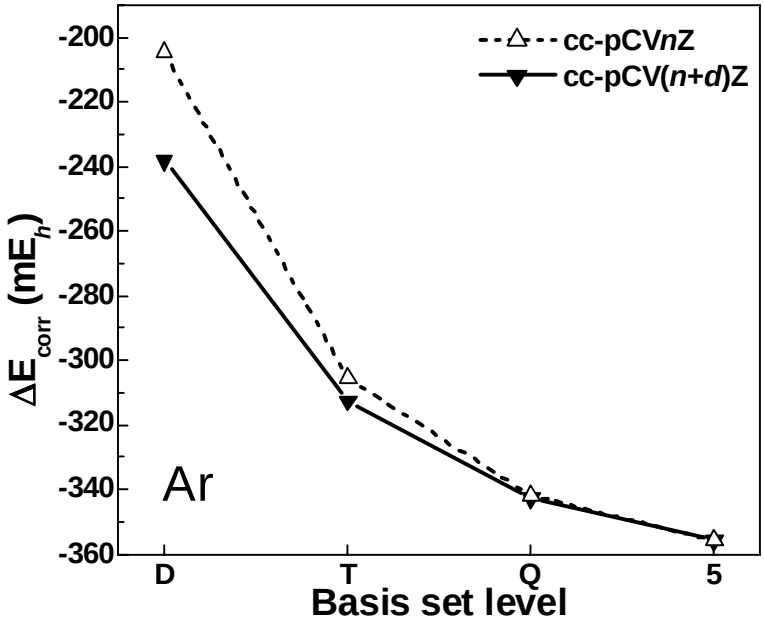

5.3. Benchmark Calculations

In order to assess the impact of the cc-pCV(n+d)Z basis sets, benchmark calculations have been performed using CCSD(T).[50-52] In these calculations, the 1*s* orbital was frozen for the second-row atoms, while no orbitals were frozen for the first-row atoms. The calculated D_e, which is shown in Table 5.2, included the ZPE correction at each basis set level. The CBS limit (n=∞) was found using the dissociation energy determined at each basis set level (n=D,T,Q,5) with the Feller exponential extrapolation.[19] In Table 5.2, the change in D_e (ΔD_e) arising from the use of the tight-*d* sets has been tabulated for the valence-only and all-electron calculations.

The benchmark molecules (SO, SO_2, S_2, AlCl, PN, Si_2) were chosen due to their previous use in performance studies of the correlation consistent basis sets.[15-17] The data reported in Table 5.2 reflects the inclusion of ZPE corrections, which were not included in the majority of this earlier work. The CCSD(T)/cc-pV*n*Z and cc-pV(n+d)Z calculations have been performed previously on all of the molecules,[15,17] while CCSD(T)/cc-pCV*n*Z benchmark studies have been done on Si_2, S_2, and PN.[16] The CCSD(T)/cc-pV*n*Z and cc-pV(n+d)Z benchmarks on SO_2 which include ZPE corrections were obtained from the earlier work by Dunning and Wilson.[17]

As shown in earlier studies,[15,17,18,143] for valence-only (cc-pV*n*Z and cc-pV(n+d)Z) calculations, the augmented tight-*d* sets improve the prediction of D_e for all basis set levels and all molecules studied. This improvement (ΔD_e) for the valence-only calculations is most noticeable at the double-ζ level and is most significant for S–O bonded systems (4.235 and 15.679 kcal/mol for SO and SO_2, respectively). Calculating the D_e with the all-electron basis set cc-pCV*n*Z improves upon the standard cc-pV*n*Z (valence-only) values, however, at the double-ζ level, the valence-only cc-pV(D+*d*)Z basis set provides a better prediction of the D_e for all of the systems. For example, the SO_2 D_e is 200.383 kcal/mol at the cc-pV(D+*d*)Z level as compared to

188.500 kcal/mol at the cc-pCVDZ basis set level. The D_e obtained while using the cc-pV(D+d)Z basis set does not include the contribution of the core and core-valence correlation, yet resulted in a larger D_e than was obtained with the all-electron cc-pCVDZ calculation, which suggestive of a deficiency in the 2*d* set for cc-pCVDZ. As discussed earlier, the core-*d* function in cc-pCVDZ does not adequately allow for a balanced description of the core-valence interactions.

As shown in Table 5.2, the modified core-valence sets, cc-pCV(*n*+*d*)Z, resulted in a larger D_e than the valence sets, cc-pV(*n*+*d*)Z. This remedied the noted problem at the double-ζ level, where the all-electron cc-pCV*n*Z D_e was actually smaller than the cc-pV(*n*+*d*)Z D_e. The ΔD_e was similar for the valence and for the core-valence basis sets. This illustrated an improved description not only for the atoms, as illustrated in Figure 5.3 for sulfur and argon, but also for the molecules, as shown in Figure 5.4 for S_2 and SO_2. The greatest impact of the cc-pCV(*n*+*d*)Z basis sets occurred for the double-ζ level basis sets, and rapidly decreased as the basis set size was increased. This decrease in ΔD_e happened much more rapidly than the decrease in ΔD_e for the valence basis sets. This was not unexpected because the all-electron basis sets are much more saturated sets. The molecules that experienced the most significant improvements in energetic description were those containing both sulfur and oxygen. For example, for cc-pCV(D+*d*)Z, the D_e of SO and SO_2 were improved by 3.557 and 13.201 kcal/mol, respectively. All of the ΔD_e determined for PN were similar to those for SO, while the smallest impact was noted for Si_2 (e.g., 1.093 kcal/mol at the double-ζ level).

Figure 5.4 depicts the D_e values for S_2 and SO_2. The impact that the augmented-*d* basis sets made on D_e is shown for both the valence-only and all-electron calculations. In comparing the D_e from the cc-pV*n*Z and cc-pCV*n*Z basis sets in Fig. 5.4, there is only a small increase in

the D_e at the double-ζ level, whereas at the triple-ζ level, there is a much larger increase of the D_e. For the augmented-*d* sets, a more consistent improvement in D_e is observed for the comparison of cc-pV(*n*+*d*)Z to cc-pCV(*n*+*d*)Z at each basis set level. However, the increase in D_e arising from the use of the core-valence sets for the augmented-*d* sets is much smaller than for the standard basis sets. This is due to the significant effect of the single tight-*d* function in the cc-pV(*n*+*d*)Z basis sets.

Table 5.2. Computed D_e (in kcal/mol) for SO, SO_2, S_2, AlCl, PN, and Si_2 using CCSD(T). Frozen-core calculations utilized the cc-pV*n*Z and cc-pV(*n*+*d*)Z basis sets, while all-electron calculations utilized the cc-pCV*n*Z and cc-pCV(*n*+*d*)Z basis sets. The ΔD_e, represents the difference between the D_e for the augmented-*d* basis set and the D_e for the standard basis set.

	n=	cc-pV*n*Z	cc-pV(*n*+*d*)Z	ΔD_e	cc-pCV*n*Z	cc-pCV(*n*+*d*)Z	ΔD_e
SO	D	94.698	98.933	4.235	96.042	99.599	3.557
	T	112.871	115.437	2.566	115.796	116.235	0.439
	Q	118.762	120.273	1.511	120.909	120.918	0.009
	5	121.955	122.285	0.331	122.860	122.861	0.001
	∞	123.11	122.90		123.29	123.38	
SO_2[a]	D	184.704	200.383	15.679	188.500	201.702	13.201
	T	228.290	237.347	9.057	237.707	239.314	1.607
	Q	242.525	247.605	5.080	249.278	249.316	0.037
	5	250.794	251.835	1.041	253.237	253.239	0.002
	∞	253.82	252.92		253.92	254.15	
S_2	D	80.661	84.046	3.385	82.017	84.877	2.860
	T	92.303	94.295	1.992	94.677	94.971	0.293
	Q	97.670	98.941	1.271	99.582	99.598	0.016
	5	100.494	100.767	0.273	101.308	101.311	0.003
	∞	102.89	102.34		102.46	102.85	
AlCl	D	107.441	109.132	1.690	108.120	111.046	2.926
	T	115.763	116.420	0.657	116.583	116.654	0.071
	Q	119.339	119.774	0.434	120.141	120.152	0.011
	5	120.858	120.958	0.100	121.299	121.300	0.001
	∞	122.01	122.05		123.62	123.62	

(table continues on next page)

(Table 5.2 continued)

	n=	cc-pVnZ	cc-pV(n+d)Z	ΔD_e	cc-pCVnZ	cc-pCV(n+d)Z	ΔD_e
PN	D	113.260	116.954	3.695	114.561	117.872	3.311
	T	130.961	132.771	1.809	133.444	133.839	0.394
	Q	138.271	139.220	0.949	140.236	140.253	0.017
	5	141.416	141.634	0.219	142.619	142.621	0.002
	∞	143.60	143.36		147.84	148.14	
Si_2	D	60.211	61.424	1.213	60.984	62.078	1.093
	T	69.536	70.205	0.668	70.355	70.455	0.100
	Q	72.815	73.224	0.409	73.558	73.554	-0.004
	5	74.154	74.277	0.122	74.533	74.540	0.006
	∞	74.82	74.82		76.57	76.66	

[a] Values for SO_2 with cc-pVnZ and cc-pV(n+d)Z were obtained from Ref. 15.

Figure 5.4. Comparison of the atomization energy from valence-only calculations with cc-pV*n*Z and cc-pV(*n*+*d*)Z basis sets and from all-electron calculation with cc-pCV*n*Z and cc-pCV(*n*+*d*)Z basis sets for both the (a) S_2 and (b) SO_2.

(a)

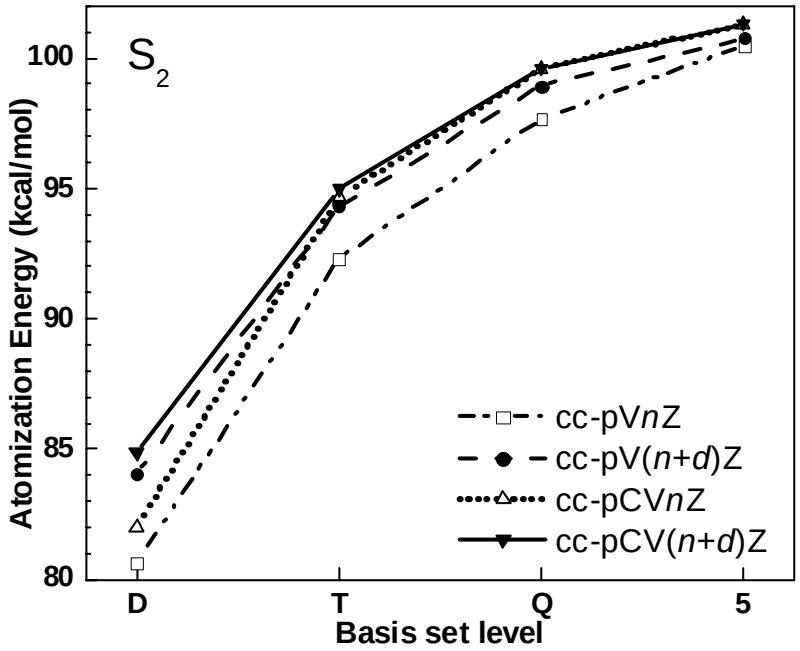

(b)

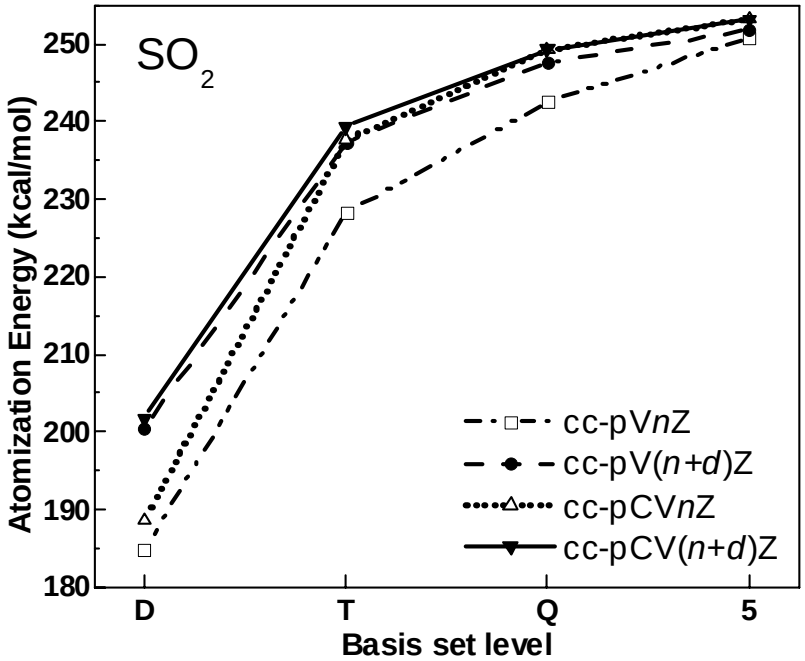

5.4. Conclusions

The cc-pCV*n*Z basis sets for second-row atoms were revisited in order to design core-valence correlation consistent basis sets that build upon the recommended valence basis sets, cc-pV(*n*+*d*)Z. These revised core-valence basis sets (cc-pCV(*n*+*d*)Z)provide a systematic description of the core-valence contribution to the total energy for all-electron calculations, and improve upon the description obtained using the cc-pCV*n*Z basis sets. As well, these revised sets remedied a problem noted in the calculation of dissociation energies for a series of molecules, where frozen core calculations using the cc-pV(D+*d*)Z basis set yielded much larger dissociation energy than all-electron calculations using the cc-pCVDZ basis set. These revised sets are recommended for use in all-electron calculations involving second-row atoms (Al-Ar).

CHAPTER 6

AN *AB INITIO* STUDY OF THE NOBLE GAS COMPOUND HKrCl[§]

6.1. Introduction

Noble gases have long been considered inert atoms due to their completely filled valence shell. However, in 1933 Linus Pauling was the first to propose that the inert gases should be capable of forming chemical bonds and further stated that "xenic acid, H_4XeO_6, should form salts as Ag_4XeO_6 and AgH_3XeO_6".[147] This hypothesis was dormant until the work of Bartlett in 1962, in which the inorganic complex $XePtF_6$ was synthesized.[148] Within a year, the first krypton bonded molecules, KrF_4[149] and KrF_2[150-153] were created. These initial studies suggested that actual chemical bonds, rather than simple van der Waal's forces, were possible for noble gas atoms.

The synthesis and characterization of noble gas-bonded molecules are difficult, and there have only been relatively few experimental studies on chemically bonded noble gas systems. Computational chemistry has therefore been instrumental in the further characterization these species, and in the prediction of new chemically bound noble gas systems. Some of the earliest *ab initio* studies have provided supporting evidence of the nature of the chemical bonding in these compounds,[154-158] and in some cases, these studies have shown that some of the earlier experiments led to incorrect assumptions. For example, a few experimental studies reported

[§] This chapter has been adapted from the publication of *Chem. Phys. Lett.*, Vol. 393, Scott Yockel, J. J. Seals III and A. K. Wilson, "An *ab initio* study of the noble gas compound HKrCl", Pages 448-452, Copyright (2004), with permission from Elsevier

evidence of XeF,[159-163] and one study suggested that XeF would have dissociation energy of ~20 kcal/mol.[164] These results are not surprising, as chemical bonding in XeF_2, XeF_4, and XeF_6 has been reported.[165-173] However, Liskow *et al.* have shown through Hartree-Fock (HF) and configuration interaction (CI) computations that the XeF radical has no minimum energy structure and, therefore, is not chemically stable.[156] Another important aspect found in the study by Liskow *et al.* was the large effect that electron correlation had on the computed potential energy surface of XeF. When CI was used, the repulsion energy dropped nearly 75% as compared to HF and resulted in a very flat potential energy well, whereas the HF repulsive surface is steep. More generally, the study by Liskow *et al.* demonstrated the importance of adequate treatment of electron correlation in any noble gas bonded systems.

A study by Collins and co-workers provided the first theoretical study of krypton-bonded systems, and showed that basis set size had a significant impact on the orbital overlap and charge distributions of KrF_2.[158] For example, the addition of 4*d* functions on krypton increased the overall overlap population for Kr—F from 0.045 to 0.419. With CI calculations, Liu and Schaefer predicted the spectroscopic constants for KrF^+, prior to any experimental analysis, and correctly identified KrF^+ to be a chemically bound system, which was in agreement with later experimental studies.[157] Computational studies by Bagus *et al.*, suggested that noble gas-bonded systems are bound by a resonance between ionic and covalent bonds.[155] These earlier studies helped provide the necessary background needed to understand the electronic structure of noble gas-halides systems, which had become the molecular source for powerful UV lasers.[154]

Recent experimental work has resulted in the isolation of new compounds, which contain a noble gas atom (Xe, Kr, or Ar) bonded to a hydrogen and a halide (HNgX).[33,34,174] These compounds have been synthesized with a low-temperature matrix-isolation technique. In this

technique, a dilute solution of the precursor is photolyzed and deposited on a surface of solid rare gas (at 20K for Kr and 7.5K for Ar),[175] then transferred to an infrared transparent window. At this point, the solid rare gas matrix is slowly heated (~1K/min) to allow for thermal mobilization of atoms in the precursor, forming the matrix isolated noble gas-bonded compounds, which are detectable by infrared spectroscopy. In low temperature matrices (< 40 K), these noble gas-bonded compounds have infrared stretching frequencies near the range of covalently bonded organic systems (~3500-1500 cm^{-1}), suggesting that these compounds are actually chemically bound, rather than van der Waals type complexes, which generally have much lower frequencies (<100 cm^{-1}). Actual chemical bonding with noble gases is still a relatively new concept,[174] which requires understanding gained by both experimental and theoretical studies.

Theoretical computations have provided further insight into the bonding and charge distribution in noble gas-bonded systems, and has assisted in the assignment of vibrational modes.[176] For example, Pettersson, Lundell, and Räsänen have synthesized HKrCl and supported their experimental findings by obtaining structures, frequencies, dipole moments, and Mulliken analysis from theoretical computations.[33] With infrared spectroscopy they observed strong absorption bands at 1476 cm^{-1} and 544 cm^{-1}, suggesting that HKrCl was not a van der Waals complex, but rather, had stronger covalent-like chemical bonds. Their initial calculations with UMP2, which used an effective core potential, LANL1DZ, for Kr, WBP for Cl, and 6-311G** for H, provided stretching modes of 977 cm^{-1} (H–Kr) and 235 cm^{-1} (Kr–Cl) and a bending mode of 492 cm^{-1}. These predicted frequencies dramatically underestimate (500 cm^{-1}) the H–Kr stretch and only qualitatively matched the observed bending mode mode (544 cm^{-1}). Pettersson *et al.* performed additional calculations, which used an all electron basis set for Kr and Cl and overestimated the H–Kr stretch by 216 cm^{-1}. It is apparent from these initial studies that accurate

prediction of the vibrational frequencies of noble gas-bonded systems requires more rigorous methods and more complete basis sets than described above. Pettersson *et al.*, used a Mulliken analysis to study the charge distribution, which gives a positive charge for both H and Kr and a negative charge for Cl. However in later work, they reexamined the geometry using MP2 with a slightly different basis set, LANL1DZ for Kr and 6-311G++(2d,2p) for H and Cl, and noted that the new Mulliken analysis resulted in a different qualitative picture than the previous calculations by showing a negative charge on both the H and Cl.[34] In recent work by Lignell *et al.,*[35] the Kr–Cl stretching mode was studied, and anharmonic *ab initio* calculations were done using the vibrational self-consistent field with corrections via second-order perturbation theory (CC-VSCF) approach.[35]

While structures of noble gas-bonded molecules can normally be determined by less expensive computational methods such as DFT, previous computational studies have suggested the need to use *ab initio* methods such as multi-reference or coupled cluster approaches in combination with large basis sets to provide accurate energetics.[177,178] As noted in Chapter 3, only when a sufficiently large (aug-cc-pVTZ) basis set is used with CCSD(T) is the atomization energy of KrF_2 even qualitatively correct. Other studies have shown that the dissociation energies of HKrF and HArF, computed with MP2 and CCSD(T) and low level basis sets, predicted the linear molecule to be higher in energy than H + Kr + F or H + Ar + F respectively, while this qualitative picture is reversed when higher level basis sets are used.[174,179] Another study correctly predicted the decomposition of HNgX into HX and Ng using MP2 and CCSD(T) for HKrF and HArF.[176] In the previous studies discussed above, accounting for electron correlation played a critical role in even the qualitative prediction of chemical properties. Thus it

is important to choose methodologies that recover ample electron correlation for a correct characterization of any noble gas-bonded systems.

In this chapter, the optimized structure, relative energetics, and vibrational properties of the HKrCl species, have been determined using an advanced correlation treatment in combination with the correlation consistent basis sets. In order to provide insight into the decomposition and stability of this compound, the minimum energy pathway of HKrCl to HCl + Kr has been computed. Studying the reaction pathways of these metastable molecules are vitally important in understanding the dissociation barriers, and relative stability compared to the dissociative products.

6.2. Computational Methods

It has been shown in Chapters 3 and 4 that the *ab initio* method, CCSD(T), [50-52] provides reliable structural and energetic properties of molecules containing third-row atoms, like Kr, when used in combination with the correlation consistent basis sets (cc-pV*n*Z). Therefore, due to the well-established accuracy of this computational approach (See, *e.g.* Refs. 4,7,8,11-13,60), it has been chosen for the characterization of HKrCl in this chapter. The augmented correlation consistent basis sets (aug-cc-pV*n*Z)[4] that include diffuse functions, were also used, as they may be useful in characterizing the bonding of the HKrCl molecule with its partial ionic character. The correlation consistent basis sets (cc-pV(*n*+d)Z) modified for second-row atoms, which were discussed in Chapter 5, have also been chosen for their usefulness in describing chlorine containing species.[15]

Several structural and chemical properties have been computed in order to further characterize HKrCl. Geometry optimizations were performed for each level of basis set through

the quintuple-ζ level, while vibrational frequencies have been obtained using basis sets through the quadruple-ζ level. The relative energies for various fragmentations of HKrCl have been determined at the quintuple-ζ level in order to assess the energy differences between a completely bound HKrCl and an infinitely separated system of HCl and Kr. Mulliken and Natural Bond Orbital (NBO)[180] analyses have been done on HKrCl, as they provide an important means of understanding the charge density in these systems by showing the relative charges on the atoms within the molecule. These analyses have been done with the HF, MP2, and CCD densities using the CCSD(T)/aug-cc-pV(5+d)Z geometry.

The Quadratic Steepest Descent method of Sun and Ruedenberg (QSD)[181] was used to locate the transition state for the separation of HKrCl into HCl and Kr. Following the location of the transition state, the minimum energy path was found with the QSD reaction path (an approximated potential energy surface method).[182] Both the transition state and the minimum energy pathways were computed at the CCSD(T) level with the augmented double- and triple-ζ basis sets.

Mulliken and NBO calculations were performed with Gaussian 98,[86] while all other calculations have been performed with the MOLPRO[85] quantum chemistry package.

6.3. Results and Discussion

6.3.1. Minimum Energy Structure

In Table 6.1, the optimized geometric parameters for HKrCl are shown. The bond lengths obtained here differ from those obtained from previous work by Lundell and co-workers,[34] which used MP2/6-311++G(2d,2p) (with an 18 electron ECP on Kr). The newly

calculated H-Kr bond length at the quintuple-ζ level for each type of basis set is ~0.1 Å greater at 1.53 Å than that reported in the previous work, while there was a decrease in the bond length for the Kr-Cl bond from 2.66 Å in the previous studies to ~2.51 Å for the basis sets used in the current study. Panek, *et. al*, have optimized several HNgX structures including HKrCl using a range of DFT approaches. Overall, their results are in reasonable agreement with those obtained in the present study.[183]

Table 6.1. Equilibrium geometry of HKrCl computed with CCSD(T) and the correlation consistent basis sets. Bond lengths in Å.

Basis Set	Equilibrium Geometry	
	$r_{(H-Kr)}$	$r_{(Kr-Cl)}$
cc-pV*n*Z		
n=T	1.554	2.517
Q	1.536	2.514
5	1.535	2.510
cc-pV(*n*+*d*)Z		
T	1.553	2.515
Q	1.535	2.513
5	1.533	2.510
aug-cc-pV*n*Z		
D	1.549	2.581
T	1.531	2.529
Q	1.531	2.519
5	1.532	2.516
aug-cc-pV(*n*+*d*)Z		
D	1.549	2.578
T	1.532	2.527
Q	1.530	2.519
5	1.531	2.512
Prev. calc.[a]	1.735	2.663
Prev. calc.[b]	1.534	2.687
Prev. calc.[c]	1.435	2.666
Prev. calc.[d]	1.500	2.563

[a] From Ref. 33 UMP2/LANL1DZ (Kr)/WBP (Cl)/6-311G**(H)
[b] From Ref. 33 UMP2/4333/433/4 (Kr)/533/5111 (Cl)/6-311G**(H)
[c] From Ref. 34 MP2/18-VE LANL1DZ (Kr)/6-311++G(2d,2p) (Cl, H)
[d] From Ref. 184 MP2(full)/aug-cc-pVDZ

6.3.2. Charge Distribution

It is evident from the Mulliken and NBO analysis data in Table 6.2 that there is a definite electronic charge transfer from krypton to the electronegative chlorine. This charge transfer suggests a hydrogen-krypton bond, despite a completely filled valence shell of krypton. The CCD/aug-cc-pVQZ calculation shows a larger charge separation between the krypton and chlorine and a smaller charge on the hydrogen than shown by an earlier UMP2 calculation [174]. Also, the CCD result is qualitatively different from the prior study,[34] which used an ECP on Kr and has a negative value on H. Charge separations, like the ones list in Table 6.2, are characteristic of the HNgX type of noble gas-bonded systems, which describe a resonance between covalent and ionic bonding (see Sec. 6.1).

Table 6.2. Partial charges (q) from Mulliken and Natural Bond Orbital (NBO) analysis on HKrCl optimized at the CCSD(T)/aug-cc-pV(5+d)Z level.

	Mulliken			NBO		
	H	Kr	Cl	H	Kr	Cl
HF/aug-cc-pVnZ						
n=D	0.1662	0.5616	-0.7278	0.1832	0.5779	-0.7610
T	0.0509	0.6598	-0.7107	0.1471	0.6062	-0.7532
Q	0.0774	0.6634	-0.7408	0.1350	0.6162	-0.7512
MP2/ aug-cc-pVnZ						
D	0.1044	0.5198	-0.6242	0.1355	0.5283	-0.6637
T	0.0068	0.5928	-0.5996	0.1119	0.5411	-0.6530
Q	0.0472	0.5817	-0.6288	0.1070	0.5445	-0.6515
CCD/ aug-cc-pVnZ						
D	0.1007	0.5505	-0.6512	0.1306	0.5561	-0.6867
T	0.0117	0.6201	-0.6318	0.1092	0.5723	-0.6815
Q	0.0551	0.6072	-0.6623	0.1064	0.5760	-0.6825
Prev. calc.[a]	0.135	0.530	-0.665			
Prev. calc.[b]	0.040	0.365	-0.405			
Prev. calc.[c]	-0.178	0.887	-0.709			

[a] From Ref. 33 UMP2/LANL1DZ (Kr)/WBP (Cl)/6-311G**(H).
[b] From Ref. 33 UMP2/4333/433/4 (Kr)/533/5111 (Cl)/6-311G**(H).
[c] From Ref. 34 MP2/18-VE LANL1DZ (Kr)/6-311++G(2d,2p) (Cl, H).

6.3.3. Relative Energy

As shown in Table 6.3, relative energies have been calculated in reference to the non-interacting acid halide and the krypton atom. The energies of the different molecular configurations are arranged in ascending order, and are reported relative to the Kr + HCl energy. The linear molecule HKrCl is the nearest in energy (4.393 eV) at the cc-pV5Z level to the combined energies of the neutral HCl and Kr atom. The relative energy of HKrCl falls between that of other similar systems, such as HXeCl at 2.6 eV[185] and HKrF at 5.72 eV.[179] The next three combinations of KrCl + H, HKr + Cl, and H + Kr + Cl only differ from one another by less than 0.02 eV, and are 0.24-0.29 eV above the energy of HKrCl. Therefore from a strictly energetic standpoint, HKrCl should dissociate to Kr + HCl. The charged species, $HKr^+ + Cl^-$ and $KrCl^+ + H^-$, are well above the linear HKrCl, with energies of 10.037 and 15.143 eV, respectively at the aug-cc-pV5Z level.

Table 6.3. Computed CCSD(T) energies relative to Kr + HCl, given in eV in ascending order.

	cc-pV5Z	aug-cc-pV5Z
Kr + HCl	0.000	0.000
HKrCl	4.393	4.358
KrCl + H	4.623	4.628
HKr + Cl	4.636	4.643
H + Kr + Cl	4.639	4.648
$HKr^+ + Cl^-$	10.138	10.037
$KrCl^+ + H^-$	15.466	15.143

6.3.4. Transition State

The optimized transition state structure for HKrCl → Kr + HCl, which is depicted in Table 6.4, has a bent geometry (Fig. 6.1), and is analogous to the transition states for the HArF and HKrF molecules.[176] From earlier work, the calculated HKrF bond angle was 102.1° using MP2/aug-cc-pVTZ,[176] whereas the calculated bond angle for HKrCl was 101.5° with CCSD(T)/aug-cc-pVQZ. The calculated bond lengths in this study for HKrCl also compare

favorably to similar noble gas systems, such as HKrF, with a slightly larger (0.02 Å) H-Kr bond length in HKrCl. The HKrCl barrier height of 1.14 eV is larger than the HKrF barrier height of 1.03 eV found by Chaban,[176] but smaller than the HXeCl barrier height of 1.4 eV found by Johansson.[185] Both aug-cc-pVDZ and aug-cc-pVTZ basis sets result in similar transition state geometries and minimum energy paths as shown in Fig. 6.2. Though the focus in this study has been upon the dissociation of HKrCl to Kr + HCl, it should be noted that a previous computational study on HXeCl has suggested that the most favorable decomposition channel for this species is HXeCl → H + Xe + Cl, and is favored for two reasons. First, the relative energy of H + Xe + Cl is lower than HXeCl, and secondly it also has a lower barrier height as compared with HXeCl→Xe+HCl dissociation.[176,185] Because H + Kr + Cl is higher in energy that HKrCl, the dissociation of HKrCl → H + Kr + Cl, was therefore, not considered, since it would be an energetically unfavored decomposition.

Table 6.4. Computed transition state geometry of HKrCl compared to HKrF and HArF. Angles are given in ° and bond lengths are given in Å.

MP2	$a_{(H\text{-}Ar\text{-}F)}$	$r_{(Ar\text{-}F)}$	$r_{(H\text{-}Ar)}$
aug-cc-pVTZ[a]	106.7	2.26	1.26
	$a_{(H\text{-}Kr\text{-}F)}$	$r_{(Kr\text{-}F)}$	$r_{(H\text{-}Kr)}$
aug-cc-pVTZ[a]	102.1	2.33	1.40
CCSD(T)	$a_{(H\text{-}Kr\text{-}Cl)}$	$r_{(Kr\text{-}Cl)}$	$r_{(H\text{-}Kr)}$
aug-cc-pVDZ	101.2	2.92	1.42
aug-cc-pVTZ	101.1	2.88	1.41
aug-cc-pVQZ	101.5	2.87	1.41

[a] From Ref. 176.

Figure 6.1. Transition state and minimum energy structure of HKrCl obtained with CCSD(T)/aug-cc-pVQZ and CCSD(T)/aug-cc-pV5Z respectively.

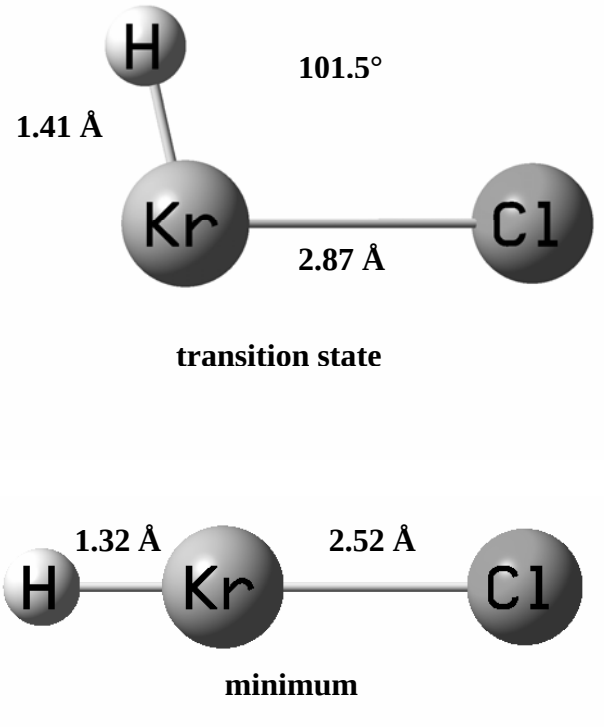

Figure 6.2. Minimum energy path for the H–Kr–Cl bending computed with CCSD(T) and the aug-cc-pV*n*Z basis sets.

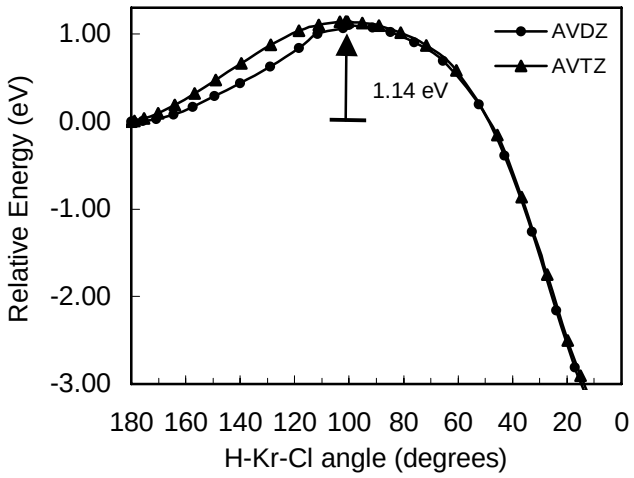

6.3.5. Vibrational Frequencies

The computed harmonic frequencies are presented in Table 6.5, and are generally higher than the experimental results. This is partially due to the lack of anharmonic corrections. As

discussed in recent work, the anharmonic corrections on HKrCl lower the H-Kr stretch by 250 cm^{-1}, reduce the H-Kr-Cl bend by 30 cm^{-1}, and shift Kr-Cl by only 1.4 cm^{-1}.[184] Matrix effects also influence the stretching frequencies of HKrCl, and should be similar to that previously noted in HArF,[179] which increased the H-Ar stretch by 30 cm^{-1}. Addition of the tight-*d* function in the basis set has very little impact in the description of the three vibrational modes. As compared with the experimentally known intense H-Kr stretch, the calculated frequency differs by approximately 135-170 cm^{-1} using the most advanced methods in this study, whereas for the degenerate bending modes, the calculated frequencies differ from experiment by ~50-60 cm^{-1}. Overall, the calculated Kr-Cl stretching modes are approximately 30 cm^{-1} from experiment.

Table 6.5. Vibrational frequencies for HKrCl computed with CCSD(T) and the correlation consistent basis sets. Frequencies in cm^{-1}.

Basis Set	Vibrational mode		
	$\nu_{(Kr-Cl)}$	$\delta_{(H-Kr-Cl)}$	$\nu_{(H-Kr)}$
cc-pV*n*Z			
n=T	284	597	1487
Q	284	601	1611
cc-pV(*n*+*d*)Z			
T	284	596	1488
Q	284	601	1613
aug-cc-pV*n*Z			
D	271	569	1497
T	280	593	1622
Q	281	597	1646
aug-cc-pV(*n*+*d*)Z			
D	271	569	1495
T	280	592	1620
Q	281	596	1643
Prev. calc.[a]	235.0	492.6	977.4
Prev. calc.[b]	272.8	566.9	1692.1
Prev. calc.[c]	275.7	604.2	1943.1
Expt.[d]	253.1	544	1476

[a] From Ref. 33 UMP2/LANL1DZ (Kr)/WBP (Cl)/6-311G**(H).
[b] From Ref. 33 UMP2/4333/433/4 (Kr)/533/5111 (Cl)/6-311G**(H).
[c] From Ref. 184 MP2(full)/aug-cc-pVDZ.
[d] From Ref. 33,184.

6.3.6. Atomization Energy

Calculated atomization energies are given in Table 6.6, and as shown, larger basis sets do have a significant impact upon the atomization energy. With the exception of the aug-cc-pV(T+*d*)Z basis set, all other basis sets at the double and triple zeta levels show a negative value for the atomization energy of HKrCl, whereas, the higher level basis sets result in positive values. This suggests that electron correlation plays an important role in the stability of these types of noble gas-bonded systems. At the aug-cc-pV5Z and aug-cc-pV(5+*d*)Z levels, the atomization energy is 4.94 and 5.54 kcal/mol, respectively.

Table 6.6. Atomization energy (kcal/mol) of HKrCl computed with CCSD(T) and the correlation consistent basis sets.

Basis set	AE (kcal/mol)
cc-pV*n*Z	
n=T	-4.51
Q	0.08
5	3.50
cc-pV(*n*+*d*)Z	
T	-4.39
Q	0.17
5	4.29
aug-cc-pV*n*Z	
D	-6.28
T	-0.07
Q	1.58
5	4.94
aug-cc-pV(*n*+*d*)Z	
D	-6.17
T	0.48
Q	1.94
5	5.54

6.4. Conclusions

Geometries, transition states, and frequencies have been calculated for HKrCl with the *ab initio* method CCSD(T) in combination with the standard and augmented correlation consistent basis sets. In comparison with the standard correlation consistent basis sets, the augmented sets

yield only slightly lower relative energies, while frequencies are overestimated. The ordering of relative energies for HKrCl is similar to other HNgX noble gas compounds that have been studied previously.

Transition state structures also are consistent with those obtained from earlier calculations on HArF, showing a bent geometry that leads to the dissociation of HKrCl into an acid halide and the neutral noble gas compound. The calculated barrier of 1.1 eV (~ 25 kcal/mol) indicates that the HKrCl molecule will be stable relative to the dissociation into Kr and the HCl.

CHAPTER 7

THE EXISTENCE OF $FKrCF_3$, $FKrSiF_3$, AND $FKrGeF_3$[§]

7.1. Introduction

As discussed in Chapter 6, krypton (once thought to be inert) was first shown to have chemical bonds (as opposed to van der Waal's forces) with fluorine in KrF_4[149] and KrF_2[150,151,186,187] and more recently with hydrogen and halides (HKrX).[33,34,174,176-178] Other neutral noble gas triatomics, HNgX (where Ng=He, Ne, Ar, Kr, Xe and X=H, F, Cl, Br, I), also have received considerable attention,[33,34,174,176-179,188-191] including computations which suggested the existence of HHeF.[190,191] Many of the new noble gas species were first suggested by theory, which then lead to observation via experiment.[192,193] Thus, the exploration of possible new species by theoretical predictions is vitally important to the discovery of new noble gas bonded molecules as well as furthering the knowledge of noble gas chemistry. The prediction of new noble gas-bonded systems is the focus of both this chapter and the subsequent chapter. When no experimental data are available to serve as a reference for computations, the historical performance of the methods and basis sets, often established via benchmark studies, must be used to gauge the reliability of computed chemical properties.

Prior experimental studies have focused primarily upon infrared spectra to characterize the stability and bonding of noble gas species. Theoretical studies, on the other hand, have been

§ This chapter has been adapted from the publication of *Chem. Phys. Lett.*, Vol. 411, Scott Yockel, Ankit Garg and A. K. Wilson, "The existence of $FKrCF_3$, $FKrSiF_3$, $FKrGeF_3$", Pages 91-97, Copyright (2005), with permission from Elsevier.

used to predict minimum energy geometries, dissociation energies, frequencies, and charge distributions. In terms of the theoretical work, there has been some debate as to what level of theory is needed to properly characterize noble gas compounds. It has been suggested that the structures of these HNgX compounds can be characterized with less expensive computational approaches such as density functional theory (DFT).[174,177-179] However, as shown by Panek *et al.*,[178] DFT with a triple-ζ quality basis set is capable of producing ground state structures (HHeI, HNeCl, HNeBr, HNeI) of compounds that are not found with *ab initio* methods such as MP2 and CCSD(T). The calculated dissociation energies for HNgX molecules vary widely with respect to the computational method. For HHeF, the computed dissociation energy ranges from –29.2 kcal/mol with the density functional PBE96 to 54.3 kcal/mol with the MP2 *ab initio* method. These studies also have suggested that *ab initio* methods, such as coupled cluster and multireference approaches, should be used to determine energetics for noble gas systems.[174,177-179] The need for more sophisticated methods is due to the importance that electron correlation plays in these molecules, which includes ground-states that are often coupled with low-lying excited states.

The investigation on HKrCl in Chapter 6 illustrated the need for higher electron correlation methods to predict accurate energetics of neutral noble gas systems.[194] To illustrate, CCSD(T) combined with large basis sets of at least quadruple- and quintuple-ζ quality was required to predict correctly a positive atomization energy. In the benchmark study with the correlation consistent basis sets in Chapter 3,[134] KrF_2 was shown to have a negative atomization energy at the cc-pVDZ level, with CCSD(T). This signifies that the bound molecule is higher in energy than the sum of the individual atoms and is therefore completely unstable. This is contrary to experimental evidence, which reported KrF_2 as a meta-stable molecule, with an

atomization energy of 21.9 kcal/mol.[152] Even at the CCSD(T)/cc-pVTZ level, where the optimized bond length is fairly close (0.01 Å) to experiment, the atomization energy was calculated to be 8.57 kcal/mol, (13.33 kcal/mol below the experimental value). For this molecule, an atomization energy within 2 kcal/mol of experiment was obtained only when the highest (quintuple-ζ) basis set level was used. Thus, method and basis set choice are important for accurate descriptions of these systems.

Recent noble gas studies, both experimental and theoretical, have targeted noble gas species of more than three atoms.[34,174,190,193,195-199] Largely, these studies have focused upon the formation and characterization of xenon compounds. To date only a few larger krypton compounds have been studied.[34,174,193,196,199,200] One of the older known krypton containing compounds is HKrCN, which has been studied using both infrared spectroscopy and *ab initio* methods (CCSD(T) with the LJ18 pseudopotential).[199] The Räsänen research group characterized the first "organokypton" molecules, HKrCCH and $HKrC_4H$, both experimentally and theoretically.[196,200] These species, as well as $HKrC_3H_3$, have been studied at the MP2 level with moderately sized basis sets, 6-311++G(2d,2p).[196] The insertion of krypton into water to form HKrOH was first predicted by McDowell with the MP2 and QCISD methods and 6-311++G(2d,2p) basis sets.[198] This study also determined the favored dissociation channel to Kr + H_2O to be through the bending mode with a barrier of ~0.52eV. It was later found by Chaban that the use of multi-reference methods shows the dissociation to H + Kr + OH to have an even lower barrier of ~0.15 eV and concluded that this path would be favored over bending mode.[197] As mentioned earlier, care must be taken when evaluating the energetics of noble gas molecules.

There is less known about argon compounds than about xenon or krypton compounds. While most studies have focused upon smaller species such as HArF,[33,176-179,201,202] little work

has been done on larger argon systems. Cohen, *et al.* focused both on FArCCH,[195] the lighter analog to FKrCCH[200] and FXeCCH,[193,203] and on $FArSiF_3$,[195] which is a non-linear compound similar to the xenon systems FXeSiF and $FXeSiF_3$[204] studied previously. This computational study was performed using an all-electron MP2 and CCSD(T) with the aug-cc-pVDZ basis set, and suggested that both of these argon species are meta-stable as indicated by their minimum energy structures, relative energies, and charge distributions. Based upon previous studies of the rare gases, the existence of meta-stable species such as $FArSiF_3$ suggests the possible existence of similar analogs for the other rare gases. Thus, this chapter examines the possible existence of $FKrCF_3$, $FKrSiF_3$, and $FKrGeF_3$. Though krypton-carbon bonding has been reported in the literature, krypton-silicon bonding in a neutral species (this is known to occur in charged species)[205] and krypton-germanium bonding have not been reported in the literature at the time of this study. Initial calculations on $FKrSiF_3$ and $FKrGeF_3$ have been done in collaboration with Ankit Garg, a high school student at the Texas Academy of Mathematics and Science.

7.2. Computational Methods

Density functional theory and *ab initio* methods have been used in combination with the standard and augmented (aug-) correlation consistent basis sets (cc-pV*n*Z).[1-4] Density functional approaches used include Becke's (B3)[56] three-parameter exchange functional with correlation functionals from Lee, Yang, and Parr (LYP)[57] and from Perdew and Wang (PW91),[206] combining to form B3LYP and B3PW91. These functionals were chosen for their computational efficiency as compared with *ab initio* correlated methods and for their demonstrated ability to predict minimum energy structures in noble gas compounds.[183] Additionally, MP2 and CCSD(T) were used to obtain the energetics for these krypton compounds. For the basis set choice, the

augmented correlation consistent basis sets have proven useful in past studies involving noble gas systems,[207-210] as these species have more dispersed bonding than seen in typical covalent bonding. Thus, diffuse functions are important. The comparison of the properties predicted with the methods in this study is important since there has been some deliberation in the past studies on which methods are appropriate for which properties.

Geometries were obtained using all four methods (B3LYP, B3PW91, MP2, and CCSD(T)). A natural bond order analysis (NBO) was done at the double- and triple-ζ basis set levels for Hartree-Fock (HF), B3LYP, and B3PW91 to characterize the bonding in these molecules. (The HF results are based upon the respective MP2 optimized geometries.) A comparison of the energies of various fragmentations of $FKrCF_3$, $FKrSiF_3$, and $FKrGeF_3$, relative to CF_4, SiF_4, and GeF_4, respectively, and Kr, has been done at the quadruple-ζ level with B3LYP, B3PW91, and MP2 and at the augmented triple-ζ level with CCSD(T). Vibrational frequencies were obtained at the double- though quadruple-ζ basis set levels with B3LYP, B3PW91, and MP2.

The density functional and Hartree-Fock calculations were performed with the GAUSSIAN98 software suite,[86] while the MP2 and CCSD(T) calculations were performed using the MOLPRO quantum chemistry programs.[85]

7.3. Results and Discussion

7.3.1. Minimum Energy Structure

The minimum energy structures are shown in Table 7.1 for $FKrCF_3$, $FKrSiF_3$, and $FKrGeF_3$. In comparing the geometries, the bond lengths generally converge more quickly when

using the augmented sets as compared with the standard sets. In $FKrSiF_3$, the bond length for F-Kr ranges from 2.08-2.10 Å at the aug-cc-pVQZ level, and is comparable to the F-Ar bond length of 2.09 Å reported for $FArSiF_3$.[211] The F-Kr distance predicted for $FKrGeF_3$ is shorter than for its silicon analog (for every method and basis set combination, with the exception of MP2/cc-pVDZ), and the F-Kr bond length (~2.0 Å) is even shorter in $FKrCF_3$ at the quadruple-ζ level with MP2. Due to the shorter F-Kr bond length, $FKrCF_3$ is expected to have the strongest F-Kr bond of the three species. Figure 7.1, compares the krypton containing bond lengths determined using CCSD(T)/aug-cc-pVTZ to (1) the sum of the covalent radii, and (2) the sum of the van der Waal's radii. As shown in this figure, the bond distances to krypton are nearer in length to the covalent radii than to the van der Waal's radii, which suggests that these systems contain chemical bonds to krypton. The Kr-Si and Kr-Ge bonds are only ~0.1 Å longer than the covalent radii, whereas Kr-C is ~0.2 Å longer. The Kr-Ge-F angles are ~2.0º larger than the Kr-Si-F and Kr-C-F bond angles.

Previous studies have questioned the usefulness of DFT in the prediction of noble gas compounds due, in large part, to the prediction of ground state structures that are not obtained when using *ab initio* correlated methods.[183] In this study, such differences were not observed.

Table 7.1. Computed optimized geometries for $FKrCF_3$, $FKrSiF_3$, $FKrGeF_3$, with bond lengths (r) in Å, and angles (a) in °. All three structures have C_{3v} symmetry.

Method		cc-pV*n*Z					aug-cc-pV*n*Z			
$FKrCF_3$		$r_{(F\text{-}Kr)}$	$r_{(Kr\text{-}C)}$	$r_{(C\text{-}F)}$	$a_{(Kr\text{-}C\text{-}F)}$		$r_{(F\text{-}Kr)}$	$r_{(Kr\text{-}C)}$	$r_{(C\text{-}F)}$	$a_{(Kr\text{-}C\text{-}F)}$
B3LYP										
	D	2.051	2.189	1.326	108.6	D	2.057	2.137	1.328	108.3
	T	2.033	2.140	1.321	108.5	T	2.049	2.131	1.320	108.3
	Q	2.035	2.129	1.319	108.4	Q	2.045	2.128	1.319	108.3
B3PW91										
	D	2.033	2.158	1.322	108.6	D	2.037	2.111	1.324	108.4
	T	2.014	2.112	1.317	108.5	T	2.029	2.106	1.316	108.4
	Q	2.016	2.105	1.315	108.5	Q	2.025	2.103	1.315	108.4
MP2										
	D	2.029	2.179	1.329	108.7	D	2.023	2.092	1.336	108.7
	T	1.983	2.077	1.320	108.9	T	2.004	2.066	1.320	108.7
	Q	1.983	2.063	1.317	108.8	Q	1.997	2.061	1.317	108.7
CCSD(T)										
						D	2.046	2.132	1.336	108.4
						T	2.023	2.092	1.319	108.6
$FKrSiF_3$		$r_{(F\text{-}Kr)}$	$r_{(Kr\text{-}Si)}$	$r_{(Si\text{-}F)}$	$a_{(Kr\text{-}Si\text{-}F)}$		$r_{(F\text{-}Kr)}$	$r_{(Kr\text{-}Si)}$	$r_{(Si\text{-}F)}$	$a_{(Kr\text{-}Si\text{-}F)}$
B3LYP										
	D	2.072	2.453	1.624	109.6	D	2.102	2.396	1.613	109.0
	T	2.075	2.376	1.580	109.0	T	2.106	2.361	1.577	108.5
	Q	2.087	2.361	1.571	108.8	Q	2.104	2.356	1.570	108.5
B3PW91										
	D	2.054	2.425	1.622	109.5	D	2.080	2.376	1.610	109.0
	T	2.057	2.354	1.578	109.0	T	2.083	2.344	1.575	108.6
	Q	2.067	2.344	1.568	108.8	Q	2.082	2.340	1.567	108.6
MP2										
	D	2.050	2.409	1.624	109.3	D	2.093	2.341	1.612	108.4
	T	2.048	2.306	1.574	108.6	T	2.091	2.295	1.572	108.0
	Q	2.060	2.288	1.565	108.3	Q	2.085	2.286	1.564	108.0
CCSD(T)						D	2.100	2.365	1.611	108.6
						T	2.099	2.309	1.570	108.1

(table continues on next page)

(Table 7.1 continued)

Method		cc-pV*n*Z					aug-cc-pV*n*Z			
$FKrGeF_3$		$r_{(F-Kr)}$	$r_{(Kr-Ge)}$	$r_{(Ge-F)}$	$a_{(Kr-Ge-F)}$		$r_{(F-Kr)}$	$r_{(Kr-Ge)}$	$r_{(Ge-F)}$	$a_{(Kr-Ge-F)}$
B3LYP										
	D	2.068	2.561	1.742	111.2	D	2.079	2.513	1.736	110.7
	T	2.053	2.500	1.716	111.0	T	2.074	2.486	1.715	110.6
	Q	2.059	2.489	1.713	110.8	Q	2.071	2.483	1.712	110.7
B3PW91										
	D	2.049	2.529	1.738	110.6	D	2.057	2.485	1.730	110.1
	T	2.034	2.471	1.710	110.4	T	2.053	2.460	1.709	110.0
	Q	2.039	2.463	1.707	110.3	Q	2.049	2.458	1.706	110.1
MP2										
	D	2.062	2.588	1.751	111.6	D	2.053	2.482	1.745	110.6
	T	2.014	2.449	1.734	111.3	T	2.044	2.430	1.735	110.7
	Q	2.021	2.427	1.734	111.1	Q	2.036	2.423	1.734	110.8
CCSD(T)										
						D	2.080	2.521	1.743	110.7
						T	2.065	2.452	1.734	110.7

Figure 7.1. Calculated krypton bond lengths determined with CCSD(T)/aug-cc-pVTZ reported relative to the van der Waals and covalent radii.

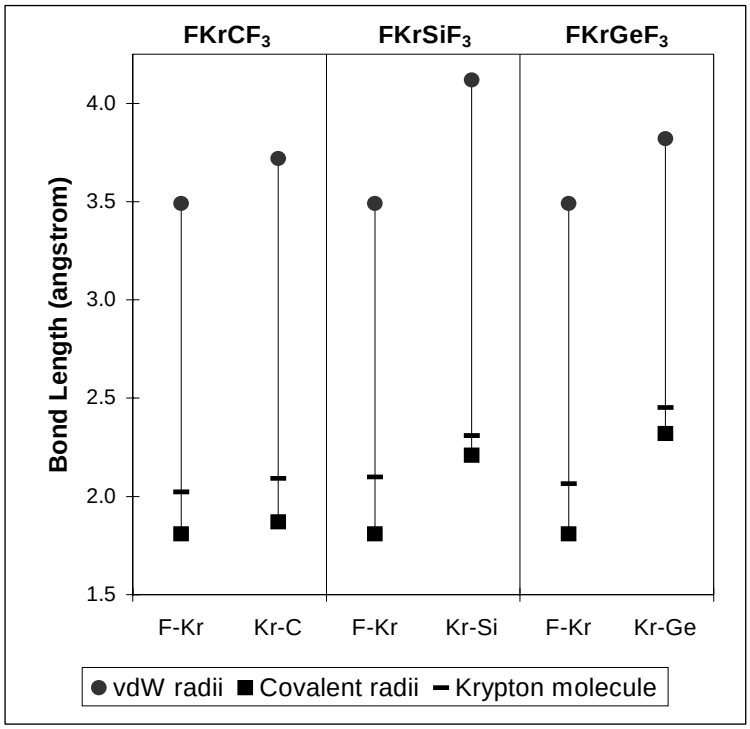

7.3.2. Charge Distribution

The magnitude of the charge distribution is shown in Table 7.2. There are only slight differences in the charge distributions for the two molecules $FKrSiF_3$ and $FKrGeF_3$, whereas $FKrCF_3$ differs from these two species. In $FKrCF_3$, krypton has a partial charge of 0.68-0.78 at the aug-cc-pVTZ level, whereas the partial charge on krypton within $FKrSiF_3$ and $FKrGeF_3$ is 0.46-0.49 and 0.48-0.56, respectively. The overall charge on the carbon (~1.0) is approximately half that of silicon and germanium (~2.0). $FKrSiF_3$ has a larger charge separation between F (most negatively charged) and Si (most positively charged) than $FKrGeF_3$ does between F and Ge, and also has a more ionic F-Kr bond. Overall, DFT at the cc-pVDZ basis set level results in the smallest charge separations for these molecules. As compared with the $FArSiF_3$ results from Ref. 211 that show a charge separation of 3.207 between F and Si, both $FKrSiF_3$ and $FKrGeF_3$ have greater charge separations; also the F-Ar bond is slightly more ionic in $FArSiF_3$.

Table 7.2. Particle charges (q) of $FKrCF_3$, $FKrSiF_3$, and $FKrGeF_3$ computed with Natural bond order (NBO) analysis.

	$FKrCF_3$				$FKrSiF_3$				$FKrGeF_3$			
	F	Kr	C	F	F	Kr	Si	F	F	Kr	Ge	F
HF/cc-pV*n*Z[a]												
D	-0.7189	0.7294	1.1916	-0.4007	-0.8394	0.4829	2.3709	-0.6715	-0.7476	0.5268	2.2301	-0.6697
T	-0.7745	0.7621	1.0715	-0.3531	-0.8767	0.4919	2.3819	-0.6657	-0.8009	0.5576	2.2424	-0.6664
HF/aug-cc-pV*n*Z[a]												
D	-0.7784	0.7912	1.1746	-0.3958	-0.8818	0.4747	2.4975	-0.6968	-0.8131	0.5267	2.3812	-0.6983
T	-0.7949	0.7776	1.0792	-0.3540	-0.8915	0.4846	2.4214	-0.6715	-0.8260	0.5383	2.3060	-0.6728
B3LYP/cc-pV*n*Z												
D	-0.5667	0.6051	0.9949	-0.3445	-0.6497	0.4347	2.0442	-0.6103	-0.5377	0.4436	1.8461	-0.5840
T	-0.6393	0.6348	0.9368	-0.3108	-0.7109	0.4638	2.1208	-0.6246	-0.6266	0.4864	1.9579	-0.6059
B3LYP/aug-cc-pV*n*Z												
D	-0.6415	0.6633	1.0113	-0.3444	-0.7105	0.4574	2.1967	-0.6478	-0.6333	0.4709	2.0606	-0.6327
T	-0.6612	0.6552	0.9424	-0.3121	-0.7468	0.4645	2.1827	-0.6335	-0.6697	0.4843	2.0393	-0.6179
B3PW91/cc-pV*n*Z												
D	-0.5793	0.6179	0.9915	-0.3434	-0.6134	0.4490	1.9849	-0.6069	-0.5475	0.4515	1.8511	-0.5850
T	-0.6457	0.6449	0.9145	-0.3046	-0.7077	0.4729	2.0938	-0.6197	-0.6452	0.4973	1.9536	-0.6028
B3PW91/aug-cc-pV*n*Z												
D	-0.6455	0.6726	0.9993	-0.3421	-0.7090	0.4617	2.1766	-0.6433	-0.6395	0.4756	2.0513	-0.6290
T	-0.6643	0.6640	0.9188	-0.3062	-0.7733	0.4658	2.1829	-0.6252	-0.6816	0.4913	2.0281	-0.6137

[a] HF calculations were performed with the respective MP2 optimized geometries.

7.3.3. Relative Energy

Relative energies have been used in computational studies on noble gas compounds as a tool to asses the stability of the noble gas compounds and their fragmented parts relative to noble gas atom and the precusor.[179,191-194,196,212] Table 7.3 shows energy differences for various molecular configurations relative to the combined energies of the krypton atom and carbon/silicon/germanium tetrafluoride. For each family of molecular configurations, the same relative energy ordering of the configurations occurs. $FKrCF_3$, $FKrSiF_3$, and $FKrGeF_3$ are the nearest configuration in energy (lowest relative energy) to the separated tetrafluoride molecule and the krypton atom. The relative energies of the corresponding carbon and germanium configurations are more similar to one another than to the relative energies of the silicon systems. As compared with $FKrCF_3$ and $FKrGeF_3$, there is a greater energy separation between $FKrSiF_3$ and the next highest relative energy configuration. For example, when using B3LYP/cc-pVQZ, the relative energy for $FKrGeF_3$ is 4.759 eV and for $FKrSiF_3$ is 5.887 eV, whereas the increases in energy to the next highest configuration ($F + Kr + GeF_3$ and $F + Kr + SiF_3$) are 0.573 eV and 1.028 eV, respectively. The carbon system has the lowest increase in energy from the full molecule ($FKrCF_3$) to the next highest combination ($F + Kr + CF_3$) at 0.463 eV with B3LYP/cc-pVQZ. As compared with DFT, nearly all of the MP2 relative energies were found to be slightly higher. Generally, with MP2 there is a larger change in the relative energies from one molecular combination to the next as shown in Table 7.3. For example, when using B3LYP/cc-pVQZ for the germanium system, the energy increase is 0.573 eV from $FKrGeF_3$ to $F + Kr + GeF_3$, while using MP2/cc-pVQZ and aug-cc-pVQZ the increases in energy are 0.753 eV and 0.918 eV, respectively. For all three systems (carbon, silicon, and germanium), the full molecule is the lowest in relative energy as compared with the relative energies of the other molecular

configurations (with the exception of the energy arising from the reference – the separated krypton atom and tetrafluoride).

Table 7.3. Relative energies computed with B3LYP, B3PW91, MP2 and CCSD(T) in eV.

Method	B3LYP		B3PW91		MP2		CCSD(T)
Basis Set	cc-pVQZ	aug-cc-pVQZ	cc-pVQZ	aug-cc-pVQZ	cc-pVQZ	aug-cc-pVQZ	aug-cc-pVTZ
$Kr + CF_4$	0.000	0.000	0.000	0.000	0.000	0.000	0.000
$FKrCF_3$	5.004	4.927	5.025	4.963	5.296	5.139	5.219
$Kr + CF_3 + F$	5.466	5.434	5.506	5.484	6.017	6.032	5.678
$KrF_2 + CF_2$	8.060	7.985	8.240	8.182	8.657	8.526	8.422
Kr + C + 4F	20.398	20.335	20.648	20.604	21.754	21.851	20.271
$Kr + SiF_4$	0.000	0.000	0.000	0.000	0.000	0.000	0.000
$FKrSiF_3$	5.887	5.735	5.827	5.747	6.220	6.037	6.053
$Kr + SiF_3 + F$	6.916	6.838	6.851	6.837	7.469	7.489	7.067
$KrF_2 + SiF_2$	10.207	10.078	10.249	10.224	11.086	10.954	10.616
Kr + Si + 4F	25.577	25.454	24.002	23.953	25.915	26.028	23.920
$Kr + GeF_4$	0.000	0.000	0.000	0.000	0.000	0.000	0.000
$FKrGeF_3$	4.749	4.677	4.748	4.690	5.155	5.008	5.025
$Kr + GeF_3 + F$	5.322	5.297	5.336	5.321	5.908	5.926	5.551
$KrF_2 + GeF_2$	7.108	7.029	7.245	7.186	8.037	7.900	7.724
Kr + Ge + 4F	19.448	19.386	19.450	19.436	21.052	21.179	19.466

7.3.4. Vibrational Frequency

Vibrational frequencies have been calculated, and only the stretching modes involving the krypton bonds are included in Table 7.4. The first mode shown in the table is purely a stretching mode, where the three fluorides are in translation with the C, Si, and Ge atoms, respectively. In each occurrence of this vibrational mode, a symmetric stretch; the displacement of the krypton relative to the fluorine changes from carbon to germanium. In the carbon system, the mode (242 cm^{-1} at MP2/cc-pVQZ) is predominantly a Kr-C stretch as the krypton and fluorine undergo similar displacement, while in the germanium system this mode is dominated

by the F-Kr bond stretch (165 cm^{-1} at MP2/cc-pVQZ). The next two modes listed (ν_s and ν_{as}) in the table consist of a stretch and bend combination. The largest change in the same mode for the three molecules is noted for the ν_{as} of the carbon system (751 cm^{-1} at MP2/cc-pVQZ) as compared to that of the silicon and germanium systems (488 and 474 cm^{-1}, respectively). For the ν_s modes calculated, the silicon and carbon systems have more similar vibrational frequencies (499 cm^{-1} and 414 cm^{-1} at MP2/cc-pVQZ, respectively) as compared with the germanium system (284 cm^{-1}). Overall there is a distinct lowering in the vibrational stretching modes involving krypton from carbon to germanium.

Table 7.4. Computed vibrational frequencies (cm^{-1}) that contain krypton bond stretching modes.

Method		cc-pV*n*Z				aug-cc-pV*n*Z		
$FKrCF_3$		$\nu_{(FKr-C)}$	$\nu_{s\ (F-Kr-C)}$	$\nu_{as\ (F-Kr-C)}$		$\nu_{(FKr-C)}$	$\nu_{s\ (F-Kr-C)}$	$\nu_{as\ (F-Kr-C)}$
B3LYP								
	D	199.2	431.0	725.2	D	217.9	425.7	721.2
	T	216.1	435.0	738.5	T	220.1	422.2	737.8
	Q	220.2	433.7	738.5	Q	220.5	424.1	738.7
B3PW91								
	D	208.4	441.7	734.8	D	228.3	438.4	730.4
	T	227.6	446.6	747.8	T	230.7	433.3	747.3
	Q	230.8	445.1	747.5	Q	231.2	435.5	748.0
MP2								
	D	174.6	480.3	730.4	D	223.0	474.6	714.5
	T	232.0	499.4	749.2	T	238.3	476.9	745.8
	Q	241.6	499.1	751.0	Q	242.4	481.9	750.3
$FKrSiF_3$		$\nu_{(FKr-Si)}$	$\nu_{s\ (F-Kr-Si)}$	$\nu_{as\ (F-Kr-Si)}$		$\nu_{(FKr-Si)}$	$\nu_{s\ (F-Kr-Si)}$	$\nu_{as\ (F-Kr-Si)}$
B3LYP								
	D	168.2	378.7	456.8	D	179.6	371.9	446.4
	T	184.6	392.5	468.4	T	188.8	377.4	460.4
	Q	188.6	390.0	467.2	Q	190.2	379.1	463.1
B3PW91								
	D	174.3	384.6	465.1	D	185.1	381.0	455.5
	T	191.2	400.1	475.8	T	194.1	386.5	467.8
	Q	194.0	398.2	474.3	Q	195.2	388.6	470.2

(table continues on next page)

(Table 7.4 continued)

Method		cc-pV*n*Z				aug-cc-pV*n*Z		
MP2								
	D	162.0	405.5	483.3	D	192.2	389.5	453.9
	T	206.3	419.7	488.3	T	212.0	391.5	477.2
	Q	213.4	414.6	487.9	Q			
$FKrGeF_3$		ν (FKr-Ge)	ν_s (F-Kr-Ge)	ν_{as} (F-Kr-Ge)		ν (FKr-Ge)	ν_s (F-Kr-Ge)	ν_{as} (F-Kr-Ge)
B3LYP								
	D	149.8	263.6	423.6	D	156.4	263.4	418.4
	T	158.4	276.1	429.3	T	160.2	274.0	415.3
	Q	160.1	275.5	426.0	Q	160.5	273.8	417.0
B3PW91								
	D	155.4	268.2	434.5	D	162.1	269.7	431.1
	T	164.6	281.5	440.5	T	166.1	279.9	426.9
	Q	166.0	281.2	437.4	Q	166.4	279.8	429.1
MP2								
	D	118.7	273.9	458.8	D	151.7	278.1	454.5
	T	159.0	285.6	480.2	T	163.4	283.7	451.2
	Q	164.6	284.7	474.3	Q	164.8	283.0	457.3

7.4. Conclusions

Three new, neutral noble gas compounds, $FKrCF_3$, $FKrSiF_3$ and $FKrGeF_3$, have been characterized using DFT and *ab initio* methods. Whereas a number of previous studies of noble gas compounds found that DFT falsely predicted bound structures that were not detectable using *ab initio* methods, both types of approaches predicted comparable structures and energetics for the molecules in this study. In a comparison of the bonding and relative energies of these three new krypton compounds, $FKrCF_3$ is more similar to $FKrGeF_3$ than to $FKrSiF_3$. Furthermore, this study suggests the existence of the first known germanium-krypton bonding.

CHAPTER 8

CHARACTERIZATION OF NEW ORGANOKRYPTON SPECIES

8.1. Introduction

The origin of noble gas bonded systems and the earliest theoretical studies on xenon and krypton bonded systems have been discussed previously (see Sec. 6.1). Recent studies,[174,177,179,183,198,213] have helped to understand the level of theory needed to predict chemical properties of these noble gas bonded systems. Similar to Chapter 7, the main focus of this chapter is on the prediction of new noble gas bonded systems.

Recent work has suggested noble gas atom insertion into hydrocarbons, yielding a new class of molecules appropriately named "organo-noble gas" compounds. Lundell *et al*. provided the first such study, in which MP2 and CCSD(T) calculations predicted structures where Xe had been inserted in C–H and O–H bonds to form HXeCCH, $HXeC_6H_5$, and $HXeOC_6H_5$.[192] Shortly thereafter, Feldman and co-workers,[203] and the Räsänen group[193] reported the experimental synthesis of HXeCCH using a matrix isolation technique as overviewed in Sec 6.1. In addition, the Räsänen group detected the formation of HXeCC and HXeCCXeH with infrared spectroscopy.[193] Both of these species had been studied by Lundell *et al*. using computational methods[192] Räsänen's work marked the first time a neutral noble gas hydride had been synthesized which contained two xenon atoms. The analogous krypton species HKrCCH was then synthesized by the Räsänen group, providing the first "organokypton" system. However, it is not believed that HKrCC or HKrCCKrH were formed during the synthesis of HKrCCH, since no vibrational bands were observed for these additional species[196] The Räsänen group also

performed theoretical computations that provided a possible reason for the absence of the HKrCC and HKrCCKrH molecules in the experimental infrared analysis. From their all-electron correlated MP2 computations with the aug-cc-pVDZ basis set, HKrCC was found to be 1.38 eV higher in energy than H + Kr + C≡C.[196] This suggests that the formation of HKrCC is energetically unfavorable and that the C≡C species, which is lower in energy, is more likely to be detected by infrared analysis. Additional experiments have included the synthesis of diacetylene xenon and krypton systems, $HXeC_4H$ and $HKrC_4H$, respectively, with characterization of the bonding through infrared spectroscopy. This work also included MP2 computations with a triple-ζ quality (6-311++G(2d,2p)) basis set on H, Kr, and C and an 18 electron RECP on Xe (LJ18).[200]

Other recent theoretical studies have examined the bonding of noble gases to silicon.[195,204,212] These studies have suggested FXeSiF, $FXeSiF_3$, $HXeSiF_3$, and $FArSiF_3$ as chemically bound molecules,[195,204] as well as $FKrSiF_3$, which was studied in Chapter 7. Furthermore, in Chapter 7 it was shown for the first time that krypton is capable of forming chemical bonds to germanium.[214]

The study in this chapter identifies two potentially new noble gas-bonded compounds, FKrCCKrF and FKrCCF, which stem from the analogous HXeCCXeH and HXeCCH molecules. It is proposed that the fluorinated systems should be more stable than the krypton-hydride species, HKrCCKrH and HKrCC,.[196] and that a di-krypton species (FKrCCKrF) may be stable enough to be detected through infrared analysis. Initial calculations in this chapter have been done in collaboration with Evan Gawlik, a high school student at the Texas Academy of Mathematics and Science.

8.2. Methodology

Optimal geometries, vibrational frequencies, charge distributions, and relative energies of the ground-state molecules, FKrCCKrF and FKrCCF, were computed. These computations were performed using the B3LYP[56,57] hybrid density functional and the *ab initio* methods, MP2[215] and CCSD(T).[50-52] These methods where used in combination with the correlation consistent basis sets (cc-pV*n*Z) developed by Dunning *et al,*.[1-3] Previously, in Chapters 3 and 4 it was shown that coupling the correlation consistent basis sets with CCSD(T), can provide accurate (~1-2 kcal/mol) energetics for krypton-flouride bonded systems. For noble gas systems that contain krypton-fluoride bonding, these computational approaches (B3LYP, MP2, and CCSD(T)) have provided qualitatively similar structural and energetic properties, as shown in Chapter 7.[214] However, the validity of using DFT for the accurate prediction of noble gas bonded systems has been questioned in the past,[178] and therefore, MP2 and CCSD(T) was also used in this study.

Due to the large computational cost, large quintuple-ζ basis sets were not applicable for geometry optimizations and vibrational frequency calculations with MP2, and furthermore, aug-cc-pVTZ was the largest basis set used in the CCSD(T) calculations. Charge distributions were calculated using the Natural Bond Order (NBO) analysis at the B3LYP/aug-cc-pVTZ level of theory, enabling a qualitative description of the charge separation in the noble gas bonds. As shown in Chapter 5, the relative charge distribution varies little with respect to choice of correlated method; thus, only one approach (B3LYP) was used in this study.

As relative energies have been useful in previous noble gas studies to provide an energy ordering of the various meta-stable species with respect to the energy of the noble gas and precursor molecule,[179,191-194,196,214] relative energies have been determined in the present study. Relative energy computations enabled the prediction that HXeCC and HXeCCXeH were stable

species,[192] prior to experimental observation. These species were later found experimentally during the characterization of HXeCCH.[193,203]

In this study, the energies are examined relative to (Kr + FCCF), which is the sum of the energies of the unbound noble gas (Kr) and the precursor molecule (FCCF). Several combinations of the constituent atoms of the FKrCCKrF compounds were considered and their relative energies were determined using B3LYP and MP2 computations paired with the aug-cc-pVQZ basis set, and also using CCSD(T) paired with the aug-cc-pVTZ basis set.

Transition-state structures were identified for both the FKrCCKrF → FKrCCF + Kr and FKrCCF → FCCF + Kr reactions using the Quadratic Steepest Descent (QSD) method,[181,182] and energy and frequency calculations for transition-state structures were performed using MP2 at the aug-cc-pVDZ, aug-cc-pVTZ, and aug-cc-pVQZ basis sets levels. Intrinsic reaction coordinate (IRC) calculations also were performed at these levels of theory to verify the transition structure as the barrier in the decomposition pathway.

Density functional computations were performed using the GAUSSIAN 03 software suite,[216] and the MP2 and CCSD(T) computations were performed using the MOLPRO quantum chemistry package.[85]

8.3. Results and Discussion

8.3.1. Minimum Energy Structures

Optimal geometries, as shown in Table 8.1, were found for the ground state structures for FKrCCKrF and FKrCCF, in which both structures were found to be linear. It must be noted that in Table 8.1, a number of double-ζ optimized geometries have been excluded because the frequency analysis provides imaginary normal modes, which indicates that the structures found

were not minimum energy structures. This is not surprising, as a double-zeta basis set did not correctly predict KrF_2 (Chapter 3) and HKrCl (Chapter 6) to be stable with respect to dissociation, though both of these species have been shown by experiment to exist.[33,35,106] However, a better account of electron correlation arising from an increase in basis set size resulted in the correct characterization of the species. As in this earlier work, the double-zeta basis sets were not useful in the description of the noble gas species, as B3LYP and MP2 computations using the cc-pVDZ basis set did not lead to a minimum energy structure for FKrCCKrF. This was remedied upon increasing the basis set size.

The typical bond length dependence on basis sets was found for FKrCCKrF and FKrCCF. Most of the krypton bond lengths have reached convergence at the quadruple-ζ level and only change ~0.005 Å from the triple-ζ level to the quadruple-ζ level, when using either B3LYP or MP2. However, there is a convergence issue with the F-Kr bond in FKrCCF when using B3LYP and the cc-pV*n*Z basis sets, in that the bond length changes from 1.973, 1.967, and 1.974 when *n*=D, T, and Q, respectively. In fact, the convergence issue with the bond lengths of F-Kr was resolved when diffuse functions are used (see the B3LYP/aug-cc-pV*n*Z results in Table 8.1) Problems with the convergence of molecular properties in DFT, with respect to the correlation consistent basis sets, are known and have been studied previously by Wang and Wilson.[98-100] The inclusion of diffuse functions in the basis sets generally provides longer F-Kr bond lengths and shorter Kr–C bond lengths than are found using the standard correlation consistent basis sets. Upon the second insertion of krypton into the acetylene derivative, there is a slight shortening (~0.008 Å) in the F–Kr bond, while the Kr–C and C–C bonds are slightly lengthened by 0.015 and 0.012 Å, respectively. A slight change in geometry was also seen in the HXeCCXeH system, in which the H–Xe and C–C bonds were lengthened by 0.027 and 0.016 Å,

respectively, while the Xe–C bond decreased by 0.008 Å. In both the current study and the HXeCCXeH study,[192] the bond distance from the noble gas atom to the most electronegative atom decreased upon the addition of the second noble gas atom.

The computed krypton-carbon bond lengths in these two new systems are slightly shorter than those predicted in previous computational studies on analogous compounds. For example, MP2/aug-cc-pVQZ calculations predict a Kr–C bond length in FKrCCF of 1.913 Å whereas the work presented in Chapter 7 predicted Kr-C bond length of 2.061 Å in $FKrCF_3$ using MP2/aug-cc-pVQZ.[214] Also, in a study by Khriachtchev *et al.*[196] on HKrCCH, the Kr–C bond length is 2.25 Å with MP2(full)/aug-cc-pVDZ. This bond length is much longer (0.28 Å) than the Kr–C length in FKrCCF, shown in Table 1. Likewise, the F–Kr bond length in FKrCCKrF as computed at the MP2/aug-cc-pVTZ level (1.954 Å), is significantly shorter than the bond length found in HKrF (2.034 Å) as computed by Chaban and co-workers[176] at the same level of theory. Knowing that a shorter bond length generally corresponds to a stronger bond, both the single and double insertion of krypton into FCCF should provide a more stable noble gas bonded system in comparison to the analogous systems, HKrCCH and HKrCCKrH. .

Table 8.1. B3LYP, MP2, and CCSD(T) computed minimum energy structures for FKrCCKrF and FKrCCF molecules. Bond lengths are in Å.

Method	Basis	FKrCCKrF			FKrCCF			
		F-Kr	Kr-C	C-C	F-Kr	Kr-C	C-C	C-F
B3LYP	cc-pV*n*Z							
	n=D	--	--	--	1.973	1.989	1.210	1.283
	T	1.961	1.965	1.205	1.967	1.952	1.196	1.274
	Q	1.966	1.955	1.203	1.974	1.941	1.194	1.273
	aug-cc-pV*n*Z							
	D	1.987	1.967	1.218	1.996	1.950	1.207	1.281
	T	1.976	1.952	1.204	1.986	1.937	1.194	1.274
	Q	1.973	1.950	1.203	1.983	1.936	1.194	1.272
MP2	cc-pV*n*Z							
	D	--	--	--	1.961	1.986	1.229	1.288
	T	1.933	1.949	1.226	1.936	1.934	1.211	1.277
	Q	1.937	1.933	1.222	1.942	1.918	1.207	1.274
	aug-cc-pV*n*Z							
	D	1.977	1.967	1.244	1.982	1.945	1.228	1.292
	T	1.954	1.934	1.225	1.961	1.917	1.210	1.276
	Q	1.947	1.929	1.222	1.955	1.913	1.207	1.273
CCSD(T)	aug-cc-pV*n*Z							
	D	1.987	1.986	1.237	1.993	1.965	1.225	1.296
	T	1.963	1.948	1.218	1.971	1.931	1.206	1.278

8.3.2. Charge Distribution

For each molecule, charge distribution calculations indicate highly positive charges on the krypton atoms, highly negative charges on the halogens, and relatively neutral charges on the carbon atoms. These computed partial charges are shown in Table 8.2. A larger charge separation generally aids in the stability of these molecules, and (as discussed in Sec 6.1) is characteristic of the resonance between the somewhat ionic and covalent nature of noble gas bonding. In a similar system, HKrCCH,[196] the charge on Kr was 0.535, which is slightly less than the charge on Kr in the FKrCCF system. The charges on carbons in these two systems are different, since in the CCH radical, the carbons are the most electronegative. Thus in HKrCCH, this causes the charge to be much larger (~ -0.4) on the carbons in HKrCCH. In the CCF radical, fluorine is the most electronegative species and carries the largest charge (~ -0.6), which causes a

significant difference to the partial atomic charges in FKrCCF as compared to HKrCCH. The highly ionic character of the F–Kr bond in the di-krypton system suggests that the formation of FKrCCKrF should be fairly stable.

Table 8.2. Charge distributions (q) for HKrCCKrF and FKrCCF from B3LYP/aug-cc-pVTZ Natural Bond Order analysis.

FKrCCKrF			FKrCCF				
F	Kr	C	F	Kr	C	C	F
-0.6130	0.7443	-0.1313	-0.6269	0.6732	0.1200	0.0031	-0.1693

8.3.3. Relative Energy

Relative energy calculations have been used in previous studies to provide an energy ordering of the various meta-stable species with respect to the energy of the noble gas and precursor molecule.[179,191-194,196,214] In Table 8.3, the computed relative energies are shown for the FKrCCF and FKrCCKrF molecules, as well as other molecular species that might occur during the formation/decomposition process. In this study, the FKrCCF molecule was the lowest in energy relative to the most stable combination of the constituent atoms, C_2F_2 + 2Kr. As shown in Table 8.3, the insertion of the second krypton has roughly twice the relative energy of the first insertion.

The relative energy ordering of each of the molecular species in Table 8.3 was found to be the same with each computational method used. The most noticeable difference in the MP2 and CCSD(T) relative energies is the energy change between FKrCCKrF and F_2 + C_2 + 2Kr; for MP2 this difference is 0.882 eV and for CCSD(T) it is 0.101 eV. It would appear that the more sophisticated CCSD(T) level of theory (which should recover more correlation energy) predicts the FKrCCKrF system to be less stable and closer to the energy of the F_2 + C_2 + 2Kr system. This is contrary to the notion that krypton-bonded systems rely heavily on electron correlation to be bound, as shown for KrF_2 in Chapter 3 and HKrCl in Chapter 6. However, closer inspection

reveals that the correlation energy in FKrCCKrF described by the MP2/aug-cc-pVQZ (-1.372697 E_h) computation is larger than that of the CCSD(T)/aug-cc-pVTZ (-1.352754 E_h) computation, which shows the large dependence on basis sets size for energetic properties of noble gas bonded systems.

In the experimental synthesis of HXeCCH, two other xenon systems were also detected by infrared spectroscopy, HXeCCXeH and HXeCC.[193] However, as mentioned previously, the HKrCCH experimental study did not detect either HKrCCKrH or HKrCC.[196] From the relative energy predictions in Table 8.3, the formation of FKrCCF likely would enable FKrCCKrF to be observed by infrared spectroscopy. The detection of FKrCC is, however, not likely because FKrCC has a much higher relative energy – 1.935 eV above the MP2 computed FKrCCKrF structure.

Table 8.3. B3LYP, MP2, and CCSD(T) computed energies (eV) relative to C_2F_2 + 2Kr.

Method:	B3LYP	MP2	CCSD(T)
Basis Set:	aug-cc-pVQZ	aug-cc-pVQZ	aug-cc-pVTZ
C_2F_2 + 2Kr	0.000	0.000	0.000
FKrCCF + Kr	4.028	3.945	4.097
FKrCCKrF	8.275	8.070	8.386
F_2 + C_2 + 2Kr	9.846	8.952	8.487
KrF_2 + C_2 + Kr	10.204	9.210	9.149
FKrCC + Kr + F	-- [a]	10.005	9.665
2F + C_2 + 2Kr	11.458	10.828	10.068
F_2 + 2C + 2Kr	15.045	15.693	17.398
2F + 2C + 2Kr	16.657	17.569	18.979
$2F^-$ + 2C+ + 2Kr	32.685	32.711	31.864
$2F^-$ + C_2^{2+} + 2Kr	39.697	39.551	38.364

[a] B3LYP/aug-cc-pVQZ does not find FKrCC as a minimum.

8.3.4. Transition States

The transition-state structures corresponding to the removal of each krypton atom from the FKrCCKrF molecules are shown in Tables 8.4 and 8.5. The favorable decomposition pathway for the removal of the first noble gas should involve a bending of the F–Kr–C bond

angle, since other dissociations would lead to unfavorable higher energy products. For FKrCCKrF, a transition state was located with an F–Kr–C angle at 98.2°, which was coupled with an increase in F–Kr bond length and a departure from linearity among the atoms in the distal CCKrF chain. The removal of the second krypton atom is similar to the first removal, and a transition state was found at a 98.0° F–Kr–C angle. The dissociation barriers were computed and are listed in Table 8.6. Interestingly, the energy barrier for the removal of the first kypton is larger (~0.045 eV) than the energy barrier for the removal of the second kypton. The dissociation barrier in FKrCCF is only slightly lower than the barrier predicted for HXeCCH (2.18 eV) by Lundell *et al.*[192] Intrinsic reaction coordinate analyses verify these structures as the transitional structures to the dissociated products and are shown in Fig. 8.1. The reaction pathways shown are plotted with respect to the F–Kr–C angle, as this angle is the principle geometric parameter that is changed from the ground state to the transition state. The bending of the F–Kr–C angle also lies on the transition vector determined from the imaginary mode of the vibrational frequencies. This figure is very similar to the one presented in the Lundell *et al.* study on HXeCCH because they both provide fairly high (~2.0 eV) and wide energy barriers.[192]

Table 8.4. The transition-state structure for FKrCCKrF (MP2/aug-cc-pV*n*Z).

Basis	Bond Length (Å)					Bond Angle (°)			
Set	F-Kr	Kr-C	C-C	C-Kr	Kr-F	FKrC	KrCC	CCKr	CKrF
n=T	2.300	1.772	1.218	1.952	1.929	98.1	174.6	179.2	180.0
Q	2.291	1.769	1.214	1.946	1.922	98.2	174.7	179.2	180.0

Table 8.5. Transition-state structure for FKrCCF (MP2/aug-cc-pV*n*Z).

Basis	Bond Length (Å)				Bond Angle (°)		
Set	F-Kr	Kr-C	C-C	C-F	FKrC	CCKr	CCF
n=T	2.318	1.769	1.203	1.264	98.0	166.8	175.0

Table 8.6. Dissociation barriers for FKrCCKrF and FKrCC in eV from MP2/aug-cc-pV*n*Z computations.

Molecule	Basis Set	Barrier
FKrCCKrF	*n*=T	1.987
	Q	1.999
FKrCCF	T	1.942

Figure 8.1. Plot of the FKrCCKrF and FCCKrF intrinsic reaction coordinate computed with MP2/aug-cc-pVTZ.

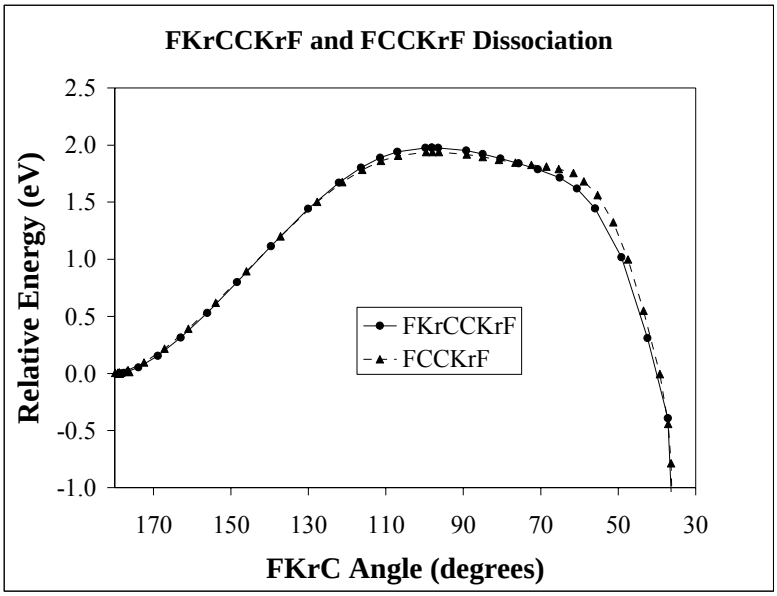

8.4. Conclusions

Two new organokrypton compounds (FKrCCF and FKrCCKrF) have been successfully identified and characterized theoretically. The optimized geometries suggest that these molecules have some of the shortest Kr–C bonds known, and vibrational frequency calculations verify them as ground state structures. FKrCCKrF is the first known metastable centrosymmetric organokrypton molecules, and is similar to the HXeCCXeH reported previously.[193] In the FKrCCKrF and FKrCCF molecules, the charge distribution predicts highly positive charges on the krypton atoms, highly negative charges on the fluorine atoms, and relatively neutral charges on the carbon atoms. Relative energy calculations predict the FKrCCF

molecules to be the lowest in energy relative to the precursor, C_2F_2 + 2Kr, and also predict FKrCCKrF to be the next most stable structure. The FKrCCKrF and FKrCCF transition structures were found with a large bent F–Kr–C angle, which should be the major channel in the decomposition. This study predicts that upon the formation of FKrCCF, the first experimentally detectable di-krypton system (FKrCCKrF) should be observed.

CHAPTER 9

THE STRUCTURE-LUMINESCENCE RELATIONSHIP IN Au(CO)Cl

9.1. Introduction

The application of the correlation consistent basis sets to krypton chemistry was presented in Chapters 6-8, and in Chapter 4, the pseudopotential series (cc-pV*n*Z-PP) of the correlation consistent sets were utilized for the benchmark study of scalar relativistic effects. In this chapter, the recently developed cc-pV*n*Z-PP sets for coinage metals (Cu, Ag, Au, Zn, Cd, and Hg)[37] will be used to study gold-bonded luminescent materials.

The first known experimental synthesis of Au(CO)Cl was in 1925,[217] in which this species was found to be extremely air- and moisture-sensitive. More recent experimental work has shown that the binding energy in Au–CO is as high as ~2.0 eV.[218] The chemical importance of L-Au-X (L = CO or RNC; X = halide or pseudohalide) compounds partially stems from their utilization as precursors to larger Au^I complexes, in which the neutral ligand can be replaced by other ligands to form molecules with a wide range of applications.[218] For example, gold(I) isonitrile complexes have been utilized for the deposition of gold films[219,220] and for the preparation of new types of liquid crystalline phases.[221-223] Transition metal carbonyl halides have received considerable attention in recent years as the photochemical and photophysical studies of Cu^I, Ag^I, and Au^I have grown.[224,225] Despite this attention, detailed studies of the excited state properties of carbonyl complexes of d^{10} metal ions are scarce.[226] Upon studying the excited state properties of metal complexes, an important distinction must be made between $d^{1\text{-}9}$ and d^{10} configurations. This is due to a fundamental difference in the electronic transitions in the

partially filled *d* shells, which create ligand-field excited states. In the closed shell d^{10} complexes, however, *d*-*d* transitions are absent. Based on this concept, the spectroscopy and photochemistry in such systems are reliant on other types of electronic excited states.[226]

Very little experimental or theoretical work has been done to explain the excited state properties of Au(CO)Cl. Kunkely and Vogler have reported that ligand field excited states should not be possible for Au^{I} systems and that only low-energy metal centered 5*d* → 6*s* or 6*p* transitions are accessible.[227] Furthermore, from their accounts, the longest wavelength absorption (*i.e.* the lowest energy transition) was at ~250 nm for Au(CO)Cl, which was assigned to a metal-based "*d*-*s* transition" localized on Au.[228]

This chapter reports a detailed analysis of the spectral, bonding, and photophysical characteristics of Au(CO)Cl molecules from a collaborative experimental and theoretical study. All of the experimental syntheses and analyses on Au(CO)Cl reported in this chapter were performed by O. Elbjeirami and M. A. Omary (Department of Chemistry, University of North Texas).[38] The focus of this chapter will be on the theoretical aspects of the analysis and, therefore, the descriptions of the various syntheses and instrumentation are purposely omitted.[38] However, pertinent details and figures from the experimental work has been included in order to provide the context for a full discussion about the electronic structure of the Au(CO)Cl species.

9.2. Computational Methodology

Møller-Plesset second order perturbation theory (MP2)[215] was used as the primary method to calculate optimized structures, frequencies, and energetics of the ground and triplet excited states of $[(CO)AuCl]_x$ (where x = 1-3). This method was chosen, in part, due to the computational cost of more sophisticated electron correlation methods that would arise when

studying the larger dimer and trimer systems. The validity of using MP2 for describing ground-state aurophilic bonding has been described previously in the literature.[229-231] To better characterize the frequencies of the C-O stretch upon complexation, CCSD(T) [15,51,52] was also used, because in previous studies,[232,233] MP2 did not account for C-O stretching frequencies with the anomalous ~20 cm^{-1} blue shift that has been seen experimentally.[234]

As shown in Chapter 3, the correlation consistent basis sets (cc-pV*n*Z)[1,2] can provide an accurate description of main-group chemistry, and therefore, were used in this study for C and O. For Cl, the tight-*d* augmented correlation consistent basis sets (cc-pV(*n*+*d*)Z)[15] were used, and their utility has been described previously (see Sec. 5.1). For Au, the newly developed correlation consistent basis sets (cc-pV*n*Z-PP)[37] were used, which are built upon the 60-electron Stuttgart relativistic pseudopotential[235] and were created in a manner akin to cc-pV*n*Z-PP sets used in Chapter 4 for third-row atoms. In addition, the popular LANL2DZ 60 electron effective core potential[115] was used for Au as a comparison to the new cc-pV*n*Z-PP sets; additional (6*p*)/[1*p*] functions were added to the Au valence basis set LANL2DZ as described by Couty and Hall,[236] and 2*f* functions developed by Pyykko.[237]

The calculated absorption energies of the monomer and dimer were determined as the vertical transitions between the minimum singlet ground state S_0 and the T_1 triplet excited state (at the optimized S_0 geometry). In addition, time-dependent density functional theory (TD-DFT) calculations with the B3PW91[56,238] functional were performed at the cc-pVTZ-PP basis set level to assess other possible excitations that contribute to the absorption spectra. The emission energies were computed from the energy difference between the optimized T_1 electronic state geometry and the S_0 state (at the optimized T_1 geometry). The dissociation energy (D_e) values for the dimer and trimer S_0 electronic states were predicted relative to dissociated complexes,

either by calculating the energy difference between the optimized oligomer and the optimized monomers or by increasing the separation between the monomeric complexes in the optimized oligomer structure to ~ 10 Å; the two methods agreed within 0.0026 eV (21 cm^{-1}) for the dimer ground state. The latter method was, therefore, adopted for the excimer D_e. None of the computed energetic properties included zero-point energy corrections, as this study was performed to provide an insight on chemical phenomena and not a quantitative benchmark study. All of these calculations were performed with the GAUSSIAN 03 software package,[216] except for CCSD(T) calculations, which were done using MOLPRO.[85]

9.3. Results and Discussion

9.3.1. Optimal Geometry

The ground- and excited-state structures have been computed to analyze the bonding in the $[Au(CO)Cl]_x$ species. The optimal bond lengths (Å) and angles (°) are presented in Table 9.1. Overall the change in bond lengths are modest (~0.02 Å) with respect to increasing basis set size, and generally the changes in the T_1 state are changes slightly more than those in the S_0 state. There is, however, a more significant difference in the bond lengths predicted in regards to the two different types of basis sets on Au (cc-pV*n*Z-PP and LANL2DZ). For these gold systems, the cc-pV*n*Z-PP sets provide bond lengths that are always shorter than those determined using LANL2DZ, with the exception of the excited-state Au–C bond length at the triple-ζ level (when *n*=T in Table 9.1). When using a correlated method, such as MP2, a shorter bond length should be representative of a greater electron correlation recovery, which has been shown to be essential in the characterization of heavy-metal bonding.[239] Even though the LANL2DZ computation

provides a reasonable Cl–Au bond distance for the dimer (2.26 Å when *n*=T), it greatly underestimates the Au···Au distance by 0.30 Å in comparison to the experimental crystallographic distance of 3.38 Å. Furthermore, the cc-pV*n*Z-PP sets provide a longer Au–Au distance of 3.17 Å than LANL2DZ, and represent the most noticeable difference in the two types of basis sets used for Au. The inflexibility in the smaller LANL2DZ basis sets in comparison to the cc-pVTZ-PP set is likely to be the cause for such dramatic underestimation of the Au···Au distances, as well as the inherent limitations of MP2. The shortcomings of MP2 were noted previously in a study by Wilson and co-workers, which compared MP2 and CCSD(T) computed bond distances for Hg_2, a simple diatomic model for metallophilic bonding.[239]

The large distortion in the Cl–Au–C angles that was computed for the excited state monomers was due to Jahn-Teller distortions, which are not expected to take place experimentally. This is because a monomer does not provide a sufficient model for the actual structure that is in the solid state or even in solution due to the packing of molecules. Furthermore, the emission energies calculated at computed excited-state geometry, should be vastly different from the experimental emissions. On the other hand, the excited state structure of the dimer exhibits a large decrease (~0.5 Å) in the Au-Au distance, which is characteristic of excimeric bonding for such d^{10} systems as shown in Figure 9.1. This large computed structural change is likely to be observed in the solid state or solution where adjacent Au^I centers can bind with one another to form Au–Au bonded excimers. Crystallographic analyses on excited state structures are not widely accessible to most experimentalists and therefore, the computational evidence provides understanding of the type of structural change that occurs upon excitation. (A rare excited-state structural study has recently demonstrated the large excimer intermolecular contraction in d^{10} systems.[240])

Table 9.1. MP2-calculated geometries for the optimized S_0 and T_1 states of $[(CO)AuCl]_x$ (x= 1-3 with antiparallel isomers for x= 2 or 3). Calculated bond lengths are in Å and bond angles in °. The basis set combinations are cc-pVnZ for C and O, cc-pV(n+d)Z for Cl and either cc-pVnZ-PP for Au or LANL2DZ.

Molecule	Basis Set	Bond lengths (Å)				Bond Angles (°)	
		Cl-Au	Au-C	C-O	Au-Au	Cl-Au-C	Au-C-O
Au(CO)Cl	cc-pVnZ-PP						
S_0	n = D	2.22	1.82	1.15			
	T	2.20	1.85	1.14			
T_1	D	2.34	1.94	1.16		84.1	155.6
	T	2.31	1.93	1.15		95.7	155.6
	LANL2DZ						
S_0	D	2.27	1.87	1.15			
	T	2.24	1.82	1.14			
T_1	D	2.59	1.97	1.15		99.1	154.4
	T	2.41	1.89	1.15		99.9	152.9
S_0	Ref. 232[a]	2.27	1.87	1.14			
S_0	Ref. 233[b]	2.25	1.86	1.14			
$[Au(CO)Cl]_2$	cc-pVnZ-PP						
S_0	D	2.23	1.87	1.15	3.20	177.0	177.8
	T	2.22	1.86	1.14	3.17	177.1	177.9
T_1	D	2.24	1.92	1.16	2.62	158.3	166.7
	T	2.22	1.90	1.15	2.61	160.3	167.7
	LANL2DZ						
S_0	D	2.28	1.88	1.15	2.98	174.6	177.2
	T	2.26	1.83	1.14	3.00	174.9	177.7
T_1	D	2.28	1.94	1.16	2.59	159.1	165.8
	T	2.26	1.88	1.15	2.60	160.7	168.5
S_0	Ref. 233	2.27	1.88	1.14	3.39		
$[Au(CO)Cl]_3$	cc-pVnZ-PP						
S_0	D	2.23	1.87	1.15	3.13	179.5	180.0
	LANL2DZ						
S_0	D	2.28	1.89	1.15	3.00	180.0	180.0
Expt.							
S_0	Ref. 241	2.26	1.93	1.11	3.38	180.0	180.0

[a] Stuttgart RECP, 8*s*3*p*5*d*2*f* (Au); McLean-Chaldler, 6*s*5*p*1*d* (Cl); 6-311G* (C, O)
[b] Stuttgart RECP, Ahlrichs, TZVP+2*f* (Au); Ahlrich, TZVP (Cl, C, O)

9.3.2. Fundamental Vibrational Frequencies

In Table 9.2, the $\nu_{C\equiv O}$ and ν_{Au-Au} vibrational frequencies from MP2 and CCSD(T) calculation are listed, as well as those from previous MP2 calculations.[232,233] There has been some discrepancy in the literature whether or not the blue shift in the $\nu_{C\equiv O}$ frequency upon

complexation with Au could be predicted theoretically. Both of the previous reported studies[232,233] predict a very slight red shift in the carbonyl frequency from the free CO to the CO in the Au(CO)Cl complex. As shown in Table 9.2, if LANL2DZ is used, it will appear that the $\nu_{C\equiv O}$ blue shift can be reproduced by MP2 calculations. However, as demonstrated previously in Sec. 9.3.1, LANL2DZ overdescribes the gold-gold bonding (*i.e.* short Au···Au distance) and is likely to underaccount for the π back-bonding to C≡O from the gold yielding a higher frequency. The $\nu_{C\equiv O}$ frequencies predicted with the cc-pV*n*Z-PP sets, should be more reliable (because they provide better Au–Au distances), but at cc-pVTZ-PP level do not display a blue shift in the carbonyl frequency. However, when CCSD(T) is used (values in parentheses), a 23 cm^{-1} blue shift is found, which is comparable to the anomalous blue shift that was seen experimentally.[234] (It must be noted that, while MP2 is not appropriate for the quantitative description of the $\nu_{C\equiv O}$ shift in the ground state, MP2 is traditionally considered an adequate level of theory to compute vibrational frequencies, and therefore, is used later in this chapter for qualitative comparisons of ground and excited states.)

From the MP2/cc-pV*n*Z-PP data shown in Table 9.2, the aurophilic association of the antiparallel linear Au(CO)Cl complexes leads to a $\nu_{Au\text{-}Au}$ frequency of 50 cm^{-1} in the dimer and two frequencies in the trimer of 44 and 67 cm^{-1}. Comparing the ground-state monomer $\nu_{C\equiv O}$ frequency to the associated dimer and trimer, the aurophilically bonded systems lead to a further blue shift (~10 cm^{-1}) of the CO frequency. This shift was presumed since the aurophilic bonding leads to less π-back bonding to the CO, which further stabilizes the C-O bond.

Upon excitation to the T_1 state, the D_e of the dimer, as shown in Table 9.2, is drastically increased by about five times to 2.49 eV in the resulting excimer. The formation of this Au–Au bonded excimer also leads to drastic changes in the vibrational frequencies. Thus, the Raman-

active $\nu_{Au\text{-}Au}$ dimer frequency calculated at the MP2 triple-ζ level exhibits a drastic blue shift to 153 cm^{-1} in the optimized T_1 excimeric phosphorescent state from the 50 cm^{-1} value in the optimized S_0 aurophilic ground state. Meanwhile, the $\nu_{C\equiv O}$ frequency in the dimer S_0 ground state is centered at 2131 cm^{-1}, which becomes two well-separated bands at 2034 and 2733 cm^{-1} in the T_1 state. The average of these two $\nu_{C\equiv O}$ values (2383 cm^{-1}) is blue shifted from the ground-state value by 252 cm^{-1}, which is likely due to the diminished π back-bonding to CO in the excimeric state caused by the now chemically bonded Au-Au centers. This is further supported by a longer Au-C bond (by ~ 0.05 Å) in the T_1 excimer than in the S_0 state dimer, which is also consistent with a weaker π back-bonding in the excimer. Based on the large decrease in the dimer Au–Au bond distance to 2.61 Å and the increase in the both the Au–Au frequency and the dissociation energy, photoexcitation leads to the formation of an excimer with an unquestionable Au–Au covalent bond after relaxation to the T_1 optimal state.

Table 9.2. Selected IR frequencies (cm^{-1}) and D_e in (eV) calculated with MP2. Additional values listed in parentheses were computed with CCSD(T). The "*" indicates a molecule in its optimized T_1 excited state.

Molecule	Basis Set	ν(C-O)	ν(Au-Au)	D_e
CO	cc-pV*n*Z			
	n=D	2113 (2143)		
	T	2121 (2153)		
	Q	2128 (2164)		
	5	2127 (2164)		
	Ref. 232[a]	2139		
	Ref. 233[b]	2129		
Au(CO)Cl	cc-pV*n*Z-PP			
	D	2119 (2168)		
	T	2121 (2176)		
	LANL2DZ			
	D	2137		
	T	2139		
	Ref. 232	2138		
	Ref. 233	2124		
Au(CO)Cl*	cc-pV*n*Z-PP			
	D	2052		
	T	2027		
$[Au(CO)Cl]_2$	cc-pV*n*Z-PP			
	D	2128, 2129[c]	50	0.44
	T	2130, 2132[c]	47	0.43
	LANL2DZ			
	D	2145, 2145	87	
$[Au(CO)Cl]_2$*	cc-pV*n*Z-PP			
	D	2033, 2594[c]	153	2.49
	T	2034, 2733[c]	160	2.27
$[Au(CO)Cl]_3$	cc-pV*n*Z-PP			
	D	2125, 2123,[c] 2137[d]	44, 67[c]	0.91
	LANL2DZ			
	D	2137, 2140,[c] 2159[d]	62, 101[c]	

[a] Stuttgart RECP, 8*s*3*p*5*d*2*f* (Au); McLean-Chaldler, 6*s*5*p*1*d* (Cl); 6-311G* (C, O)

[b] Stuttgart RECP, Ahlrich, TZVP+2*f* (Au); Ahlrich, TZVP (Cl, C, O)

[c] Symmetric and asymmetric stretch, respectively.

[d] The mode is primarily from the CO stretch on the central Au while the two others are primarily from the carbonyls on the two peripheral Au atoms.

9.3.3. Photophysics

Photophysical aspects of the Au(CO)Cl systems has been computed using MP2 and the results are shown in Table 9.3. These computed values are compared to the experimental crystalline and dilute solution spectral data from excitation/emission (Figure 9.1) and from absorption (Figure 9.2) studies. Overall, there is very little change in the excitation wavelength with increasing basis set size, whether the cc-pV*n*Z-PP or LANL2DZ basis sets are used for Au. The emission wavelengths, however, do change fairly significantly as the basis set size increases from double- to triple-ζ. There is a fairly large (~4000 cm^{-1}) difference in the Stokes' shift found using LANL2DZ rather than cc-pV*n*Z-PP for Au. The excitations wavelengths found with MP2 are only qualitatively similar to the experimental solid data, and the computed emission wavelengths (~400 nm) are not near the experimentally-observed solid-state emission at 674 nm. This exemplifies the difficulties at modeling excited solid-state phenomena by gas-phase computations that are devoid of lattice constraints. Due to computational cost, studies on larger oligomeric chains of Au(CO)Cl were not feasible. Therefore, it was hypothesized that upon freezing, dilute solutions of Au(CO)Cl should result in the formation of much shorter chains. Figure 9.2 is representative of this idea, in that drastic changes in the lowest-energy absorptions were found with more dilute solutions of Au(CO)Cl. In fact, curves (c) and (d) give rise to absorptions of wavelengths at 195 and 220 nm, respectively. These results are similar to the results found from TD-DFT calculations listed in Table 9.3, which provide support for the above hypothesis. Furthermore, observations from dilute frozen-solution luminescence experiments, as shown in Figure 9.3, provide the most conclusive evidence that shorter dimeric Au(CO)Cl

species do provide the correct photophysical predictions for these systems. The overlay of the dimer, MP2 computed emissions coincides rather well with the dilute solution emission data, which lose intensity upon increasing concentration to form a longer chain with a correspondingly much longer wavelength emission that approach the solid-state emission. All the emission bands in Figure 9.1 and 9.3 represent phosphorescence (based on lifetime data[38]), thus allowing good comparisons with the $T_1 \rightarrow S_0$ phosphorescent emissions computed herein.

Table 9.3. Computed photophysical parameters for the monomer and antiparallel dimer of Au(CO)Cl in comparison with experimental data for the solid and frozen solutions of Au(CO)Cl. The λ_{exc} and λ_{em} values for the spin-forbidden transitions are calculated via MP2 while the λ_{abs} values for spin-allowed transitions are calculated via TD-DFT with the oscillator strength values listed in parentheses. The basis set combinations are cc-pV*n*Z for C and O, cc-pV(*n*+*d*)Z for Cl, and both cc-pV*n*Z-PP and LANL2DZ for Au.

Molecule	Basis Set	λ_{exc} ($S_0 \rightarrow T_1$)/nm	λ_{em}($T_1 \rightarrow S_0$)/nm	Stokes' shift/cm^{-1}	λ_{abs} ($S_0 \rightarrow S_n$)/nm
Au(CO)Cl	cc-pV*n*Z-PP				
	n=D	220	824	33,344	
	T	220	788	32,851	227 (0.27), 240 (0.03), 197 (0.01)
	LANL2DZ				
	D	211	1024	37,606	
	T	212	776	34,256	
$[Au(CO)Cl]_2$	cc-pV*n*Z-PP				
	D	246	407	16,088	
	T	244	394	15,573	265 (0.06), 251 (0.01)
	LANL2DZ				
	D	257	406	14,257	
	T	256	391	13,418	
Expt., solid[38]		322	674	16,200	
Expt., frozen soln.[38]		282	412	11,200	

Figure 9.1. Experimental photoluminescence excitation and emission spectra of crystals of Au(CO)Cl at (a) 295 K, (b) 235 K, (c) 180 K, (d) 135 K, (e) 100 K, and (f) 77 K.

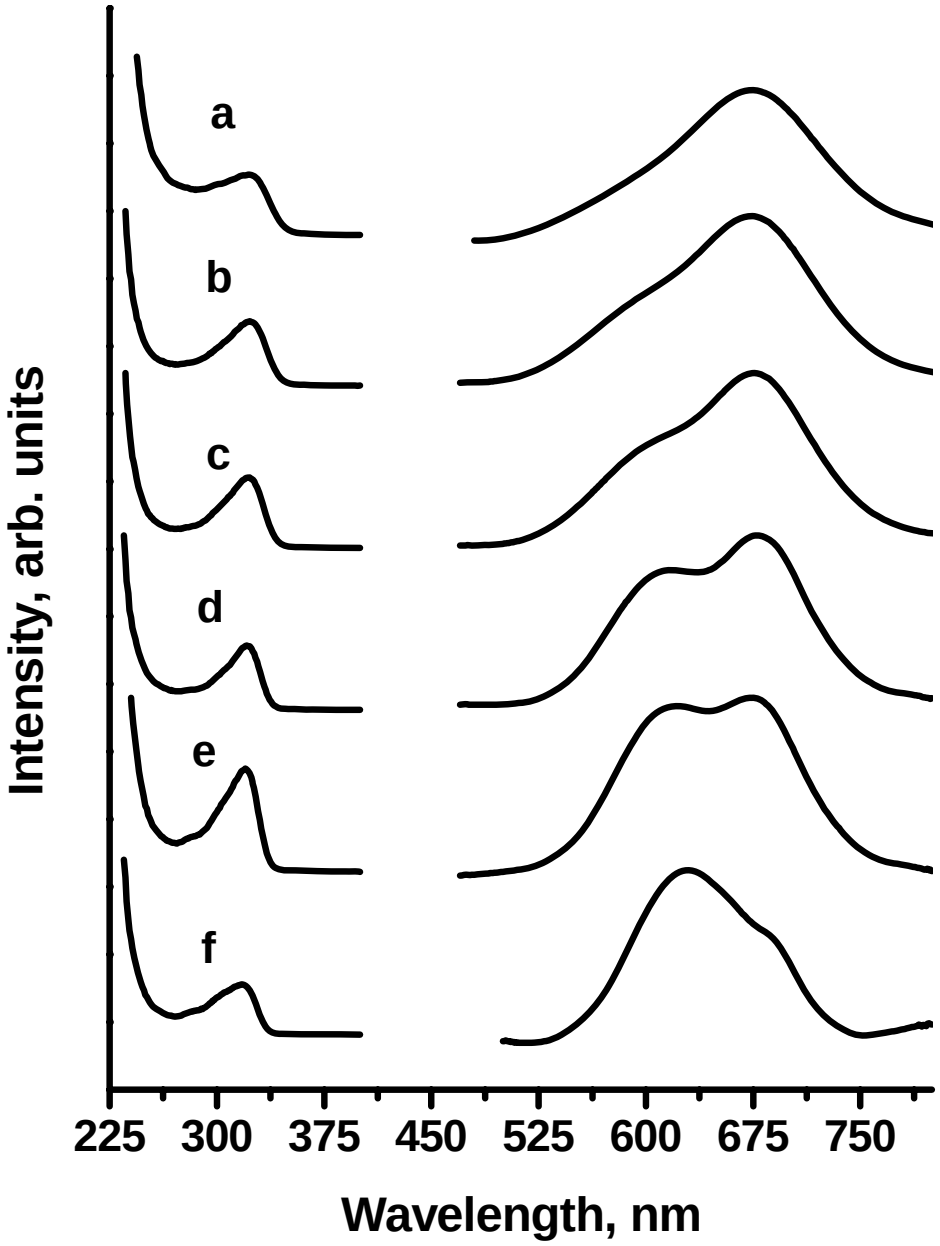

Figure 9.2. Experimental absorption spectra for solutions of Au(CO)Cl in acetonitrile with concentrations of: (a) 2.56×10^{-3} M, (b and c) 5.10×10^{-4} M, and (d, top-to-bottom, respectively) 5.10×10^{-5}, 2.56×10^{-5}, 1.27×10^{-5}, and 6.30×10^{-6} M. Left axis is for (d) and (c) and the right axis is for (a) and (b).

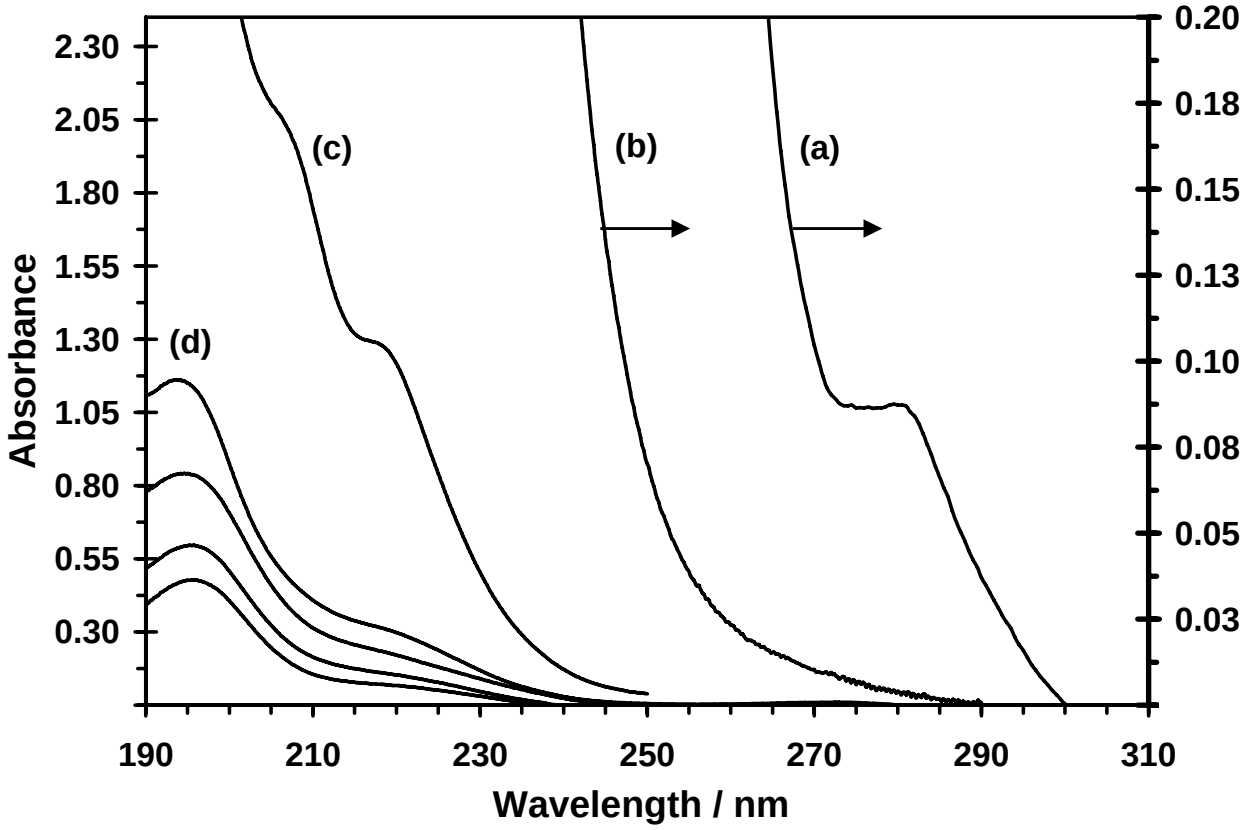

Figure 9.3. Photoluminescence excitation and emission spectra of frozen solutions (77 K) of Au(CO)Cl in CH_2Cl_2 at different concentrations: (a) 5.0×10^{-5} M, (b) 5.0×10^{-3} M, and (c) 5.0×10^{-2} M. The compute phosphorescence from the calculated MP2 emission (left) and the experimental solid-state phosphorescence study (right) are shown by the vertical bars.

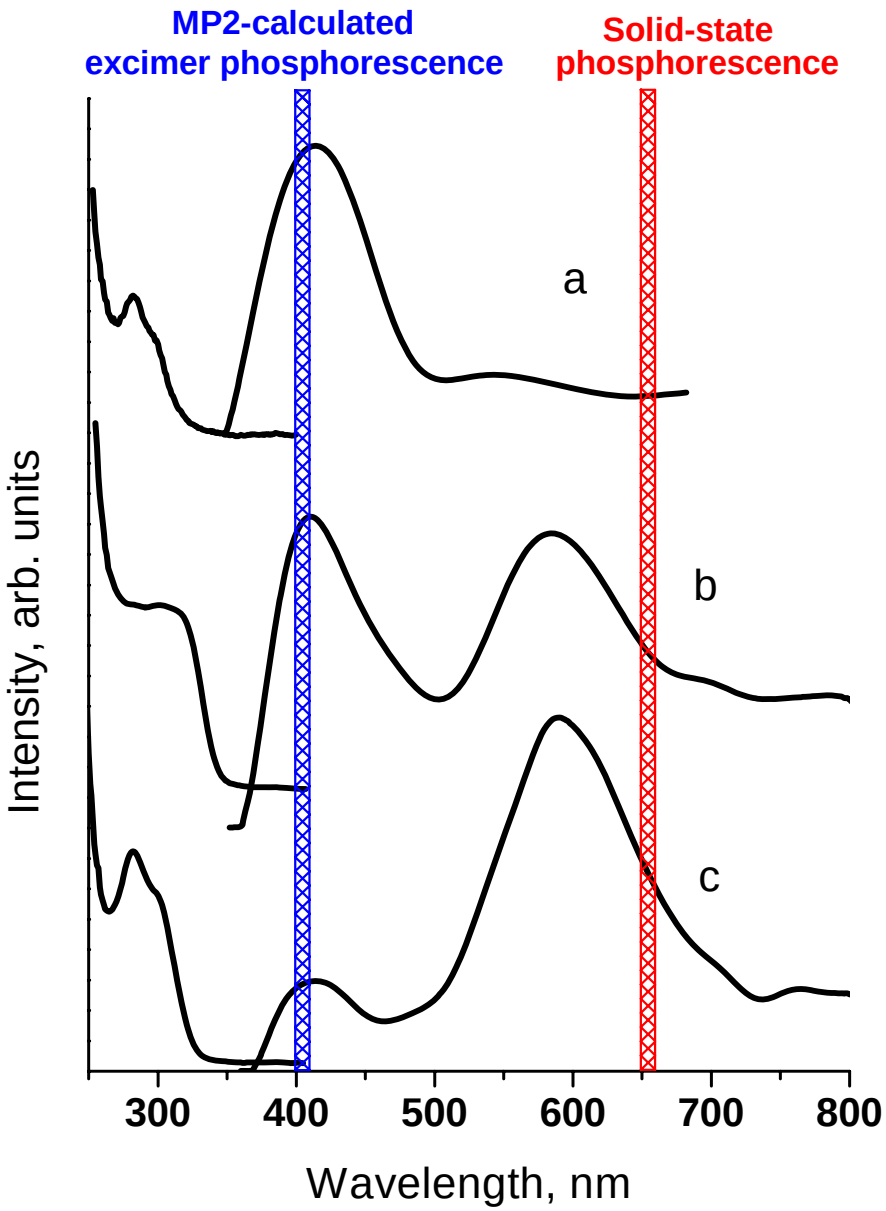

9.4. Conclusions

The characterization of Au(CO)Cl linear chains has been completed using a number of computational and compared to experimental observations. Minimum energy structures of the S_0 ground- and T_1 excited-states suggested a large contraction in the Au–Au bond upon excitation, which is due to an electron in the antibonding HOMO of the S_0 being excited into a bonding orbital in the T_1 state. The computed vibrational frequency analysis reproduced the anomalous blue shift in the carbonyl frequency (~23 cm^{-1}) that was observed experimentally upon complexation with gold,[234] only after CCSD(T) was employed. Most importantly, the dimeric absorption and emissions computed with MP2 were shown to agree with concentration-dependent frozen solution spectral data,[38] and provide conclusive evidence that in the solid state, longer oligomeric species should be responsible for the predominate phosphorescent bands, which is contrary to what earlier studies had predicted.[227]

CHAPTER 10

CONCLUDING SUMMARY

Employing the correlation consistent basis sets (cc-pV*n*Z, where *n*= D, T, Q, 5) coupled with electronic structure methods has enabled accurate predictions of chemical properties for second- and third-row main group and transition metal molecular species. In Chapter 3, the evaluation of the correlation consistent basis sets for third-row atoms (Ga-Kr) was done in a benchmark study that compared *ab initio* and density functional methodologies, CCSD(T) and B3LYP, respectively. For the 40 energies in this study (19 atomization energies, 15 ionization energies, 4 electron affinities, and 2 proton affinities), the mean absolute deviation from experiment for the CCSD(T) computed energies was ~1.0 kcal/mol (which is considered to be "chemical accuracy"), when using an extrapolation to the complete basis set (CBS) limit that utilized values from higher that a triple-ζ level. The extrapolation procedure that was found to have the lowest mean absolute deviation of 0.87 kcal/mol was the two-point CBS_{Q5}, which used quadruple-ζ and quintuple-ζ values. The resulting mean absolute deviation from B3LYP was 2-3 kcal/mol, and it must be noted that B3LYP inconsistently described the ionization energies for these third-row systems. The Douglas-Kroll (cc-pV*n*Z-DK) and pseudopotential (cc-pV*n*Z-PP) basis sets were paired with CCSD(T) in Chapter 4 to investigate the impact of scalar relativity on the energetic and structural properties of the third-row molecules used in the test suite in Chapter 3. Slight contractions in the bond length were noted due to the inclusion of scalar relativity, while the magnitude was more significant for energies (~1.0 kcal/mol on average). The atomization energy of GeH_4 was altered the most (-3.18 kcal/mol at the aug-cc-pV5Z-PP level)

as compared with the other test species when scalar relativity was considered. These benchmark studies provide calibration for the accuracy that should be expected for future computations with CCSD(T) and the correlation consistent basis sets.

The benchmark studies lead to the application of the correlation consistent basis set to study novel krypton bonded compounds. Atoms chemically bonded to noble gases, like krypton, are still a relatively new concept and are not fully understood. Chapter 6, entailed a theoretical study of HKrCl which previously had been synthesized experimentally, to gain greater insight about its existence. In this study, the minimum energy geometry, vibrational frequencies, charge distribution, relative energies, atomization energy, and lowest energy dissociation pathway were computed. Most importantly it was found that with electron correlated methods, such as CCSD(T), sufficiently larger (quadruple-ζ level) basis sets were needed in order to provide correct predictions of the energetics of HKrCl. In fact, smaller basis sets did not correctly predict HKrCl to be bound. With the understanding of the computational approaches needed to study krypton-bonded compounds, Chapters 7 and 8 focused on the prediction of new krypton bonded compounds. The molecular properties of $FKrCF_3$, $FKrSiF_3$, $FKrGeF_3$, FKrCCF, and FKrCCKrF were characterized in these studies. Of these molecules, $FKrGeF_3$ provided the first ever reported Kr–Ge bond, while FKrCCKrF should be stable enough to be the first di-krypton molecule to be detectable by infrared spectroscopy.

For second-row atoms (Al-Ar) the core-valence correlation consistent basis sets (cc-pCV*n*Z) were revisited in order to construct core-valence basis sets (cc-pCV(*n*+*d*)Z) that are built upon the recommended valence cc-pV(*n*+*d*)Z sets. All-electron correlated calculations with cc-pCVDZ did not result in dissociation energies that were an improvement over the valence-only correlated calculations using cc-pV(D+*d)*Z, as expected. A modification of the cc-pCV*n*Z

sets to include an additional core-*d* basis function remedies this problem, and allows for a systematic improvement in molecular properties over the cc-pV(n+d)Z values. These new sets, cc-pCV(n+d)Z, are much more suitable than the original core-valence basis sets for use in composite approaches, as these new sets provide a much more consistent description of core-valence effects. This consistency is particularly important when treating core-valence effects as additive effects. As a result of this work, the cc-pCV(n+d)Z basis sets are now recommend for use in all-electron correlated calculations involving second-row atoms.

The correlation consistent basis sets have also been applied to study the structural, vibrational, energetic, and luminescent properties of Au(CO)Cl. It is normally difficult to obtain qualitative values from the gas phase computational models in comparison with the experimental solid state or even solution spectral data. However, this theoretical study provided conclusive evidence for the dimer absorption and emission energies that coincided with the experimental concentration-dependent frozen-solution spectral data. Most importantly, this study proved that longer oligomeric species of Au(CO)Cl are responsible for the predominant phosphorescent bands seen in the solid state, which is contrary to the prediction from earlier studies which suggested that phosphorescence resulted from metal-based electronic transitions within a monomer.

REFERENCES

[1] T. H. Dunning, Jr., J. Chem. Phys. **90**, 1007 (1989).

[2] D. E. Woon and T. H. Dunning, Jr., J. Chem. Phys. **98**, 1358 (1992).

[3] A. K. Wilson, D. E. Woon, K. A. Peterson, and T. H. Dunning, Jr., J. Chem. Phys. **110**, 7667 (1999).

[4] R. A. Kendall, T. H. Dunning, Jr., and R. J. Harrison, J. Chem. Phys. **96**, 6796 (1992).

[5] K. A. Peterson, R. A. Kendall, and T. H. Dunning, Jr., J. Chem. Phys. **99**, 1930 (1993).

[6] K. A. Peterson, R. A. Kendall, and T. H. Dunning, Jr., J. Chem. Phys. **99**, 9790 (1993).

[7] D. E. Woon and T. H. Dunning, Jr., J. Chem. Phys. **101**, 8877 (1994).

[8] K. A. Peterson and T. H. Dunning, Jr., J. Chem. Phys. **102**, 2032 (1995).

[9] D. E. Woon and T. H. Dunning, Jr., J. Chem. Phys. **103**, 4572 (1995).

[10] K. A. Peterson, A. K. Wilson, D. E. Woon, and T. H. Dunning, Jr., Theo. Chem. Acct. **97**, 251 (1997).

[11] A. K. Wilson and T. H. Dunning, Jr., J. Chem. Phys. **106**, 8718 (1997).

[12] K. A. Peterson and T. H. Dunning, Jr., J. Chem. Phys. **106**, 4119 (1997).

[13] D. E. Woon, K. A. Peterson, and T. H. Dunning, Jr., J. Chem. Phys. **109**, 2233 (1998).

[14] T. van Mourik, A. K. Wilson, and T. H. Dunning, Jr., Mol. Phys. **96**, 529 (1999).

[15] T. H. Dunning, Jr., K. A. Peterson, and A. K. Wilson, J. Chem. Phys. **114**, 9244 (2001).

[16] K. A. Peterson and T. H. Dunning, Jr., J. Chem. Phys. **117**, 10548 (2002).

[17] A. K. Wilson and T. H. Dunning, Jr., J. Chem. Phys. **119**, 11712 (2003).

[18] A. K. Wilson and T. H. Dunning, Jr., J. Phys. Chem. A **108**, 3129 (2004).

[19] D. Feller, J. Chem. Phys. **96**, 6104 (1992).

[20] D. Feller and K. A. Peterson, J. Chem. Phys. **108**, 154 (1998).

[21] D. Feller and D. A. Dixon, J. Chem. Phys. **115**, 3484 (2001).

[22] D. Feller, K. A. Peterson, W. A. de Jong, and D. A. Dixon, J. Chem. Phys. **118**, 3510 (2003).

[23] B. Ruscic, A. F. Wagner, L. B. Harding, R. L. Asher, D. Feller, D. A. Dixon, K. A. Peterson, Y. Song, X. Qian, C.-Y. Ng, J. Liu, W. Chen, and D. W. Schwenke, J. Phys. Chem. A **106**, 2727 (2002).

[24] D. Feller and K. A. Peterson, J. Chem. Phys. **110**, 8384 (1999).

[25] D. A. Dixon and K. A. Peterson, J. Chem. Phys. **115**, 6327 (2001).

[26] K. A. Peterson, D. Figgen, E. Goll, and H. Stoll, J. Chem. Phys. **119**, 11113 (2003).

[27] K. A. Peterson, J. Chem. Phys. **119**, 11099 (2003).

[28] W. A. de Jong, R. J. Harrison, and D. A. Dixon, J. Chem. Phys. **114**, 48 (2001).

[29] C. W. Bauschlicher, Jr. and H. Partridge, Chem. Phys. Lett. **240**, 533 (1995).

[30] C. W. Bauschlicher, Jr. and A. Ricca, J. Phys. Chem. A **102**, 8044 (1998).

[31] J. M. L. Martin, J. Chem. Phys. **108**, 2791 (1998).

[32] J. M. L. Martin and O. Uzan, Chem. Phys. Lett. **282**, 16 (1998).

[33] M. Pettersson, J. Lundell, and M. Räsänen, J. Chem. Phys. **102**, 6423 (1995).

[34] J. Lundell, L. Khriachtchev, M. Pettersson, and M. Räsänen, Low Temp. Phys. **26**, 680 (2000).

[35] A. Lignell, J. Lundell, M. Pettersson, L. Khriachtchev, and M. Räsänen, Low Temp. Phys. **29**, 844 (2003).

[36] N. B. Balabanov and K. A. Peterson, J. Chem. Phys. **123**, 064107 (2005).

[37] K. A. Peterson and C. Puzzarini, Theo. Chem. Acct. **114**, 283 (2005).

[38] O. Elbjeirami, S. Yockel, C. F. Campana, A. K. Wilson, and M. A. Omary, *for publication.*

[39] E. Schrödinger, Ann. Phys. **79**, 489 (1926).

[40] E. Schrödinger, Physical Rev. **28**, 1049 (1926).

[41] E. Schrödinger, Ann. Phys. **79**, 361 (1926).

[42] E. Schrödinger, Ann. Phys. **79**, 734 (1926).

[43] M. Born and J. R. Oppenheimer, Ann. Physik **84**, 457 (1927).

[44] J. C. Slater, Physical Rev. **35**, 210 (1930).

[45] D. R. Hartree, Proc. Cambridge Phil. Soc. **24**, 426 (1928).

[46] D. R. Hartree, Proc. Cambridge Phil. Soc. **24**, 111 (1928).

[47] D. R. Hartree, Proc. Cambridge Phil. Soc. **24**, 89 (1928).

[48] V. Fock, Z. Physik **61**, 126 (1930).

[49] A. Szabo and N. S. Ostlund, *Modern Quantum Chemistry: Introduction to Advanced Electronic Structure Theory*. (Dover Publications, Inc., Mineola, New York, 1989).

[50] K. Raghavachari, G. W. Trucks, J. A. Pople, and M. Head-Gordon, Chem. Phys. Lett. **157**, 479 (1989).

[51] G. D. I. Purvis and R. J. Bartlett, J. Chem. Phys. **76**, 1910 (1982).

[52] J. D. Watts, J. Gauss, and R. J. Bartlett, J. Chem. Phys. **98**, 8718 (1993).

[53] F. Jensen, *Introduction to Computational Chemistry*. (John Wiley and Sons Ltd., Chichester, England, 1999).

[54] T. Helgaker, P. Jorgensen, and J. Olsen, *Molecular Electronic-Structure Theory*. (John Wiley and Sons, Ltd., Chichester, England, 2000).

[55] W. Kohn and L. Sham, Phys. Rev. A **140**, 1133 (1965).

[56] A. D. Becke, J. Chem. Phys. **98**, 5648 (1993).

[57] C. Lee, W. Yang, and R. G. Parr, Phys. Rev. **B37**, 785 (1988).

[58] C. D. Sherrill and H. F. Schaefer III, "The Configuration Interaction Method: Advances in Highly Correlated Approaches", in *Advances in Quantum Chemistry*, edited by P.-O. Lowdin (Academic Press, New York, 1999), Vol. 34, p. 143.

[59] N. C. Handy, Chem. Phys. Lett. **74**, 280 (1980).

[60] D. E. Woon, J. Chem. Phys. **100**, 2838 (1994).

[61] J. A. Pople, M. Head-Gordon, D. J. Fox, K. Raghavachari, and L. A. Curtiss, J. Chem. Phys. **90**, 5622 (1988).

[62] L. A. Curtiss, K. Raghavachari, G. W. Trucks, and J. A. Pople, J. Chem. Phys. **94**, 7221 (1991).

[63] L. A. Curtiss, K. Raghavachari, P. C. Redfern, V. Rassolov, and J. A. Pople, J. Chem. Phys. **109**, 7764 (1998).

[64] J. A. Montgomery Jr., M. J. Frisch, J. W. Ochterski, and G. A. Petersson, J. Chem. Phys. **110**, 2822 (1999).

[65] J. W. Ochterski, G. A. Petersson, and J. A. Montgomery Jr., J. Chem. Phys. **104**, 2598 (1996).

[66] N. J. DeYonker, T. R. Cundari, and A. K. Wilson, J. Chem. Phys. **124**, 114104 (2006).

[67] N. J. DeYonker, T. Grimes, S. Yockel, A. Dinescu, B. Mintz, T. R. Cundari, and A. K. Wilson, J. Chem. Phys. **125**, 104111 (2006).

[68] L. A. Curtiss, M. P. McGrath, J.-P. Blaudeau, N. E. Davis, R. C. Binning, Jr., and L. Radom, J. Chem. Phys. **103**, 6104 (1995).

[69] J.-P. Blaudeau, M. P. McGrath, L. A. Curtiss, and L. Radom, J. Chem. Phys. **107**, 5016 (1997).

[70] P. C. Redfern, J.-P. Blaudeau, and L. A. Curtiss, J. Phys. Chem. A **101**, 8701 (1997).

[71] B. J. Duke and L. Radom, J. Chem. Phys. **109**, 3352 (1998).

[72] L. A. Curtiss, P. C. Redfern, V. Rassolov, G. Kedziora, and J. A. Pople, J. Chem. Phys. **114**, 9287 (2001).

[73] V. Ramakrishna and B. J. Duke, J. Chem. Phys. **118**, 6137 (2003).

[74] T. Azzam, R. Schinke, S. C. Farantos, M. Joyeux, and K. A. Peterson, J. Chem. Phys. **118**, 9643 (2003).

[75] D. A. Dixon, W. A. de Jong, K. A. Peterson, and J. S. Francisco, J. Phys. Chem. A **106**, 4725 (2002).

[76] K. A. Peterson, B. A. Flowers, and J. S. Francisco, J. Chem. Phys. **115**, 7513 (2001).

[77] R. Vetter, T. Ritschel, L. Zulicke, and K. A. Peterson, J. Phys. Chem. A **107**, 1405 (2003).

[78] L. Sari, Y. Yamaguchi, and H. F. Schaefer III, J. Chem. Phys. **115**, 5932 (2001).

[79] Q. Li, G. Li, W. Xu, Y. Xie, and H. F. Schaefer III, J. Chem. Phys. **111**, 7945 (1999).

[80] L. Sari, K. A. Peterson, Y. Yamaguchi, and H. F. Schaefer III, J. Chem. Phys. **117**, 10008 (2002).

[81] L. Sari, Y. Yamaguchi, and H. F. Schaefer III, J. Chem. Phys. **119**, 8266 (2003).

[82] A. K. Wilson and T. H. Dunning, Jr., *for publication*.

[83] L. A. Curtiss, K. Raghavachari, P. C. Redfern, and J. A. Pople, Chem. Phys. Lett. **270**, 419 (1997).

[84] L. A. Curtiss, K. Raghavachari, P. C. Redfern, and J. A. Pople, J. Chem. Phys. **106**, 1063 (1997).

[85] MOLPRO, *a package of ab initio programs designed by H.-J. Werner and P. J. Knowles*; R. D. Amos, A. Bernhardsson, A. Berning, P. Celani, D. L. Cooper, M. J. O. Deegan, A. J. Dobbyn, F. Eckert, C. Hampel, G. Hetzer, P. J. Knowles, T. Korona, R. Lindh, A. W. Lloyd, S. J. McNicholas, F. R. Manby, W. Meyer, M. E. Mura, A. Nicklass, P. Palmieri, R. Pitzer, G. Rauhut, M. Schütz, U. Schumann, H. Stoll, A. J. Stone, R. Tarroni, T. Thorsteinsson, and H.-J. Werner.

[86] Gaussian 98, M. J. Frisch, G. W. Trucks, H. B. Schlegel, G. E. Scuseria, M. A. Robb, J. R. Cheeseman, V. G. Zakrzewski, J. A. Montgomery Jr., R. E. Stratmann, J. C. Burant, S. Dapprich, J. M. Millam, A. D. Daniels, K. N. Kudin, M. C. Strain, O. Farkas, J. Tomasi, V. Barone, M. Cossi, R. Cammi, B. Mennucci, C. Pomelli, C. Adamo, S. Clifford, J. Ochterski, G. A. Petersson, P. Y. Ayala, Q. Cui, K. Morokuma, P. Salvador, J. J. Dannenberg, D. K. Malick, A. D. Rabuck, K. Raghavachari, J. B. Foresman, J. Cioslowski, J. V. Ortiz, A. G. Baboul, B. B. Stefanov, G. Liu, A. Liashenko, P. Piskorz, I. Komaromi, R. Gomperts, R. L. Martin, D. J. Fox, T. Keith, M. A. Al-Laham, C. Y. Peng, A. Nanayakkara, M. Challacombe, P. M. W. Gill, B. Johnson, M. Chen, M. W. Wong, J. L. Andres, C. Gonzalez, M. Head-Gordon, E. S. Replogle, and J. A. Pople, (Gaussian, Inc., Pittsburgh PA, 2001).

[87] C. E. Moore, U.S. Patent No. 1 (1952).

[88] J.-P. Blaudeau and L. A. Curtiss, Int. J. Quantum Chem. **61**, 943 (1997).

[89] A. Halkier, T. Helgaker, P. Jorgensen, W. Klopper, H. Koch, J. Olsen, and A. K. Wilson, Chem. Phys. Lett. **286**, 243 (1998).

[90] H. Hofmann, E. Hansele, and T. Clark, J. Comput. Chem. **11**, 1147 (1990).

[91] S. Petrie, J. Phys. Chem. A **102**, 6138 (1998).

[92] K. Huber and G. Herzberg, *Molecular Spectra and Molecular Structure 4*. (Van Nostrand, Princeton, 1979).

[93] K. Ohno, H. Matsumura, Y. Endo, and E. Hirota, J. Mol. Spectrosc. **118**, 1 (1986).

[94] J. H. Callomon, E. Hirota, K. Kuchitsu, W. J. Lafferty, A. G. Maki, and C. S. Pote, "Structure Data of Free Polyatomic Molecules", in *Landolt-Bornstein, New Series, Group II* (Springer, Berlin, 1976), Vol. 7.

[95] M. K. Gilles, M. L. Polak, and W. C. Lineberger, J. Chem. Phys. **96**, 8012 (1992).

[96] Y. Koga, H. Takeo, S. Kondo, M. Sugie, C. Matsumura, G. A. McRae, and E. A. Cohen, J. Mol. Spectrosc. **138**, 467 (1989).

[97] G. Graner, J. Mol. Spectrosc. **90**, 394 (1981).

[98] N. X. Wang and A. K. Wilson, Mol. Phys. **103**, 345 (2005).

[99] N. X. Wang and A. K. Wilson, J. Chem. Phys. **121**, 7632 (2004).

[100] N. X. Wang, K. Venkatesh, and A. K. Wilson, J. Phys. Chem. A **110**, 779 (2006).

[101] B. Ruscic, M. Schwarz, and J. Berkowitz, J. Chem. Phys. **92**, 1865 (1990).

[102] S. R. Gunn and L. G. Green, J. Phys. Chem. **65**, 779 (1961).

[103] *NIST-JANAF Thermochemical Tables*, edited by M. W. Chase, Jr. (American Chemical Society and American Institute of Physics, 1985), Vol. Monograph No. 9.

[104] J. Berkowitz, J. Chem. Phys. **89**, 7065 (1988).

[105] S. T. Gibson, J. P. Greene, and J. Berkowitz, J. Chem. Phys. **85**, 4815 (1986).

[106] L. V. Gurvich, I. V. Veyts, and C. B. Alcock, *Thermodynamic Properties of Individual Substances*, 4th ed. (Hemisphere, New York, 1989).

[107] P. A. G. O'Hare and L. A. Curtiss, J. Chem. Thermodynamics **27**, 643 (1995).

[108] S. A. Kudchadker and A. P. Kudchadker, J. Phys. Chem. Ref. Data **4**, 457 (1975).

[109] B. Ruscic and J. Berkowitz, J. Chem. Phys. **101**, 7795 (1994).

[110] S. Lias, J. E. Bartmess, J. F. Liebman, J. L. Holmes, R. D. Levin, and W. G. Mallard, J. Phys. Chem. Ref. Data **17**, Suppl. No. 1 (1998).

[111] M. N. Glukhovtsev, J. E. Szulejko, T. B. McMahon, J. W. Gauld, A. P. Scott, B. J. Smith, A. Pross, and L. Radom, J. Phys. Chem. **98**, 13099 (1994).

[112] V. A. Rassolov, M. A. Ratner, J. A. Pople, P. C. Redfern, and L. A. Curtiss, J. Comput. Chem. **22**, 976 (2001).

[113] N. L. Haworth, M. B. Sullivan, A. K. Wilson, J. M. L. Martin, and L. Radom, J. Phys. Chem. A **109**, 9156 (2005).

[114] P. A. M. Dirac, *The Principles of Quantum Mechanics*, 4th ed. (Oxford Univ Press, Oxford, 1981).

[115] P. J. Hay and W. R. Wadt, J. Chem. Phys. **82**, 299 (1985).

[116] P. J. Hay and W. R. Wadt, J. Chem. Phys. **82**, 270 (1985).

[117] P. J. Hay and W. R. Wadt, J. Chem. Phys. **82**, 284 (1985).

[118] B. Metz, H. Stoll, and M. Dolg, J. Chem. Phys. **113**, 2563 (2000).

[119] W. J. Stevens, M. Krauss, H. Basch, and P. G. Jasian, Can. J. Chem. **70**, 612 (1992).

[120] E. van Lenthe, E. J. Baerends, and J. G. Snijders, J. Chem. Phys. **99**, 4597 (1993).

[121] R. D. Cowan and D. C. Griffin, J. Opt. Soc. Am. **66**, 1010 (1976).

[122] K. G. Dyall, J. Chem. Phys. **109**, 4201 (1998).

[123] K. G. Dyall, J. Chem. Phys. **106**, 9618 (1997).

[124] W. Kutzelnigg, E. Ottschofski, and R. Franke, J. Chem. Phys. **102**, 1740 (1995).

[125] B. A. Hess, Phys. Rev. A **32**, 756 (1985).

[126] B. A. Hess, Phys. Rev. A **33**, 3742 (1986).

[127] M. Douglas and N. M. Kroll, Ann. Phys. **82**, 89 (1974).

[128] C. W. Bauschlicher, Jr., J. Phys. Chem. A **104**, 2281 (2000).

[129] C. W. Bauschlicher, Jr., J. M. L. Martin, and P. R. Taylor, J. Phys. Chem. A **103**, 7715 (1999).

[130] C. W. Bauschlicher, Jr., Theo. Chem. Acct. **101**, 421 (1999).

[131] A. Ricca and C. W. Bauschlicher, Jr.e, J. Phys. Chem. A **103**, 11121 (1999).

[132] G. Kedziora, J. A. Pople, V. Rassolov, M. A. Ratner, P. C. Redfern, and L. A. Curtiss, J. Chem. Phys. **110**, 7123 (1999).

[133] G. Kedziora, J. A. Pople, M. A. Ratner, P. C. Redfern, and L. A. Curtiss, J. Chem. Phys. **115**, 718 (2001).

[134] S. Yockel, B. Mintz, and A. K. Wilson, J. Chem. Phys. **121**, 60 (2004).

[135] B. A. Hess, Phys. Rev. A **32**, 756 (1985).

[136] B. A. Hess, Phys. Rev. A **33**, 3742 (1986).

[137] M. Dolg, Chem. Phys. Lett. **250**, 75 (1996).

[138] M. Dolg, J. Chem. Phys. **104** (1996).

[139] T. Leininger, A. Nicklass, H. Stoll, M. Dolg, and P. Schwerdtfeger, J. Chem. Phys. **105**, 1052 (1996).

[140] B. Metz, M. Schweizer, H. Stoll, M. Dolg, and W. Liu, Theo. Chem. Acct. **104**, 22 (2000).

[141] C. E. Moore, (U.S.), Circ. No. 467, (1949).

[142] T. H. Dunning, Jr., K. A. Peterson, and D. E. Woon, "Basis Sets: Correlation Consistent Sets", in *Encyclopedia of Computational Chemistry - Online* (John Wiley and Sons, Ltd., 2002).

[143] R. D. Bell and A. K. Wilson, Chem. Phys. Lett. **394**, 105 (2004).

[144] S. Yockel and A. K. Wilson, Chem. Phys. Lett. **429**, 645 (2006).

[145] N. X. Wang and A. K. Wilson, J. Phys. Chem. A **107**, 6720 (2003).

[146] P. R. Taylor, in *Lecture Notes in Quantum Chemistry*, edited by B. O. Roos (Springer-Verlag, Berlin, 1992), p. 406.

[147] L. Pauling, J. Am. Chem. Soc. **55**, 1895 (1933).

[148] N. Bartlett, presented at the Proc. Chem. Soc., 1962 (unpublished).

[149] A. V. Grosse, A. D. Kirschenbaum, A. G. Streng, and L. V. Streng, Science **139**, 1047 (1963).

[150] J. J. Turner and G. C. Pimentel, Science **140**, 975 (1963).

[151] D. R. MacKenzie, Science **141**, 1171 (1963).

[152] S. R. Gunn, J. Phys. Chem. **71**, 2934 (1967).

[153] W. F. Howard and L. Andrews, J. Am. Chem. Soc. **96**, 7864 (1974).

[154] P. J. Hay and T. H. Dunning, Jr., J. Chem. Phys. **66**, 1306 (1977).

[155] P. S. Bagus, B. Liu, and H. F. Schaefer III, J. Am. Chem. Soc. **94**, 6635 (1972).

[156] D. H. Liskow, H. F. Schaefer III, P. S. Bagus, and B. Liu, J. Am. Chem. Soc. **95**, 4056 (1973).

[157] B. Liu and H. F. Schaefer III, J. Chem. Phys. **55**, 2369 (1971).

[158] G. A. D. Collins, D. W. J. Cruickshank, and A. Breeze, Chem. Commun. **881** (1970).

[159] W. E. Falconer and J. R. Morton, presented at the Proc. Chem. Soc., London, 1963 (unpublished).

[160] J. R. Morton and W. E. Falconer, J. Chem. Phys. **39**, 427 (1963).

[161] V. A. Legasov, V. N. Prusakov, and B. B. Chaivanov, Z. Fizich. Khim. **42**, 1167 (1968).

[162] H. S. Johnston and R. Woolfolk, J. Chem. Phys. **41**, 269 (1964).

[163] F. O. Sladky, P. A. Bulliner, and N. Bartlett, J. Chem. Soc. **14**, 2179 (1969).

[164] N. Bartlett and F. O. Sladky, *Comprehensive Inorganic Chemistry*. (Pergamon Press, London, 1973).

[165] T. Ogrin, B. Zemva, M. Bohinc, and J. Slivnik, J. Chem. Eng. Data **17**, 418 (1972).

[166] J. Berkowitz, W. A. Chupka, P. M. Guyon, J. Holloway, and R. Spohr, Advan. Mass. Spectrom. **5**, 112 (1971).

[167] C. R. Brundle, M. B. Robin, and G. R. Jones, J. Chem. Phys. **52**, 3383 (1970).

[168] B. Brehm, M. Menzinger, and C. Zorn, Can. J. Chem. **48**, 3193 (1970).

[169] J. D. Morrison, A. J. C. Nicholson, and T. A. O'Donnell, J. Chem. Phys. **49**, 959 (1969).

[170] U. Nielsen and W. H. E. Schwarz, Chem. Phys. **13**, 195 (1976).

[171] H. J. Svec and G. D. Flesch, Science **142**, 954 (1963).

[172] C. R. Brundle, G. R. Jones, and H. Basch, J. Chem. Phys. **55**, 1098 (1971).

[173] J. Berkowitz, W. A. Chupka, P. M. Guyon, J. Holloway, and R. Spohr, J. Chem. Phys. **75**, 1461 (1971).

[174] M. Pettersson, J. Lundell, and M. Räsänen, Eur. J. Inorg. Chem. **5**, 729 (1999).

[175] M. Pettersson, L. Khriachtchev, A. Lignell, and M. Räsänen, J. Chem. Phys. **116**, 2508 (2002).

[176] G. M. Chaban, J. Lundell, and R. B. Gerber, Chem. Phys. Lett. **364**, 628 (2002).

[177] J. Lundell, G. M. Chaban, and R. B. Gerber, Chem. Phys. Lett. **331**, 308 (2000).

[178] J. Panek, Z. Latajka, and J. Lundell, Phys. Chem. Chem. Phys. **4**, 2504 (2002).

[179] N. Runeberg, M. Pettersson, L. Khriachtechev, and J. Lundell, J. Chem. Phys. **114**, 836 (2001).

[180] A. E. Reed, L. A. Curtiss, and F. Weinhold, Chem. Rev. **88**, 899 (1988).

[181] J. Sun and K. Ruedenberg, J. Chem. Phys. **101**, 2157 (1994).

[182] J. Sun and K. Ruedenberg, J. Chem. Phys. **99**, 5269 (1993).

[183] J. Panek, Z. Latajka, and J. Lundell, Physical Chemisry Chemical Physics **4**, 2504 (2002).

[184] A. Lignell, J. Lundell, M. Pettersson, L. Khriachtchev, and M. Räsänen, Low Temp. Phys. **29**, 844 (2003).

[185] M. Johansson, M. Hotokka, M. Pettersson, and M. Räsänen, Chem. Phys. **244**, 25 (1999).

[186] S. R. Gunn, J. Phys. Chem. **71**, 2934 (1967).

[187] W. F. Howard and L. Andrews, J. Am. Chem. Soc. **96**, 7864 (1974).

[188] M. Johansson, M. Hotokka, M. Pettersson, and M. Räsänen, Chem. Phys. **244**, 25 (1999).

[189] L. Khriachtchev, M. Pettersson, N. Runeberg, J. Lundell, and M. Räsänen, Nature **406** (2000).

[190] T. Takayanagi, Chem. Phys. Lett. **371**, 675 (2003).

[191] M. W. Wong, J. Am. Chem. Soc. **122**, 6289 (2000).

[192] J. Lundell, A. Cohen, and R. B. Gerber, J. Phys. Chem. A **106**, 11950 (2002).

[193] L. Khriachtchev, H. Tanskanen, J. Lundell, M. Pettersson, H. Kiljunen, and M. Räsänen, J. Am. Chem. Soc. **125**, 4696 (2003).

[194] S. Yockel, J. J. Seals III., and A. K. Wilson, Chem. Phys. Lett. **393**, 448 (2004).

[195] A. Cohen, J. Lundell, and R. B. Gerber, J. Chem. Phys. **119**, 6415 (2003).

[196] L. Khriachtchev, H. Tanskanen, A. Cohen, R. B. Gerber, J. Lundell, M. Pettersson, H. Kiljunen, and M. Räsänen, J. Am. Chem. Soc. **125**, 6876 (2003).

[197] G. M. Chaban, Chem. Phys. Lett. **395**, 182 (2004).

[198] S. A. C. McDowell, Phys. Chem. Chem. Phys. **2003**, 1530 (2003).

[199] M. Pettersson, J. Lundell, L. Khriachtchev, and M. Räsänen, J. Chem. Phys. **109**, 618 (1998).

[200] H. Tanskanen, L. Khriachtchev, J. Lundell, H. Kiljunen, and M. Räsänen, J. Am. Chem. Soc. **125**, 16361 (2003).

[201] S.-Y. Yen, C.-H. Mou, and W.-P. Hu, Chem. Phys. Lett. **383**, 606 (2004).

[202] S. Jolkkonen, M. Pettersson, and J. Lundell, J. Chem. Phys. **119**, 7356 (2003).

[203] V. I. Feldman, F. F. Sukhov, A. Y. Orlov, and I. V. Tyulpina, J. Am. Chem. Soc. **125**, 4698 (2003).

[204] J. Lundell, J. Panek, and Z. Latajka, Chem. Phys. Lett. **348**, 147 (2001).

[205] A. Cunje, V. I. Baranov, Y. Ling, A. C. Hopkinson, and D. K. Bohme, J. Phys. Chem. A **105**, 11073 (2001).

[206] J. P. Perdew and Y. Wang, Phys. Rev. B **45**, 13244 (1992).

[207] A. K. Wilson and T. H. Dunning, Jr., J. Chem. Phys. **106**, 8718 (1997).

[208] S. Yockel, J. J. Seals, III., and A. K. Wilson, Chem. Phys. Lett. **393**, 448 (2004).

[209] D. E. Woon, K. A. Peterson, and T. H. Dunning, Jr., J. Chem. Phys. **109**, 2233 (1998).

[210] D. E. Woon, J. Chem. Phys. **100**, 2838 (1994).

[211] A. Cohen, J. Lundell, and R. B. Gerber, J. Chem. Phys. **119**, 6415 (2003).

[212] S. Yockel, A. Garg, and A. K. Wilson, Chem. Phys. Lett. **411**, 91 (2005).

[213] G. M. Chaban, Chem. Phys. Lett. **395**, 182 (2004).

[214] S. Yockel, A. Garg, and A. K. Wilson, Chem. Phys. Lett. **411**, 91 (2005).

[215] C. Møller and M. S. Plesset, Phys. Rev. B **46**, 618 (1934).

[216] Gaussian 03, M. J. Frisch, G. W. Trucks, H. B. Schlegel, G. E. Scuseria, M. A. Robb, J. R. Cheeseman, J. A. Montgomery, T. V. Jr., K. N. Kudin, J. C. Burant, J. M. Millam, S. S. Iyengar, J. Tomasi, V. Barone, B. Mennucci, M. Cossi, G. Scalmani, N. Rega, G. A. Petersson, H. Nakatsuji, M. Hada, M. Ehara, K. Toyota, R. Fukuda, J. Hasegawa, M. Ishida, T. Nakajima, Y. Honda, O. Kitao, H. Nakai, M. Klene, X. Li, J. E. Knox, H. P. Hratchian, J. B. Cross, V. Bakken, C. Adamo, J. Jaramillo, R. Gomperts, R. E. Stratmann, O. Yazyev, A. J. Austin, R. Cammi, C. Pomelli, J. W. Ochterski, P. Y. Ayala, K. Morokuma, G. A. Voth, P. Salvador, J. J. Dannenberg, V. G. Zakrzewski, S. Dapprich, A. D. Daniels, M. C. Strain, O. Farkas, D. K. Malick, A. D. Rabuck, K. Raghavachari, J. B. Foresman, J. V. Ortiz, Q. Cui, A. G. Baboul, S. Clifford, J. Cioslowski, B. B. Stefanov, G. Liu, A. Liashenko, P. Piskorz, I. Komaromi, R. L. Martin, D. J. Fox, T. Keith, M. A. Al-Laham, C. Y. Peng, A. Nanayakkara, M. Challacombe, P. M. W. Gill, B. Johnson, W. Chen, M. W. Wong, C. Gonzalez, and J. A. Pople, (Gaussian, Inc., Pittsburgh PA, 2001).

[217] W. Manchot and H. Gall, Berichte **58**, 2175 (1925).

[218] F. Calderazzo, J. Orangomet. Chem. **400**, 303 (1990).

[219] P. R. Norton, P. A. Young, Q. Cheng, N. Dryden, and R. J. Puddephatt, Surf. Sci. **207** (1994).

[220] L. G. Vaughan, U.S. Patent No. 3661659-19720509 (1972).

[221] R. E. Bachman, M. S. Fioritto, S. K. Fetics, and T. M. Cocker, J. Am. Chem. Soc. **123**, 537 (1002).

[222] T. Kaharu, R. Ishii, and S. Takahashi, J. Chem. Soc., Chem. Commun., 1349 (1994).

[223] R. Ishii, T. Kaharu, N. Pirio, S. W. Zhang, and S. Takahashi, J. Chem. Soc., Chem. Commun., 1215 (1995).

[224] C. Kual, Coord. Chem. Rev. **99**, 213 (1990).

[225] P. C. Ford and A. Vogler, Acc. Chem. Res. **26**, 220 (1993).

[226] L. Shao, L. Zhang, M. Zhou, and Q. Qun, Organometallics **20**, 1173 (2001).

[227] A. Vogler and H. Kunkely, Coord. Chem. Rev. **219-221**, 489 (2001).

[228] H. Kunkely and A. Vogler, J. Orangomet. Chem. **541**, 177 (1997).

[229] P. Pyykko, Chem. Rev. **97**, 597 (1997).

[230] P. Pyykko, Angew. Chem. Int. Ed. **43**, 4412 (2004).

[231] P. Pyykko, Inorg. Chim. Acta **358**, 4113 (2005).

[232] I. Antes, S. Dapprich, and P. Schwerdtfeger, Inorg. Chem. **35**, 2089 (1996).

[233] A. Fortunelli and G. Germano, J. Phys. Chem. A **104**, 10834 (2000).

[234] D. B. DellAmico and F. Calderazzo, Gazz. Chim. Ital. **103**, 1099 (1973).

[235] D. Figgen, G. Rauhut, M. Dolg, and H. Stoll, Chem. Phys. **311**, 227 (2005).

[236] M. Couty and M. B. Hall, J. Comput. Chem. **17**, 1359 (1996).

[237] P. Pyykko, N. Runeberg, and F. Mendizabal, Chem. Eur. J. **3**, 1451 (1997).

[238] J. P. Perdew, J. A. Chevary, S. H. Vosko, K. A. Jackson, and M. R. Pederson, Phys. Rev. B **46**, 6671 (1992).

[239] M. A. Omary, P. Sinha, P. S. Bagus, and A. K. Wilson, J. Phys. Chem. A **109**, 690 (2005).

[240] I. I. Vorontsov, A. Kovalevsky, A. Yu, Y.-S. Chen, T. Graber, I. V. Novozhilova, M. A. Omary, and P. Coppens, Phys. Rev. Lett. **94**, 193003 (2005).

[241] P. G. Jones, Naturforsch. **37**, 823 (1982).